MR elastomers for structural control

Yang Zhou
University of Wollongong

MR Elastomers for Structural Control

A thesis submitted in fulfillment of the requirements

for the award of the degree of

Master of Engineering – Research

Yang ZHOU

Faculty of Engineering, University of Wollongong

June 2009

Wollongong, New South Wales, Australia

CERTIFICATION

I, Yang ZHOU, declare that this thesis, submitted in partial fulfillment of the requirements for the award of Master of Engineering – research, in the School of Civil, Mining and Environmental Engineering, Faculty of Engineering, University of Wollongong, is wholly my own work unless otherwise referenced or acknowledged. The document has not been submitted for qualifications at any other academic institution.

Yang ZHOU

18th June 2009

ACKNOWLEDGEMENTS

I wish to thank my supervisors, Dr. Weihua Li and Assoc. Prof. Muhammad Hadi, for their enthusiastic support, professional direction and constant encouragement that inspired me to overcome the challenges on my road of life and study.

Particular thanks are extended to Xianzhou Zhang, Quanzhi Teng and Bin Liu for their help on electrical design and mechanical manufacturing for this project. Without the assistance of my lab mates I could not complete this dissertation. I thank all who helped me during my graduate studies.

Finally, I specially would like to thank my wife Meihua Gu and my parents for their understanding, patience and unwavering support throughout the course of my graduate studies.

ABSTRACT

This dissertation focuses on a basic understanding of the behaviour of Magnetorheological elastomers (MREs) and their application as MRE bearings for vibration controlling the structural systems. MREs are an important member of the group of smart materials and as such have attracted increasing interest because their modulus can be controlled by an external magnetic field.

Because MRE based devices usually work in a dynamic mode, the study of MRE properties under these conditions is essential for its practical application. The relationship between the dynamic shear stress and shear strain in various magnetic fields, including different strain amplitudes and frequencies, were measured. The stress-strain data forms elliptical curves which show that MRE behaves as if it possessed linear viscoelastic properties.

Based on these experimental results, a viscoelastic solid model with four parameters was proposed to predict the performance of MRE. In this model a spring element was placed in parallel with a 3-parameter standard viscoelastic solid model. A MATLAB optimization algorithm was used to identify the four parameters under various working conditions (magnetic field, strain amplitude and frequency). A comparison between the experimental results and the model predictions proved that the four-parameter viscoleastic model can accurately predict the performance of MRE.

A building model, three stories high, was constructed using MATLAB SIMULINK to evaluate the performance of an MRE device in structural control. Three controllers, passive on, passive off and bang-bang control strategy were used to compare the response of each storey to displacement and acceleration. In addition, the performance of an MRF damper and an MRE device in structural control, where the resultant peak force was selected as a criterion in the evaluation process, was compared and discussed. The effectiveness of an MRE bearing in structural control was well justified.

TABLE OF CONTENTS

ACKNOWLEDGEMENTS i

ABSTRACT ii

TABLE OF CONTENTS iii

LIST OF FIGURE CAPTIONS vi

LIST OF TABLE CAPTIONS ix

LIST OF SYMBOLS x

CHAPTER 1 INTRODUCTION 1

1.1 BACKGROUND AND MOTIVATION 1

1.2 AIMS AND OBJECTIVES 2

1.3 THESIS OUTLINE 2

CHAPTER 2 LITERATURE REVIEW 4

2.1 INTRODUCTION 4

2.2 MRE MATERIALS 4

2.2.1 MRE Material components 4

2.2.2 Fabrication a sample of MRE 6

2.3 MRE PROPERTY 7

2.3.1 Steady-state and dynamic properties of MRE 7

2.3.2 Influence factors of MRE 8

2.4 MODEL STUDIES OF MREs 12

2.4.1 Dipole model 12

2.4.2 Equivalent linear model 15

2.4.3 Phenomenological model 16

2.5 APPLICATIONS OF MRE 18

2.6 CONCLUSION 19

CHAPTER 3 STUDY OF THE VISCOELASTIC PROPERTIES OF MREs 20

3.1 INTRODUCTION 20

3.2 EXPERIMENTAL 20
3.2.1 Materials 20
3.2.2 Magneto-rheological Measurement 21
3.2.3 Experimental results 23
3.3 MODELLING MR ELASTOMERS 27
3.4 SYSTEM IDENTIFICATION 30
3.4.1 Parameter Identification 30
3.4.2 Comparison between experimental results and modelling predictions 32
3.5 CONCLUSION 38
CHAPTER 4 PHENOMENOLOGICAL MODEL OF MRE BEARINGS 39
4.1 INTRODUCTION 39
4.2 EXPERIMENTAL 39
4.2.1 Design and fabrication of MRE bearings 39
4.2.2 Experimental setup 40
4.2.3 Results and discussion 42
4.3 PHENOMENOLOGICAL MODEL 45
4.3.1 Modelling analysis 45
4.3.2 Parameter Identification 47
4.3.3 A comparison between experimental and model 50
4.3.4 Discussion of the MRE device 51
4.4 CONCLUSION 53
CHAPTER 5 SIMULATED EVALUATION OF AN MRE BEARING FOR STRUCTURAL CONTROL 54
5.1 INTRODUCTION 54
5.2 THREE STOREY BUILDING MODEL INCORPORATING AN MRE BEARING 54
5.2.1 Model of multi-storied structures 54
5.2.2 A three-storied benchmark model incorporating an MRE bearing 56
5.3 SIMULINK IMPLEMENTATION AND ANALYSIS 59
5.3.1 External seismic excitations 59

5.3.2 Three controllers 61
5.3.3 Performance evaluation 63
5.3.4 Discussion 78
5.4 CONCLUSION 80
CHAPTER 6 A COMPARISON BETWEEN THE MRF DAMPER AND MRE ISOLATOR 81
6.1 INTRODUCTION 81
6.2 STUDY OF AN MRF DAMPER 81
6.3 SIMULATING AN MRE DEVICE 83
6.4 PERFORMANCE EVALUATION 86
6.4.1 Dissipated energy of an MRF damper and MRE device 86
6.4.2 Structural responses evaluation 88
6.5 DISCUSSION 95
6.6 CONCLUSION 97
CHAPTER 7 CONCLUSIONS AND FUTURE WORK 98
7.1 SUMMARY 98
7.1.1 An experimental study of a multi-layer MRE bearing 98
7.1.2 A four-parameter viscoelastic phenomenological model 98
7.1.3 A simulation program for building structures 99
7.1.4 Performance evaluation 99
7.2 FUTURE WORK 100
REFERENCES 101
Appendix A: The Stress-Strain relationship of 1% and 5% amplitude input 108
Appendix B: MATLAB Program of four-parameter viscoelastic model 109
Appendix C: The relationship between magnetic flux density and current intensity 110
Appendix D: The simulation program of a three-storey building model 111
Appendix E: Peak response of building structure due to Northbridge earthquake 112

LIST OF FIGURE CAPTIONS

Figure 2.1 The dipole model 13

Figure 2.2 Particle saturation model 13

Figure 2.3 Hysteresis loop of MRE bearing in a different magnetic flux density 16

Figure 2.4 MRE phenomenological model 17

Figure 3.1 A diagram of the experimental setup 21

Figure 3.2 Plot of magnetic flux density (B_{MRE}) versus current (I) for the samples of MRE 22

Figure 3.3 Strain-stress curve of sample in different magnetic fields 24

Figure 3.4 Stress-Strain relationship of 10% amplitude input 25

Figure 3.5 Stress-Strain relationships for different strain amplitudes in 1000mA 26

Figure 3.6 Stress-Strain relationships for different frequency inputs in 1000mA 27

Figure 3.7 Four-parameter viscoelastic model for MR elastomers 28

Figure 3.8 A comparison between experimental data with model-predicted results (Strain) 33

Figure 3.9 A comparison between experimental data with model-predicted results (Frequency) 34

Figure 3.10 The relationship of current inputs with the storage and loss modulus 36

Figure 3.11 The relationship of frequency inputs with the storage and loss modulus 37

Figure 4.1 Schematic cross-section of the MR elastomers bearing 40

Figure 4.2 Schematic of experiment setup for MRE devices 41

Figure 4.3 Photograph of experiment setup for MRE devices 41

Figure 4.4 Relationship of displacement and force for MRE devices 42

Figure 4.5 Relationship of effective stiffness and effective viscous damping constant with external magnetic flux density 44

Figure 4.6 The four-parameter viscoelastic model for the MRE device 45

Figure 4.7 The relationship of four parameters with magnetic flux density inputs 48

Figure 4.8 Comparison of experimental results and analytical model results 51

Figure 4.9 The relationship of the real part and the imaginary part with magnetic flux density inputs 52

Figure 5.1 Idealised structural model 55

Figure 5.2 Schematic of a three storied building model incorporating an MRE bearing 57

Figure 5.3 Time-scaled ground acceleration of a typical seismic excitation record 60

Figure 5.4 The bang-bang control logic schematic for building 63

Figure 5.5 Displacement for each floor with an MRE device for passive off control logic 64

Figure 5.6 Acceleration for each floor with an MRE device for passive off control logic 66

Figure 5.7 Displacement for each floor with an MRE device for passive on control logic 69

Figure 5.8 Acceleration for each floor with an MRE device for passive on control logic 70

Figure 5.9 Displacement for each floor with an MRE device for Bang-bang control logic 73

Figure 5.10 Acceleration for each floor with an MRE device for Bang-bang control logic 75

Figure 6.1 A simple mechanical model of an MR damper 82

Figure 6.2 The relationship between displacement and force for an MR damper 83

Figure 6.3 The relationship between K_1 and K_2 with different frequency inputs for an MRE device 84

Figure 6.4 The relationship between displacement and force for an MRE device 86

Figure 6.5 The relationship between displacement and force for an MRF damper and MRE device 87

Figure 6.6 Displacement for each floor with an MRE device for passive off control logic 89

Figure 6.7 Acceleration for each floor with an MRE device for passive off control logic 90

Figure 6.8 Displacement for each floor with an MRE device for passive on control logic 92

Figure 6.9 Acceleration for each floor with an MRE device for passive on control logic 93

LIST OF TABLE CAPTIONS

Table 2.1 Parameters of an MRE phenomenological model 17

Table 3.1 Identified parameters 31

Table 3.2 Parameters identified for different frequencies with strain amplitude of 10% 32

Table 4.1 Four parameters at different magnetic flux density inputs 47

Table 4.2 Identification of the function parameters for the viscoelastic model 50

Table 5.1. Structural model parameters 58

Table 5.2 Peak responses due to the El Centro earthquake (Passive Off) 68

Table 5.3 Peak responses due to the El Centro earthquake (Passive On) 72

Table 5.4 Peak responses due to the El Centro earthquake (Bang-bang) 77

Table 5.5 Peak responses due to the El Centro earthquake 78

Table 6.1 Parameters of linear exploration for K_1 and K_2 85

Table 6.2 K_1 and K_2 of MRE device at 2.5 Hz frequency input 85

Table 6.3 Dissipation energy of an MRF damper and MRE device 88

Table 6.4 Peak response due to the El Centro earthquake (MRF) 88

Table 6.5 Peak response due to the El Centro earthquake (MRE) 95

Table 6.6 A comparison between an MRF damper and MRE device 95

LIST OF SYMBOLS

A	test displacement amplitude
B	magnetic flux density
C	damping matrices of structure
c_b	damping coefficient of MREs bearing without control current
c_e	effective viscous damping constant
c_n	viscous damping coefficient for the n^{th} storey
E_{loop}	energy dissipation per cycle of loading
F^+	experimental positive forces
F^-	experimental negative forces
F_{MRE}	control force of MREs bearing
G	pre-yield modulus
G_1	storage modulus
G_2	loss modulus
I	external intensity current inputs
I_{max}	maximum value of the input current
I_{min}	minimum value of the input current
J_p	dipole moment magnitude per unit particle volume
J_s	saturation polarization of the particles
K	stiffness matrices of structure
k_b	stiffness of MREs bearing without control current
k_e	effective stiffness
k_n	elastic stiffness coefficient for the n^{th} storey
M	total mass of the base
m_n	mass of the n^{th} storey
m_b	mass of MRE bearing
M	mass matrices of structure
N	experimental number of one loop

V_i	volume of particle
u_1	relative permeability of the medium
u_0	vacuum permeability
x_0	amplitude of displacement
x_n	displacement of the n^{th} storey
σ	shear stress of MRE sample
ω	angle frequency of shear strain
ε_0	amplitude of shear strain
ε	shear strain of MRE sample
ϕ	phase angle
Δ^+	experimental positive displacement
Δ^-	experimental negative displacement
η	damping loss factor for structure

CHAPTER 1

INTRODUCTION

1.1 BACKGROUND AND MOTIVATION

The tragic consequences of earthquakes will cause a tremendous loss in an economy. The recent earthquakes in Japan and China have underscored, in terms of both human and economic factors, the importance of the way in which building and bridges respond to them. For several decades significant efforts have been devoted to the possibility of using various smart materials in the design of engineering structures to increase their safety and reliability in strong earthquakes. Various semi-active devices have been developed to reduce the response of the structural system. Some examples that have been considered for civil engineering applications include variable orifice dampers, controllable friction braces, controllable friction isolators, variable stiffness devices, and electro-rheological (ER) dampers. Moreover, in Japan, variable stiffness systems have already proven their effectiveness.

Nowadays, smart materials such as Magneto-Rheological (MR) are used because their rheological properties change under a magnetic field. MR materials can generally be classified into two main groups, MR fluids and MR elastomers. Although MR fluids have wide applications in mechanic and civil engineering, MR fluids have distinct shortcomings because liquid leakage can result in environmental contamination and particle residue can degrade the performance of MR devices. These shortages are mainly due to the liquid state of MR fluids. MR elastomers, the solid analogs of MR fluids, may be a good solution to overcome the disadvantages of MR fluids. MR elastomers (MREs) are smart materials where polarised particles are suspended in a non-magnetic solid or gel-like matrix. Polarised particles can be arranged as chains in polymer media such as silicon rubbers and natural rubbers. The viscoelasticity of MRE is changed by controlling the external magnetic field.

Until now, not too many models have been developed to investigate MR elastomers. However, there are models such as the dipole model and phenomenological model which can accurately express the behavior of MR fluid. This thesis presents a four-parameter viscoelastic model, a phenomenological model, to perform the characteristics of MRE materials and MRE devices. Then, based on the experiments and verification of the MRE material and devices, a three storey building model was simulated to use the MRE devices in the area of structural control. Although there has been a lot of research into structural control with an MR fluid damper, an MRE device is not widely used to control the response of buildings to deformation.

1.2 AIMS AND OBJECTIVES

The objectives of this study consist of fabrication, testing, modelling MRE and studying its applications in structural control. The project is divided into several parts in terms of the functions of the different components of the system. The specific objectives are as follows:

1) Fabrication and testing MRE materials
2) Development and test of the mechanical performance of an MRE device
3) Simulation and evaluation of a building structure incorporating an MRE device

1.3 THESIS OUTLINE

This thesis begins with a literature review on MRE material, MRE property, and a mathematical model for MRE and MRE applications in *Chapter 2*, which gives a comprehensive overview of the achievements of previous research and the aim of this project. *Chapter 3* gives a deduction of a four parameter viscoelastic model based on experiments with samples of MREs materials. The detailed experimental procedures and verification of the four parameter viscoelastic model are also explained in this chapter. *Chapter 4* explains the development and study of an MRE device and the applications of a four parameter viscoelastic model to express the behaviour of MRE

devices. *Chapter 5* addresses the simulated three storey building model that incorporates an MREs device. An evaluation of the performance and a comparison between an MR fluid damper and the proposed MRE device are discussed in *Chapter 6.* In this chapter, the performance of an MRE device and an MRF damper for controlling displacement and acceleration, with criteria of peak control force, are verified. *Chapter 7*, concludes with a review and summary of the project and suggestions for further research work.

CHAPTER 2

LITERATURE REVIEW

2.1 INTRODUCTION

The purpose of this study is to develop an effective Magnetorheological elastomers (MREs) device for use in structural control. Thus, this literature review deals with the combined technologies of MRE material, MRE property, approaches to modelling, and applications of MRE.

MRE material consists of suspensions of polarised particles in a non-magnetic solid or gel-like matrix. These polarised particles can be arranged in chains in polymer media such as silicon rubber and natural rubber [1, 2, 3]. When a magnetic field is applied MRE materials can perform a controllable shear modulus with the magnetic field. Although many mathematical models for applications of MR materials [4, 5, 6] have been developed, they have not often been used to express the character of MRE materials. In this study, a four-parameter phenomenological model was proposed to investigate different approaches to modelling MRE materials.

2.2 MRE MATERIALS

2.2.1 MRE Material components

Three components, the matrix, particles and additives are used in the sample of MRE [4, 7]. The physical phenomena seen in MR elastomers are very similar to those in MR fluids. MREs are materials that have polarised particles arranged in chains in polymer media such as silicon and natural rubbers. However, the particle chains within the elastomer composite are intended to operate in the preyield regime, whereas MR fluids typically operate within a postyield continuous shear or flow regime [8]. Thus a typical MRE consists of viscoelastic materials, powdery solids (metals) and viscous liquids. All these have either a zero or limited mutual solubility or compatibility, even if they

can be thoroughly dissolved into each other. The interaction between the matrix and the filler particles can be either strong or weak and will influence the rheological and mechanical properties of the composite.

A) Particles

Spherical carbonyl iron particles are generally used as the filler material to fabricate MREs. They were prepared by a thermal decomposition of iron pentacarbonyl and the general size of each particle is a few microns. Iron has one of the highest saturation magnetisation values of metallic elements with Ms = 2.1 Tesla. It also has high permeability, low remnant magnetisation and high saturation magnetisation. High permeability and saturation magnetisation are thought to provide high inter-particle attraction and thereby a high MR effect. A low remnant magnetisation is also recommended because the highly remnant particles will stick together when the magnetic field is turned off [9, 10]. The magnetostriction of iron particles is also low [11].

B) Matrix

Typical matrixes are natural rubber and silicone rubber. Natural rubber is an elastomer, an elastic hydrocarbon polymer that originally derived from a milky colloidal suspension or latex, found in the sap of some plants. The purified form of natural rubber is the chemical polyisoprene which can also be produced synthetically. Heat is normally required to vulcanise silicone rubber. The silicone rubber and a vulcanising silicon sealant (at room temperature), is mixed with silicon oil to changing its ductility. The silicon oil is selected on the basis of preliminary studies with different elastomers. Polydimethylsiloxanes (PDMS) is one example of silicon rubber. Elastosil M4644 and M4601 are two-component high strength PDMS that vulcanise at room temperature. The silicones have different values of hardness, M4644 has a Shore A hardness of 41 and M4601 has a Shore A hardness of 28. The advantage of these silicones is that the moulded samples do not shrink during curing. The PDMS have a low surface tension

and are capable of wetting most surfaces. The stability and chemical neutrality of the system also enables the adhesive to bond to the metals [12, 13].

C) Additives

In addition, additives are used to decrease the basis modulus of MRE materials. When the molecules of additives enter into rubber, the gaps between the molecules of rubber are increased and the conglutination of molecules is decreased. The additives not only increase the plasticity and fluidity of the matrix, they also average the distribution of internal stress in the materials, which makes them ideal for fabricating MRE materials [14].

2.2.2 Fabrication a sample of MRE

The general procedure for fabricating an anisotropic MR elastomer with natural rubber is similar to conventional rubber. Normally, the ingredients are natural rubber, zinc oxide, stearic acid, sulfur, and iron particles. After all the ingredients are evenly mixed in a mixing machine under a high temperature such as 120°, the mixture is packed in a mould and then cured under an electric-magnetic field for some time. The samples are then left at the room temperature for more than one day prior to testing. The chain formation results from the anisotropic magnetic forces among the particles. The MREs fabricated with this method are called anisotropic MREs.

However, MREs fabricated under an external magnetic field using conventional methods have many shortcomings which greatly limit their industrial applications. Firstly, the conventional rubber-producing equipment must be modified in order to provide a magnetic field during crosslinking. Secondly, thick MREs cannot be fabricated practicably because the density of the magnetic flux will decrease sharply as the thickness of the MRE increases. Thirdly, the chain direction of the anisotropic MRE must be considered when it is to be used in a particular device. In order to overcome these drawbacks, some attempts have been tried to prepare isotropic MREs without

external fields [15]. By using special particles and high concentration of particles the absolute MR effect in isotropic MR rubbers is larger than previously reported. However, these materials with such high concentrations of iron particles have a high zero-field modulus so that the relative MR effect is quite low. This means there are many challenges remaining for the study of isotropic MREs.

2.3 MRE PROPERTY

2.3.1 Steady-state and dynamic properties of MRE

MREs contain viscoelastic properties. The shear modulus is changed by controlling an external magnetic field. Compared to other parameters, the flux density of magnetic energy, which is perpendicular to the magnetic field, can change significantly and so too can the shear properties of MREs. MRE materials generally operate at the pre-yield region and behave the same as material with viscoelastic properties [3].

The MR effect of MR elastomers is described as a reversible change in modulus in an applied magnetic field. This has been confirmed in several studies [16, 17, 18, 19, 20]. Aligned MREs have mostly been characterised at relatively low frequencies (1 to 20 Hz) to measure the changes in the dynamic shear modulus induced by the external magnetic field [3, 21]. Ginder et al. [21] found a substantial MR effect over the entire frequency range studied. The increase in the shear modulus varied initially with the strength of the magnetic field but saturated at higher strength fields. When the magnetic field was increased from 0 to 0.56 Tesla the consequent increase in shear modulus was nearly 2 MPa and the frequency of the resonance was shifted upward by over 20%. Zhou et al. [3] started that the changes of dynamic shear storage modulus can be over 50%, while Gong et al.[1] said it can be over 100%. Lokander et al. [9, 17] studied the dynamic shear modulus for isotropic MR elastomers with different filler particles and matrix materials. They measured the MR effect as a function of the amplitude of strain and found that the MR effect decreases rapidly with increasing strain within the measured range, and is not dependent on the frequency of testing. The fact that the absolute MR

effect is independent of the matrix material means that softer matrix materials will show a greater relative MR effect.

2.3.2 Influence factors of MRE

2.3.2.1 Influence of magnetic field

The magnetic field is a key parameter in the effect that MR has on MR elastomers. Filling an elastomeric material with magnetised particles influences the mechanical properties of the composite when an external magnetic field is applied. The origin of the field dependence of these properties is the existence of field-induced dipole type magnetic forces between the separate particles. The behaviour of MR elastomers is thought to be a combination of the properties of the matrix and the internal network of magnetised particles. Because these magnetic particles interact the elastomers exhibit a field dependent modulus at low strains. A field-induced increase in shear modulus reaching over 60% has been reported for applied magnetic field strength values of about 0.8 Tesla [4, 22].

2.3.2.2 Influence of the matrix material

When the material in the matrix is magnetic, the polarisation of the particles will be less effective and the MR effect therefore smaller. The addition of magnetically active additives (other than MR particles) decreases the MR effect [9, 22].

The overall properties of the elastomer composite are also influenced by the additives, as the filler material causes the volume to increase, so the previous effect also increases. Lokander et al. [17] have shown that the absolute effect of MR (the difference between the zero-field modulus and modulus measured under an external magnetic field) is independent on the matrix material. However, the zero-field modulus can be much higher for hard matrix material, where materials with high volume fraction of iron already have a high zero-field modulus, which means that the relative MR effect is quite low [9, 17].

2.3.2.3 Influence of particle size, shape and volume fraction

In conventional MREs the size of the particle varies typically from 0.1 to 10 μm and is from one to three orders of magnitude larger than typical particles of colloidal ferrofluid. Typical micron-sized MR filler particles will support hundreds of magnetic domains. Larger particles allow for obtaining stable, highly magnetic materials and reversible particle aggregation. Thus the particles should be large enough to support at least several magnetic domains in order to have a substantial MR effect.

Lokander et al. [9, 17] have shown experimentally that the shape and size of the particle has an influence on the properties of MR. They measured the magnetorheological effect for isotropic nitrile rubber MRE with varying sizes and content of iron particles. The MR effect was larger for materials with ASC300 iron (particle size < 60 μm) than for materials with carbonyl iron (particle size 3.9-5.0 μm). For particles larger than 60μm, the MR effect appeared to be slightly smaller. Demchuk and Kuzmin [23] have also studied the effect that the size of the filler particles has on the shear storage modulus and loss of isotropic and aligned MR elastomers. They found that without the field the modulus for MRE with larger particles (13 μm) was smaller than for fine particles (3.5 μm). Under a magnetic field the situation was reversed because as that the field strength increased the modulus of the MRE with larger particles exceeded the modulus of the MRE with fine particles significantly. Alternatively the loss factor decreased as either the magnetic field became stronger or the filler particles increased in size. According to Lokander et al. [9], if the air is replaced by an elastomer, then the critical particle concentration is defined as that at which the particles are in touch with each other and the voids between them are completely filled with the elastomer. But at concentrations higher than critical particle concentration there is not enough elastomer to fill all the voids between the particles and therefore the mechanical properties of the composite will be poor. The stiffness of the material due to an increased filler content will also increase substantially and therefore the relative MR effect will not increase significantly.

The optimal particle volume fraction for the largest relative change in modulus at saturation was predicted to be 27% [7]. Shiga et al. [18] measured the increase in shear modulus as a function of the particle volume fraction. For aligned MREs the change in shear modulus increases with an increasing particle volume fraction. When the concentration of filler is higher than 30 vol.%, the mechanical properties of the composite deteriorate rapidly and the stiffening of the material is larger than the increase of the MR effect. Lokander et al. [9, 17] measured the tensile strength of isotropic MR elastomers and found that the fracture stress as a function of the content of iron was almost constant when the iron contents were up to approximately 30% by volume. When the content if iron is higher, the fracture stress was much lower [9].

Moreover the filler materials influence the overall properties of the elastomers without an external magnetic field. This influence can increase when the volume of the filler material increases. Lokander et al. [17] have shown that the absolute MR effect of isotropic MREs (the difference between the zero-field modulus and the modulus measured under an external field) was quite independent of the matrix material. However, the zero-field modulus can be much larger for a harder matrix material which means that softer matrix materials may show a greater relative MR effect. Materials with a high volume of rigid filler material already have a high zero-field modulus so the relative MR effect can be quite low [17]. In addition, tensile tests by Lokander et al. [9] showed that increasing the filler over 30 vol.% would deteriorate the mechanical properties of the elastomer composite [9]. Bellan and Bossis [24] noted that in the absence of an external magnetic field the Young's modulus was much higher for the aligned material in the chain direction than for the homogeneous material with the same volume of filler. Homogeneous MREs with a random distribution of particles can be considered as isotropic materials. A solid, which is isotropic in its elastic constants, is a material where the elastic moduli are not dependent on directions [20].

2.3.2.4 Influence of working modes on the MREs properties

Borcea and Bruno [16] and Dorfmann and Ogden [25] have shown theoretically that the existence of a magnetic field stiffens the shear response of an isotropic MRE. Farshad and Benine [26] characterised isotropic and aligned MREs in tension and compression. The aligned MREs were either longitudinally or transversely oriented to the applied load. They found that the direction of alignment influences the tensile properties of the MRE. Samples aligned longitudinally to the direction of the tensile load exhibited the highest tensile strength. In shear static compression the applied magnetic field increased the stiffness of both isotropic and aligned MREs. The results of Shiga et al. [18] suggest that the increasing shear modulus in aligned MREs is quadratically dependent on the strength of the magnetic field. Bellan and Bossis [24] also considered aligned MREs to be analogous to fibre-reinforced composites. In MREs, the fibres consist of chains of particle whose stiffness is sensitive to the amount of polymer in the gaps between the particles. The stiffness of the fibres formed by particles is increased when a magnetic field was applied while the stiffness of the composite depends on the cross section of the number of chains per unit.

According to Yalcintas and Dai [19], the external magnetic field will affect the strain amplitude, loss factor, and natural frequency of the vibrating MRE system when dynamically testing in the pre-yield regime. When the strength of the magnetic field increases, the strain amplitude decreases and natural frequencies shift to higher values. The loss factors (tan δ) were found to increase with the strength of the magnetic field in every vibration mode. When an external magnetic field but no mechanical loads was applied the MREs deformed slightly. Borcea and Bruno [16] showed theoretically that an isotropic MRE would expand in the direction of the applied magnetic field while an aligned MRE will compress if the field is parallel to the oriented structure. Zhou and Jiang [20] proved this experimentally and also stated that the deformations are related to the strength of the field applied. The magnetically induced deformation of an aligned MRE in the direction of the chain only changes slightly with different volumes of filler. The deformation of an aligned MRE driven by an external magnetic field is smaller

than an isotropic MRE of the same volume. This means that aligned MREs are stiffer than isotropic MREs [20] in the direction of the chain.

2.4 MODEL STUDIES OF MREs

Similar to MRF studies, models such as an equivalent linear model and phenomenological model were developed to simulate the behaviour of MR elastomers.

2.4.1 Dipole model

Most models of MR material behaviour are based on the magnetic dipole interaction between two adjacent particles in the chain. These inter-particle interactions are then averaged over the entire sample to yield a model of the bulk magnetorheological behaviour. Jolly et al. [4] proposed a quasi-static, one-dimensional model that assumed that a magnetic interaction only occurs between the adjacent particles within a chain. On the basis of this point-dipole model, the MR effect was studied as a function of particle magnetisation. This model was based on previous studies of MR fluids. According to the model the ferrous particles are magnetised linearly and it was assumed that in MR materials the strength was related to particle magnetisation quadratically. Figure 2.1 shows the chart of a dipole model and Figure 2.2 shows particle saturation model

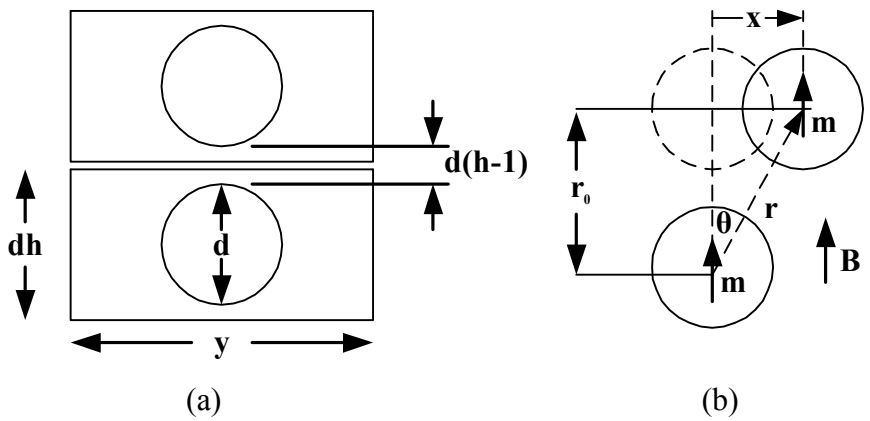

Figure 2.1. Particle saturation model [4]
(a) Geometry of two particles of diameter d within a particle chain. Adjacent chains are a distance y apart and h = r_0/d. (b) Magnetic interaction of the two particles modelled as dipole moments m and sheared with respect to one another.

In this model the average particle polarisation J_p is the dipole moment magnitude per unit particle volume, $|M| = J_p V_i$, where V_i is the volume of the particle. The pre-yield modulus G of the particle network is stress divided by strain and can be expressed as

$$G \cong \frac{\varphi J_p^2}{2\mu_1 \mu_0 h^3} \qquad \varepsilon < 0.1 \tag{2.1}$$

where μ_1 is the relative permeability of the medium, $\varepsilon = x/r_0$ is defined as the scalar shear strain of the particle chain. ϕ is the volume of particles in the composite and h is an indication of the gap between the particles in a chain.

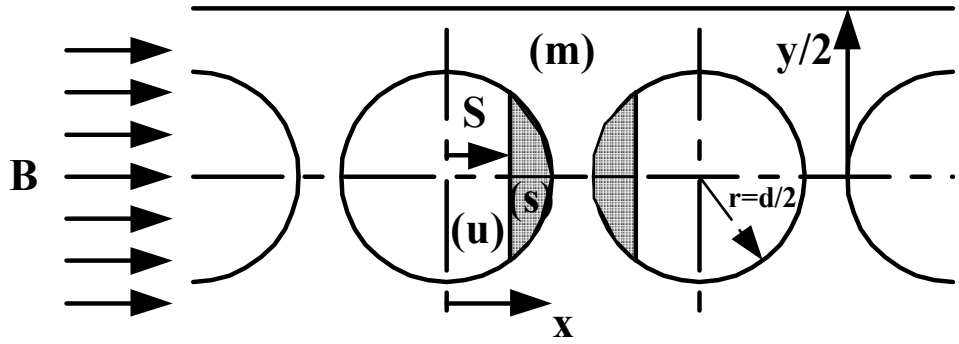

Figure 2.2. Particle saturation model [4]
Quantities are consistent with those defined in figure 2.2. Letters in parentheses indicate different regions: (s) region where particle is saturated (shaded), (u) region where particle is unsaturated, (m) matrix region with assumed relative permeability $\mu_m = 1$. Letters in parentheses also correspond to subscripts used in theory development.

$$J_p = \langle J_p \rangle = \frac{3/2(s/r)^3 B + (1-(s/r)^3)J_s}{1+3/2\phi(s/r)^3} \tag{2.2}$$

where J_s is the saturation polarisation of the particles, B is magnetic flux density, *s/r* is the ratio of the unsaturated gap and diameter of the particle.

Furthermore the maximum possible field induced change in stress (and modulus) occurs when the aligned particles become magnetically saturated, i.e. when $J_p = J_s$. It can be seen that the maximum field-induced stress rises quadratically with saturation magnetisation J_s of the particle material.

Gong et al.[1] fabricated MREs without the help of a magnetic field. Carbonyl iron particles are mixed with silicon oil before being blended with rubber material. The silicon oil helps the particles to attach to each other and self-assemble a partial microstructure. This is because of the surface tension of the additive. To analyse the influence of the assembled structure on the absolute variation of shear modulus of this kind of isotropic MRE, a simple self-assembled model was proposed. The increase in the shear modulus ΔG_{db} can be expressed as equation 2.3.

$$\Delta G_{db} = \frac{36\sqrt{2}\varphi\mu_m\mu_0\beta^2 H_0^2\left(\frac{R}{d}\right)^3\zeta}{2-\beta} \approx 1.4\Delta G_{da} \tag{2.3}$$

where μ_0 is the vacuum permeability, $\beta=(\mu_p-\mu_m)/(\mu_p+2\mu_m)$, μ_p is the relative permeability of particles and μ_m is the relative permeability of the matrix. For carbonyl iron particle and silicone rubber, μ_p=1000, μ_m=1 and β =1.

The point-dipole model is basically quasi-static and one-dimensional and it concentrates on the magnetomechanical properties of parallel chains of magnetically permeable spherical particles. A magnetic field was applied parallel to the chains and the shear strength caused by inter-particle forces was conducted. It was assumed that these particle chains were then embedded within a viscoelastic material and the viscoelastic properties of the composite were the sum of the viscoelastic properties of

the composite with no field applied and the elastic/plastic properties were induced by inter-particle forces [4]. Jolly's model suggests that MR material stress is quadratically related to particle magnetisation. Since the model was quasi-static the particles were assumed to be uniformly distributed, homogenous spheres that can be magnetically modeled as identically induced dipole moments. It was also assumed that the particles were aligned in perfect chains and that quasi-static shear strains and associated stresses were distributed uniformly over the length of each particle chain [4].

It was stated that the stress-strain relationship in the point-dipole model was independent of the size of the particle but the length of the gap between the particles in a chain was a very important parameter and the magnetic field- induced stress was inversely proportional to the third power of this gap. Therefore it is useful to select filler materials with high saturation magnetisation [4, 9]. The model by Jolly et al. [4] included a theory developed on the basis that saturation begins in the particle's polar regions at very low applied field strengths and increases towards total particle saturation as the strength of this field increases. Average particle polarisation is then calculated as a function of average composite flux density [4]. In reality however, the magnetic interaction between adjacent particle chains and packing arrangements is more complex than that occurring in simple linear chains. If the particles are spherical with the same size particles they will probably form face-centred cubic (FCC) and hexagonal close packed (HCP) microstructures [4]. Furthermore, a common weakness in modelling MR materials is still a lack of understanding of how magnetic flux density distributes itself within the particle network.

2.4.2 Equivalent linear model

Another kind of model was developed that depended on the hysteresis loop of deformation-force behaviour of the MREs [6]. This method was widely used to analyse a number of materials. Shown in Figure 2.3, the MREs express a linear viscoelastic characterisation in a certain magnetic field and strain. The deformation-force behaviour

of MREs at an applied magnetic field can be modelled by an equivalent linear model through effective elastic stiffness and viscous damping.

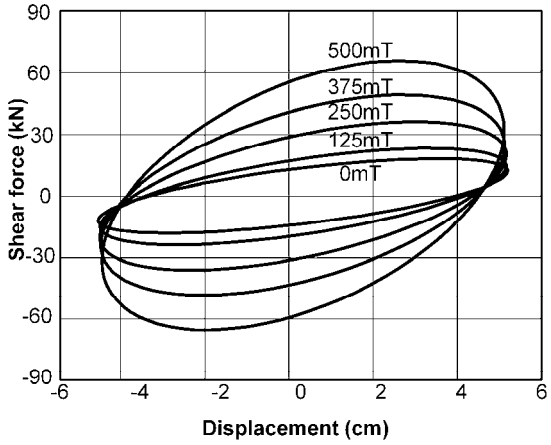

Figure 2.3 Hysteresis loop of MRE bearing in a different magnetic flux density [6]

The linear force developed in the isolation system can be expressed as

$$f_b = k_e x_b + c_e \dot{x}_b \tag{2.4}$$

where k_e is the effective stiffness, the slope of the main axis of the force-displacement ellipse loop; c_e is the effective viscous damping constant.

The equivalent linear elastic stiffness for each cycle of loading is calculated from the force-deformation curve of MREs. The effective viscous damping coefficient of the isolator unit calculated for each cycle of loading is specified as

$$c_{eff} = \frac{E_{loop}}{\pi \omega_{eff} A^2} \tag{2.5}$$

where E_{loop} is the energy dissipation per cycle of loading, ω_{eff} is the angle frequency and A is the test displacement amplitude.

2.4.3 Phenomenological model

Although the dipole models are capable of describing the force-displacement behaviour of MR materials reasonably well they cannot describe the non-linear force-velocity behaviour of the damper [27]. To overcome this deficiency different dynamic models have been developed. In order to develop a high-fidelity model for MR fluids, many phenomenological models such as the Bingham model [28, 29, 30, 31], the viscoelastic

model [32] and the Bouc-Wen model [33] have been used in the design and analysis of structural control with an MRF damper. Although these phenomenological models were widely used to predict the behaviour of an MR fluid damper [25, 34, 35, 36], there is not much investigation in modelling MRE materials and devices.

Koo et al. [5] recently developed a phenomenological model to capture the dynamic behaviour of MREs under compression loadings. Three key parameters were used in their model to predict the characteristics of MRE materials. These parameters (k_0, k_1 and c_0), were expressed with various external magnetic flux densities (B) in (2.6). The schematic figure of the model is shown in figure 2.4. and the parameters are listed in table 2.1.

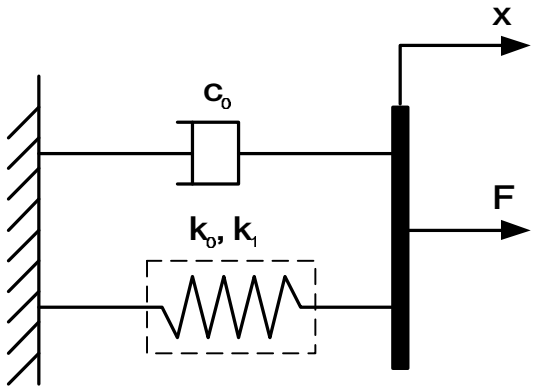

Figure 2.4 MRE phenomenological model [5]

$$\begin{cases} k_0 = k_{0a} + k_{0b}B \\ k_1 = k_{1a} + k_{1b}B \\ c_0 = c_{0a} + c_{0b}B \end{cases} \tag{2.6}$$

Table 2.1 Parameters of an MRE phenomenological model [5]

Parameters	c_{0a}	c_{0b}	k_{0a}	k_{0b}	k_{1a}	k_{1b}
Values	0.8342	0.2670	4.1072	1.2435	0.1677	0.0002

2.5 APPLICATIONS OF MRE

Until now there were many applications of MRF damper in structural control. Spencer et al. [37] developed a three-storey benchmark building incorporating an MRF damper to control the structural response stemming from the excitation of external ground., Many researchers have now done a lot of investigation into structural control incorporating MRF damper [38, 39, 40, 41] based on this benchmark.

Although MRF damper has been widely used for structural control there are not many applications of MRE materials and devices although they have been used in other different areas. One application for MRE is to use variable stiffness or resonance tunability which are countless, among these are dynamic vibration absorbers (DVA) invented by Frahm [42], which are a classic solution to suppress vibration in machines and structures. Ginder et al. [21] did pioneer work on the development of an adaptive tuneable vibration absorber (ATVA) using MREs. This device was not only used to explore the performance of such tuneable components but also to extend the measurement of the shear module of these materials to much higher frequencies than has previously been reported. Meanwhile, tuneable stiffness mounts and suspensions are other applications of MREs. The application of MR elastomers include automotive bushings and engine mounts where significant changes in the spring constant due to an applied magnetic field can be used to dynamically control stiffness and damping properties [10]. Additionally, MREs have also been used to construct new devices such as sandwich beams [43]. Zhou et al. [44] indicated that the sandwich configuration is an alternative to developing smart structures because it takes advantage of the field-controllable shear modulus of MRE and enhances the bulk flexural rigidity through the skins.

2.6 CONCLUSION

In this chapter the recent advances in various aspects of MR elastomers were described and reviewed. They include MRE materials, MRE properties, approaches to modelling MREs and applications of MRE. MR elastomers are now classified as smart materials particularly well suited to provide effective performance in structural control. The MR properties of MRE materials relate directly to practical applications of MRE. Therefore, on going research based on previous researches of MR elastomers and MR fluid will investigate a suitable model to represent the MR properties of MRE materials and devices, and evaluate its performance in structural control that incorporates an MRE device.

CHAPTER 3

STUDY OF VISCOELASTIC PROPERTIES OF MRES

3.1 INTRODUCTION

MRE devices generally operate at dynamic loading where they are subject to harmonic loading and therefore a study of their dynamic performance is crucial. As with MRFs, MREs act as viscoelastic properties at harmonic loading. This chapter aims to study the properties of MRE under dynamic loading. Experimental studies were conducted using an MR rheometer from which it was proposed that a four-parameter viscoelastic model be made to study the results. The four parameters were identified by using a MATLAB optimisation tool box. A comparison between the experimental studies and the predictive values from the model were discussed.

3.2 EXPERIMENTAL

3.2.1 Materials

In this project there were three material components, including particles, matrix and additives, were used to fabricate a sample of MRE. The particles used were carbonyl iron power, C3518 (Sigma-Aldrich Pty LTD) with a mean particle size of approximately 5μm. Silicone rubber (HB Fuller Pty. LTD) was used for the matrix of MR elastomers. The particles were wetted with silicone oil (DC 200/200cs, Dow Corning Corporation, U.S.A.) and then mixed with silicone rubber and silicone oil. All the ingredients were stirred in a beaker for about 5 min at room temperature. The mixture was put into a vacuum case to remove the air bubbles and then poured into a mould. After being cured for approximately 24 hours at room temperature under a constant magnetic flux density of 1 Tesla (electromagnetic system, Peking EXCEEDLAN Inc., China), the MR elastomer samples were prepared. The weight of the particles, silicone oil, and silicone rubber was in a ratio of 3:1:1.

3.2.2 Magneto-rheological Measurement

The mechanical properties of the MREs was measured with a rotational rheometer (MCR 301, Anton Paar Companies, Germany) and a Magneto Rheolgical Device (MRD 180), equipped with an electromagnetic kit that can generate a magnetic field perpendicular to the direction of the shear flow. A 20mm diameter parallel-plate measuring system with 1 mm gap was used. The samples were sandwiched between a rotary disk and a base. In this study a steady-state rotary shear and oscillatory shear were both used for the experiments.

The schematic of the experimental setup is shown in Figure 3.1. The stress and stain signals were output from two ports which were detected and processed by a Data Acquisition (DAQ) board (Type: LABVIEW PCI-6221, National Instruments Corporation. U.S.A) and a computer.

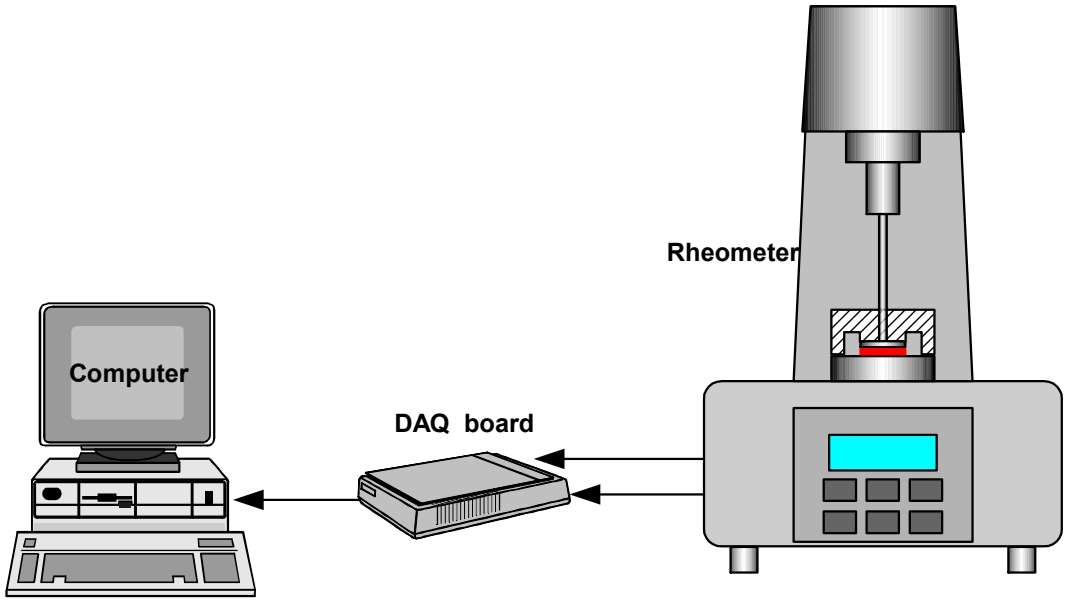

Figure 3.1: A diagram of the experimental setup

In this experiment the magnetic flux density of the sample of MRE (B_{MRE}) in the measuring gap depends not only on the current (I) applied to the samples, but also on the magnetic properties of MRE materials.

Figure 3.2 shows the dependence of the magnetic flux density (B_{MRE}) with the

measuring gap on current (I) for the sample of MRE. The relationship between B_{MRE} versus I is found to be:

$$B_{MRE} = 220I \text{ (mT)} \quad (3.1)$$

where the units of B_{MRE} and I are in mT and amp (A), respectively.

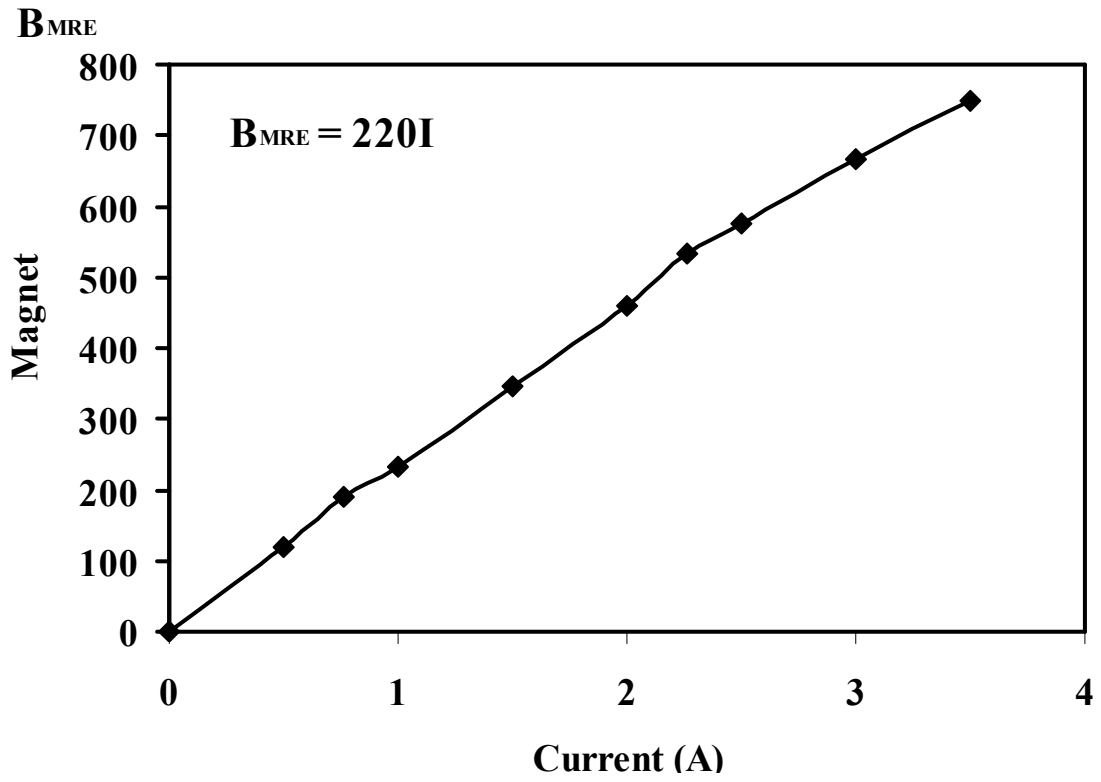

Figure 3.2 Plot of magnetic flux density (B_{MRE}) versus current (I) for the samples of MRE

A. Steady-shear testing

Under rotary shear the shear stress and shear strain of MREs under fields varying from 0~3.5A were measured. The MR effect was evaluated by measuring the shear strain-stress curve of the sample with and without a magnetic field applied.

B. Dynamic testing

In order to obtain the dynamic mechanical behaviour of MRE, the strain-stress hysteresis loop of MRE at different magnetic flux densities were measured with the oscillation mode. Once the set-up was completed the computer was then used to

transmit the input sine waveform to the test machine. To ensure the homogeneity of the MR elastomers, the experiments were carried out at different amplitudes of oscillation. These amplitudes were selected input stains at 1%, 5%, 10% respectively. Five sets of data were collected for different amplitudes of oscillation, according to the various magnetic fields input to the sample of MR elastomers.

Seven different magnetic fields, 0, 125, 250, 375, 500, 625 and 750mT, were used in this experiment. The current intensities in the coil are ranged from 0 to 3.5A. Three amplitudes of shear strain, 1%, 5%, and 10%, and three input frequencies, 1, 5 and 10Hz, were used. The real time strain and stress signals were recorded by the PC and then used to reconstruct the hysteresis loop.

3.2.3 Experimental results

3.2.3.1 Steady-state results

Figure 3.3 shows the strain-stress curve of the sample at 7 different magnetic field intensities ranging from 0 to 750mT. The slope of the strain-stress curve is the shear modulus of the material. As the figure shows, the shear modulus of the increased with the magnetic fields, proves that the MREs exhibited obvious MR effects. The shear stress shows a linear relationship with the shear strain when the strain is within 10%. This means the MRE acts with linear viscoelastic properties when the strain is below 10%. This finding is totally different from MR fluids where the linear viscoelastic region is generally below 0.1% [15]. This also demonstrated that MREs generally operate at the pre-yield region while MRF operates at the post-yield region. When the strain is above 10%, the modulus reaches a saturation (maximum value) and decrease steadily. This could be due to sliding effect.

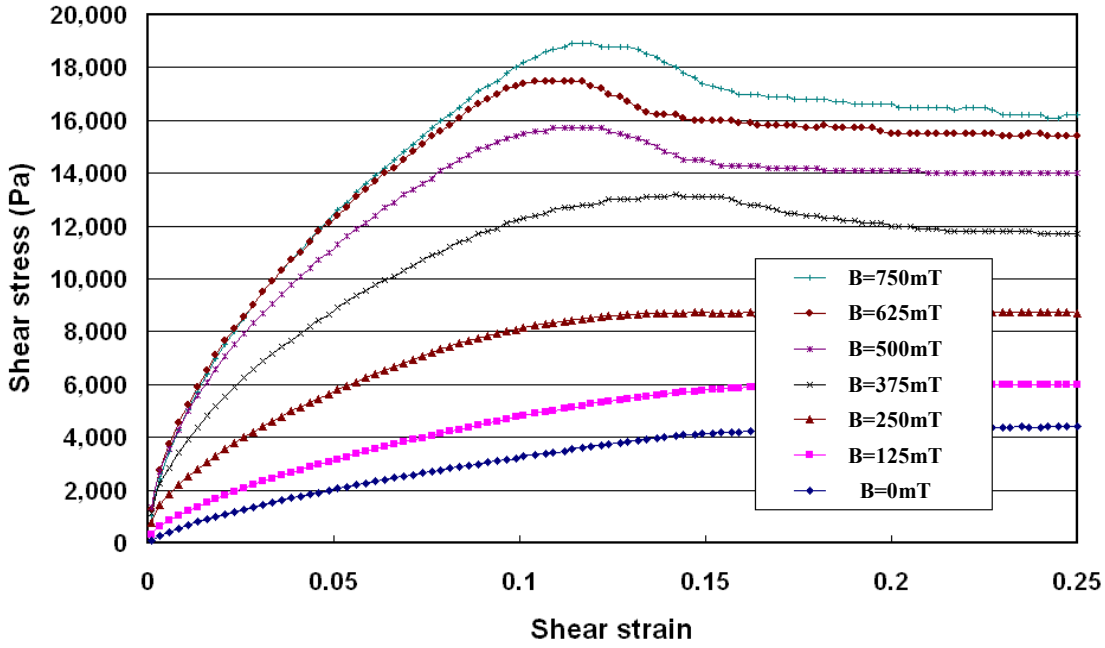

Figure 3.3 Strain-stress curve of sample in different magnetic fields

3.2.3.2 Dynamic performances

A. The effect of a magnetic field

A typical relationship of shear stress versus shear strain under various strength magnetic fields of MR elastomers is shown from Figure 3.4. The results show that such materials have controllable mechanical properties. An increase in the stress-strain loop area with the magnetic field demonstrates that the damping capacity of the MR elastomers is a function of the applied magnetic field. When the strain amplitudes are 1% and 5% with a 1Hz frequency input the experimental results also show the same characteristics. These two figures are shown in Appendix A. These experimental results demonstrate that not only are the areas dependent on the magnetic fields, the shape of the ellipse loops are also different. In particular, the slope of the main axis of the elliptical loops varies with the magnetic field. This is totally different from MR fluids [45] where the slope of the ellipse loops represents elastic properties.

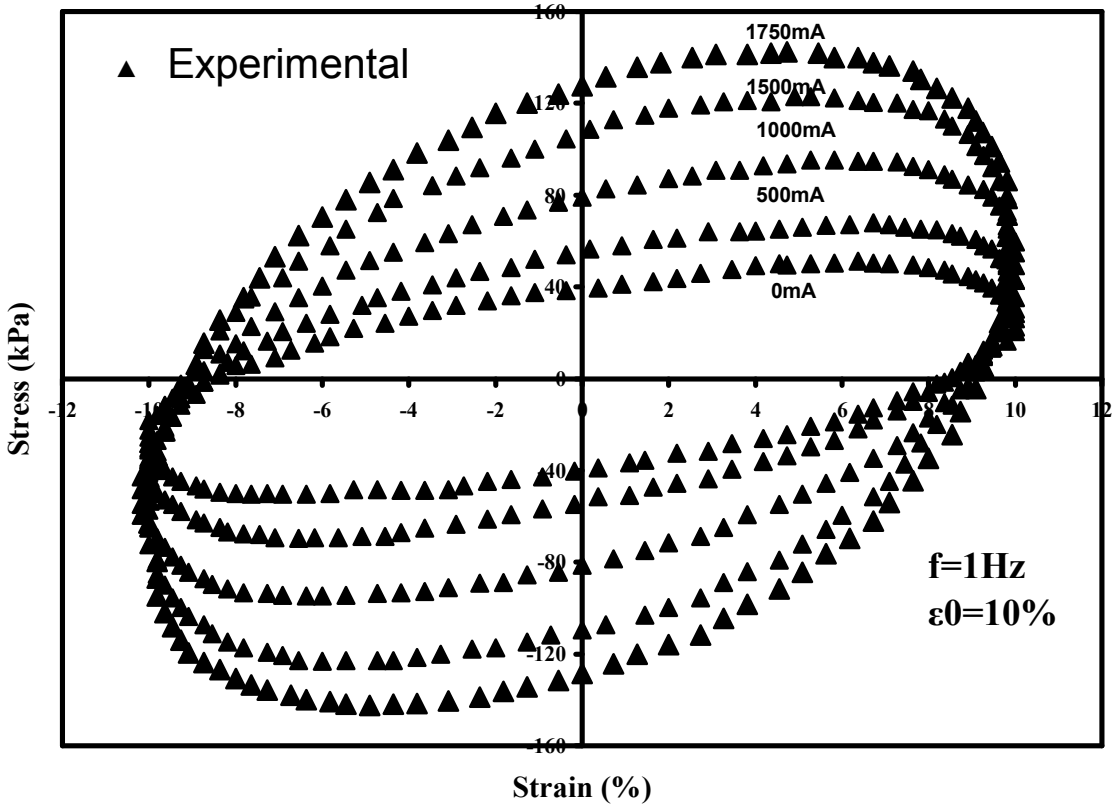

Figure 3.4 Stress-Strain relationship of 10% amplitude input

B. The effect of strain amplitude

Figure 3.5 shows the relationships between shear strain and shear stress for 1%, 5%, 10% and 50% inputs of strain amplitude when a 1000mA current is applied to the MRE sample. Here the maximum stress tends to increase and the slope of the main axis shows the positive value when strain amplitude is below 10%. However, when strain amplitude is 50% the slope of the main axis changes from positive to negative, which could be due to the effect of sliding. When the strain is above 10%, the modulus reaches the saturation (maximum value) and increases steadily.

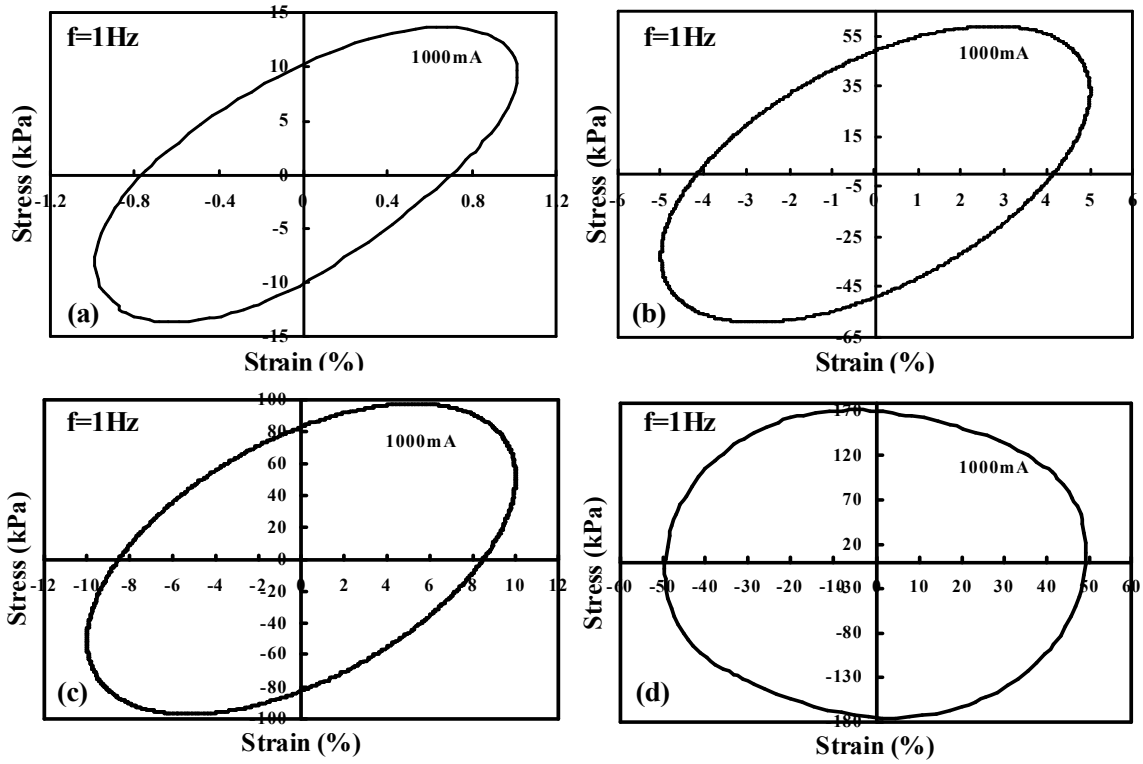

Figure 3.5 Stress-Strain relationships for different strain amplitudes in 1000mA (a) 1% Strain amplitude (b) 5% Strain amplitude (c) 10% Strain amplitude (d) 50% Strain amplitude

C. Effect of frequencies

Figure 3.6 shows the effects of shear strain frequency inputs on MRE performance. The slope of the main axis of the elliptical loops increased with an increasing shear strain frequency inputs while the maximum stress amplitudes of different strain frequency inputs changed steadily. The shear strain frequency inputs mainly influences the slope of main axis of the ellipses. When the strain frequency inputs change from 1Hz to 5Hz, the slope of the main axis increases steadily. When the strain frequency inputs change from 5Hz to 10Hz, the slope of the main axis can increase slightly.

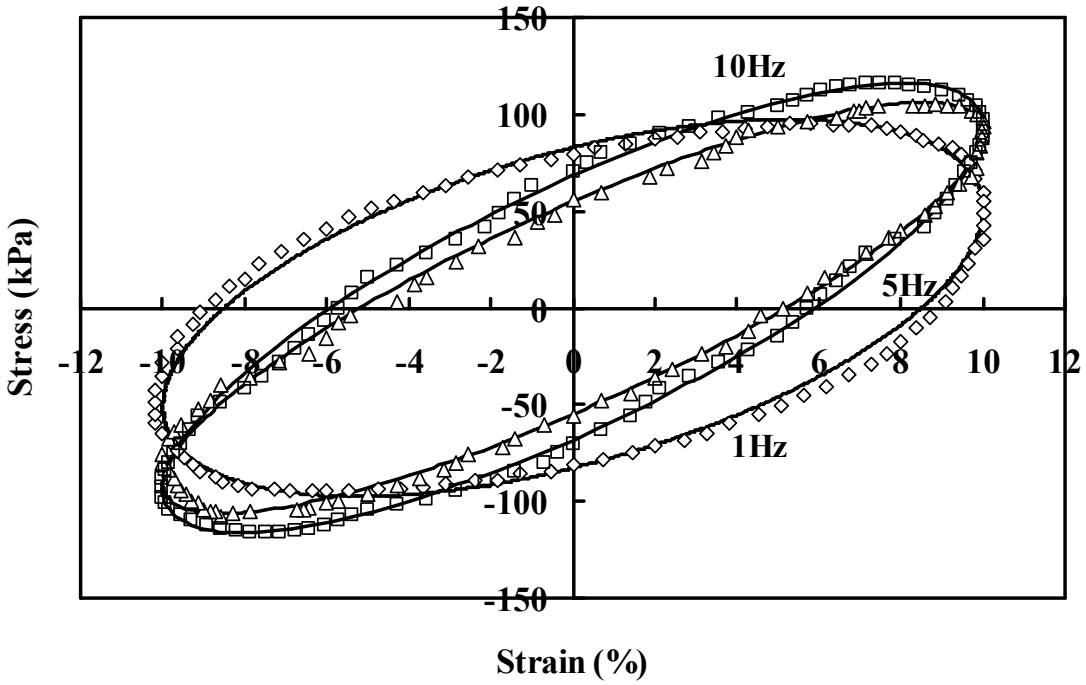

Figure 3.6 Stress-Strain relationships for different frequency inputs in 1000mA

3.3 MODELLING MR ELASTOMERS

The effects of magnetic field, amplitude and frequency on the properties of MRE were discussed in the section above. Obviously, except for very large strain amplitudes (50%), the stress-strain plots are excellent elliptical loops which indicate that MREs behave with linear viscoelastic properties. A linear Kelvin-Voigt model was used to model the viscoelastic properties of MR fluid [46]. MREs, unlike MR fluid, also depend on a magnetic field for the modulus on stiffness. To this end we proposed a four-parameter viscoelastic model to describe the properties of MRE because it is an extension of the Kelvin-Voigt model. A spring is included in the model to represent change in the field dependence modulus. Figure 3.7 shows the plot of the four parameter viscoelastic model for MR elastomers.

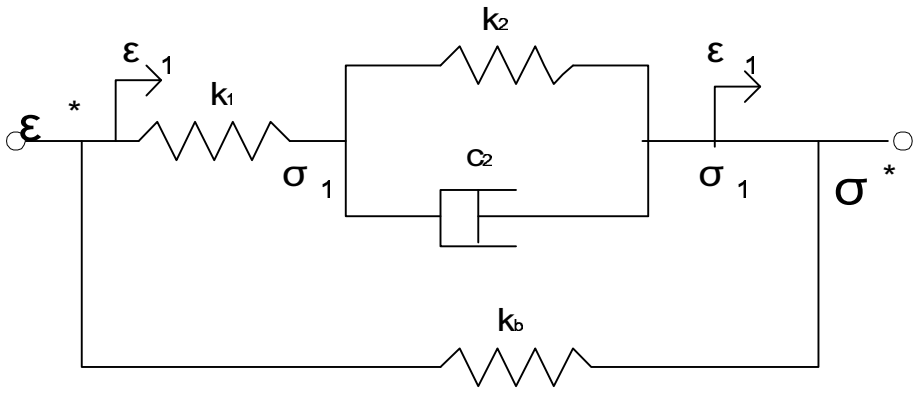

Figure 3.7: Four-parameter viscoelastic model for MR elastomers

In this model, k_1, k_2 and c_2 are for a standard solid and k_b is placed from on a viscoelastic theory so the relationship of shear stress and shear strain can be represented as:

$$\sigma^* = k_b\varepsilon^* + \sigma_1 \tag{3.2}$$

$$\sigma_1 = k_1\varepsilon_1 \tag{3.3}$$

We may use a complex stress-strain equation for representation

$$\sigma_1 = k_2(\varepsilon^* - \varepsilon_1) + c_2(\dot{\varepsilon}^* - \dot{\varepsilon}_1) \tag{3.4}$$

Where k_1, k_2 and c_2 are the three parameters in the Kelvin-Voigt model respectively, k_b is the stiffness of spring which is in a parallel connection with the Kelvin-Voigt model, and ε^* and σ^* are represented as shear strain inputs and shear stress outputs respectively. ε_1 and σ_1 are the shear strain and shear stress for the internal node.

It was suggested that the equations be simplified so from equation (3.2) we can obtain the following equations (3.5) and (3.6):

$$\sigma_1 = \sigma^* - k_b\varepsilon^* \tag{3.5}$$

$$\dot{\sigma}_1 = \dot{\sigma}^* - k_b\dot{\varepsilon}^* \tag{3.6}$$

From equation (3.3) we can obtain following equations (3.7) and (3.8):

$$\varepsilon_1 = \sigma_1 / k_1 \tag{3.7}$$

$$\dot{\varepsilon}_1 = \dot{\sigma}_1 / k_1 \tag{3.8}$$

By substituting equations (3.5), (3.6) into (3.4), the shear strain and shear stress for the internal node can be eliminated

$$\sigma_1 + k_2\sigma_1 / k_1 + c_2\dot{\sigma}_1 / k_1 = k_2\varepsilon^* + c_2\dot{\varepsilon}^* \tag{3.9}$$

As such, all the shear strain and shear stress for the internal node can be eliminated by substituting equations (3.5) and (3.6) into (3.9)

$$(1 + k_2 / k_1)(\sigma^* - k_b\varepsilon^*) + c_2(\dot{\sigma}^* - k_b\dot{\varepsilon}^*) / k_1 = k_2\varepsilon^* + c_2\dot{\varepsilon}^* \tag{3.10}$$

Similarly, equation (3.11) can be derived by an arrangement of equation (3.10)

$$(1 + k_2 / k_1)\sigma^* + c_2\dot{\sigma}^* / k_1 = (k_b + k_b k_2 / k_1 + k_2)\varepsilon^* + c_2(1 + k_b / k_1)\dot{\varepsilon}^* \tag{3.11}$$

Because the materials behave with linear viscoelastic properties the stress-strain relationship is given by

$$\sigma^* = G^*\varepsilon^* = (G_1 + iG_2)\varepsilon^* \tag{3.12}$$

$$\dot{\sigma}^* = G^*\dot{\varepsilon}^* \tag{3.13}$$

Hence, by substituting equations (3.12) and (3.13) into (3.11), the items related to σ^* can be eliminated. After arrangement, equation (3.11) can be expressed as

$$[(1 + k_2 / k_1)G^* - k_b - k_b k_2 / k_1 - k_2]\varepsilon^* = (c_2 + c_2 k_b / k_1 - c_2 G^* / k_1)\dot{\varepsilon}^* \tag{3.14}$$

Suppose the input strain ε^* is harmonic, which is given by

$$\varepsilon^* = \varepsilon_0 e^{i\omega t} \tag{3.15}$$

$$\dot{\varepsilon}^* = i\omega\varepsilon_0 e^{i\omega t} \tag{3.16}$$

Where ω and ε_0 are angle frequency and amplitude of the strain, respectively. By substituting equations (3.15) and (3.16) into (3.14), the complex modulus G^* can be expressed as

$$G^* = \frac{(k_b + k_b k_2 / k_1 + k_2) + (c_2\omega + c_2\omega k_b / k_1)i}{(1 + k_2 / k_1) + c_2\omega i / k_1} \tag{3.17}$$

Comparing equation (3.12) and (3.17), the storage and loss modulus of MRE are given

by equation (3.18) and (3.19), respectively

$$G_1 = \frac{(k_1k_b + k_2k_b + k_1k_2)[(k_1+k_2)^2 + c_2^2\omega^2] + c_2^2\omega^2k_1^2}{(k_1+k_2)[(k_1+k_2)^2 + c_2^2\omega^2]} \tag{3.18}$$

$$G_2 = \frac{c_2\omega k_1^2}{[(k_1+k_2)^2 + c_2^2\omega^2]} \tag{3.19}$$

Suppose that the strain input ε is a harmonic input

$$\varepsilon(t) = \varepsilon_0 \sin(\omega t) \tag{3.20}$$

The steady-state response of the strain can be obtained as

$$\sigma(t) = \varepsilon_0\sqrt{G_1^2+G_2^2}\,\sin(\omega t + \phi) \tag{3.21}$$

where ϕ is the phase angle difference between the input and output, which can be calculated as $\phi = \tan^{-1}(G_2/G_1)$.

3.4 SYSTEM IDENTIFICATION

3.4.1 Parameter Identification

The proposed viscoelastic model includes four parameters, i.e. k_b, k_1, k_2, c_2. The model uses the shear strain as an input, calculates the modulus G_1 and G_2 needed for the model, and then gives the shear stress, given by the equation (3.21). The four parameters are estimated on the base of the least squares method to minimise the error between the model-predicted stress of *Sm* and the experimental result of *Se*. The error in the model is represented by the objective function *J* given by

$$J = \sum_{i=1}^{N} (Sm_i - Se_i)^2 \tag{3.22}$$

where *N* is the experimental number of one loop. *Sm* is the shear stress value as predicted by equation (3.22). This optimisation was done with the MATLAB optimisation function.

Different groups of four parameters can be identified for each experimental case. Table

3.1 shows these four parameters k_b, k_1, k_2, c_2 for different shear strain input and current input.

Table 3.1 Identified parameters

I (mA)	k_b (kPa)	k_1 (kPa)	k_2 (kPa)	c_2 (kPa s)
0	1.8809	39.164	0.3222	0.3905
500	2.5703	40.4525	0.6477	0.8716
1000	3.657	46.7411	1.0463	1.487
1500	4.293	56.9859	1.533	2.0786
1750	5.0697	63.642	1.9357	2.8359

(a) 1% Strain amplitude.

I (mA)	k_b (kPa)	k_1 (kPa)	k_2 (kPa)	c_2 (kPa s)
0	3.3692	216.3603	0.385	0.7124
500	3.7867	250.1231	0.6002	0.9852
1000	5.1198	282.2121	1.2942	1.5042
1500	5.9124	332.3151	2.577	2.1967
1750	6.861	393.6399	4.2381	3.5514

(b) 5% Strain amplitude.

I (mA)	k_b (kPa)	k_1 (kPa)	k_2 (kPa)	c_2 (kPa s)
0	3.1211	514.3752	1.6998	0.9632
500	3.9307	557.1895	1.9307	1.3598
1000	4.604	564.2137	2.406	1.7294
1500	5.9847	578.1652	2.9161	2.4605
1750	8.11	621.3341	3.919	4.1876

(c) 10% Strain amplitude.

From table 3.1 we found that the four parameters k_b, k_1, k_2, c_2 increase steadily with an

increase in current. Similarly, the four-parameter viscoelastic model can also be used to identify parameters for other cases such as the 5Hz and 10Hz frequency inputs. The strain amplitude input chosen for these two cases was 10%. Similar results were also identified and shown in table 3.2.

Table 3.2 Parameters identified for different frequencies with strain amplitude of 10%

I (mA)	k_b (kPa)	k_1 (kPa)	k_2 (kPa)	c_2 (kPa s)
0	2.2753	76.7461	2.4739	1.0848
500	2.7546	81.9691	2.855	1.5438
1000	3.4167	86.8016	3.2278	2.1046
1500	3.8057	98.2675	3.4332	2.7632
1750	4.5669	130.2478	3.5331	4.4902

(a) 5Hz frequency input.

I (mA)	k_b (kPa)	k_1 (kPa)	k_2 (kPa)	c_2 (kPa s)
0	2.1115	88.7629	3.2691	1.1681
500	2.5278	90.0953	3.4262	1.4958
1000	3.1703	95.2552	4.1533	2.1012
1500	3.8967	109.9699	4.5025	2.6982
1750	5.5704	122.4474	4.6711	4.2005

(b) 10Hz frequency input.

3.4.2 Comparison between experimental results and modelling predictions

Using the parameters estimated from the system identification process, the stress versus strain was reconstructed and compared with the experimental data curve. Figures 3.8 (a), (b), and (c) show the reconstructed stress versus strain loops compared with the practical experimental curves. It can be seen from the plots that the model can simulate the experimental data very well.

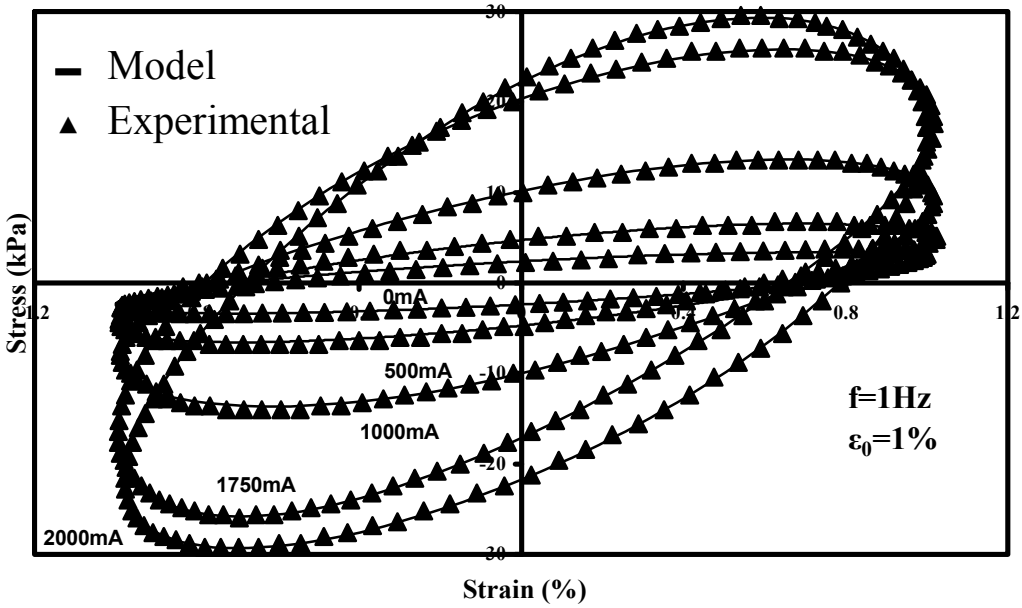
Model
Experimental
Stress (kPa)
Strain (%)
0mA
500mA
1000mA
1750mA
2000mA
f=1Hz
ε0=1%

(a)

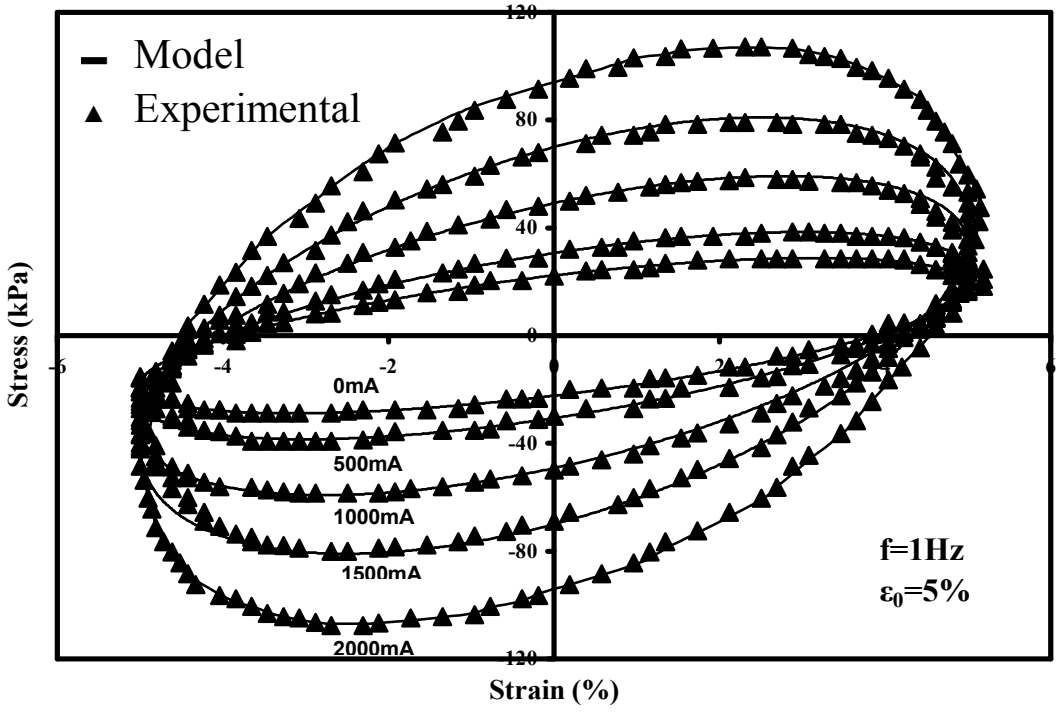
Model
Experimental
Stress (kPa)
Strain (%)
0mA
500mA
1000mA
1500mA
2000mA
f=1Hz
ε0=5%

(b)

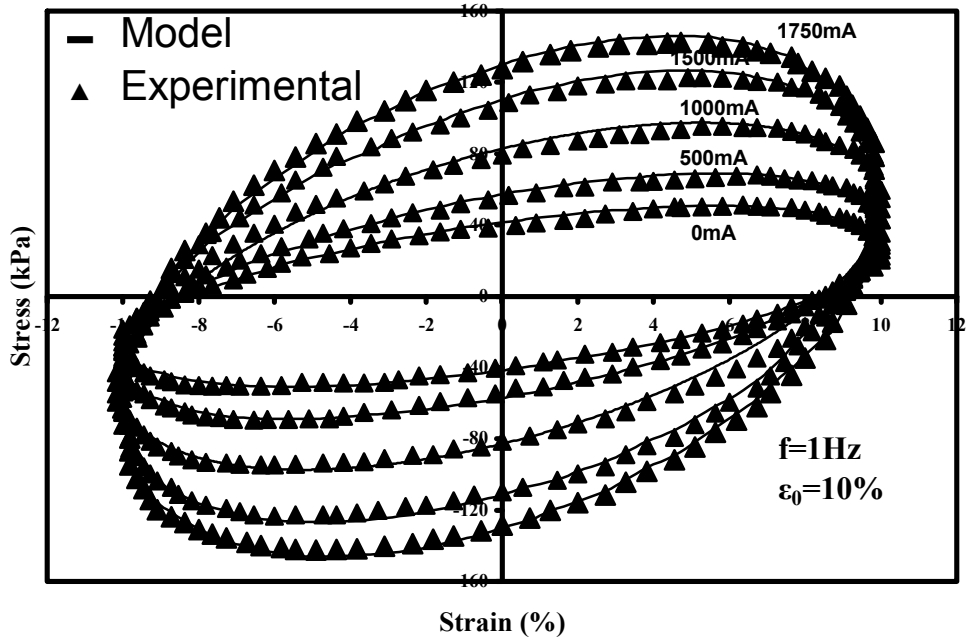

(c)

Figure 3.8: A comparison between experimental data with model-predicted results. (a) Amplitude input with 1%. (b) Amplitude input with 5%. (c) Amplitude input with 10%.

Similarly, the process for identifying the parameters can also be implemented with different frequency inputs. From figure 3.9 (a) and (b), it can be seen that the model can simulate the experimental data very well.

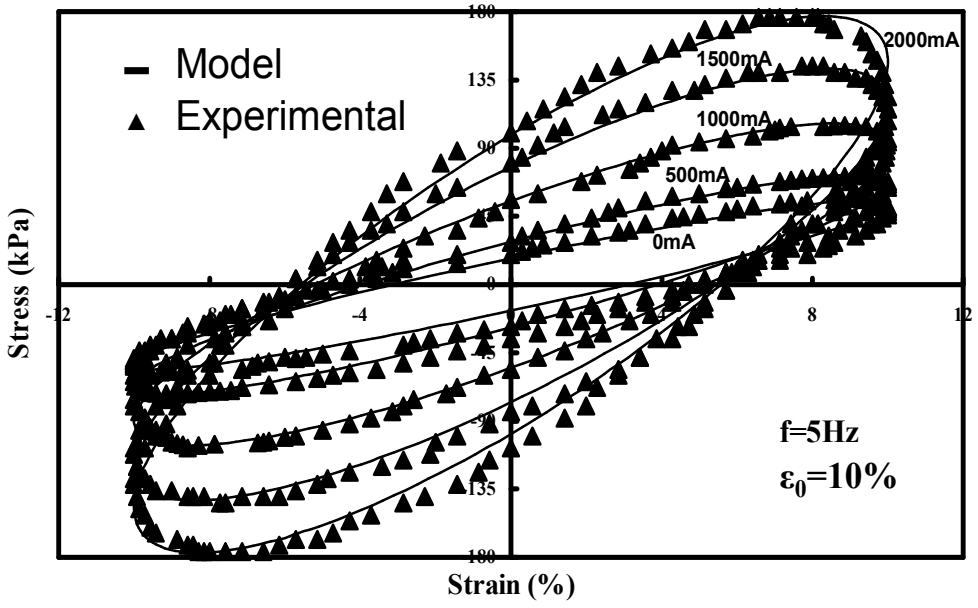

(a)

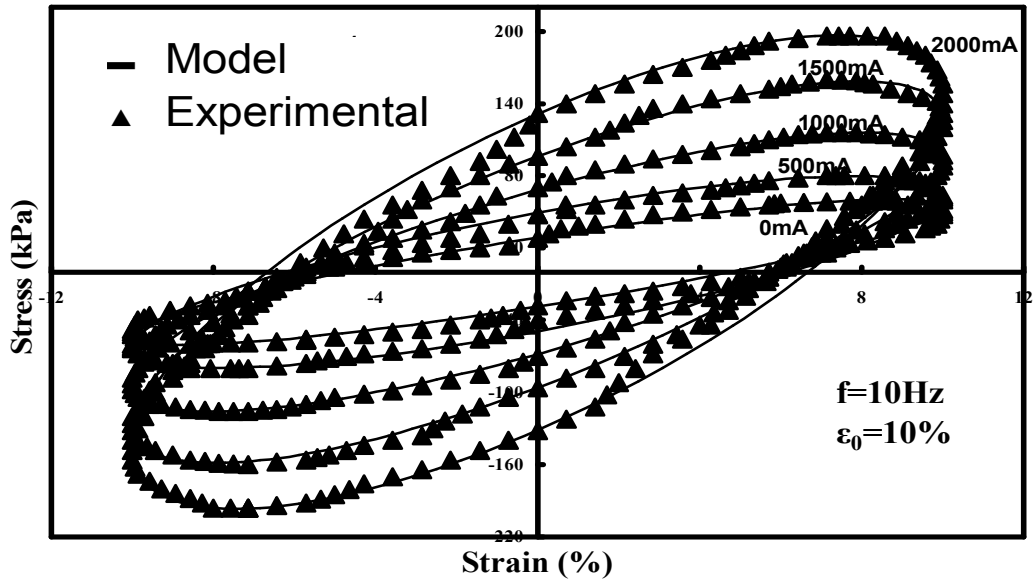

(b)

Figure 3.9: A comparison between experimental data with model-predicted results: (a) Strain frequency input with 5Hz. (b) Strain frequency input with 10Hz.

From table 3.1 listed in the previous section, we can obtain G_1 and G_2 based on equation (3.18) and (3.19). Figure 3.10 shows the relationship of the storage and loss modulus of MRE with current inputs. These figures show that when the current inputs increase from 0mA to 2000mA, the storage modulus (G_1) and loss modulus (G_2) both increase steadily. This trend exists in all strain amplitude inputs such as 1%, 5% and 10%. Moreover, the strain amplitude also influences the storage modulus (G_1) and loss modulus (G_2). When the strain amplitude changes from 1% to 10%, the storage modulus (G_1) and loss modulus (G_2) both increase slightly.

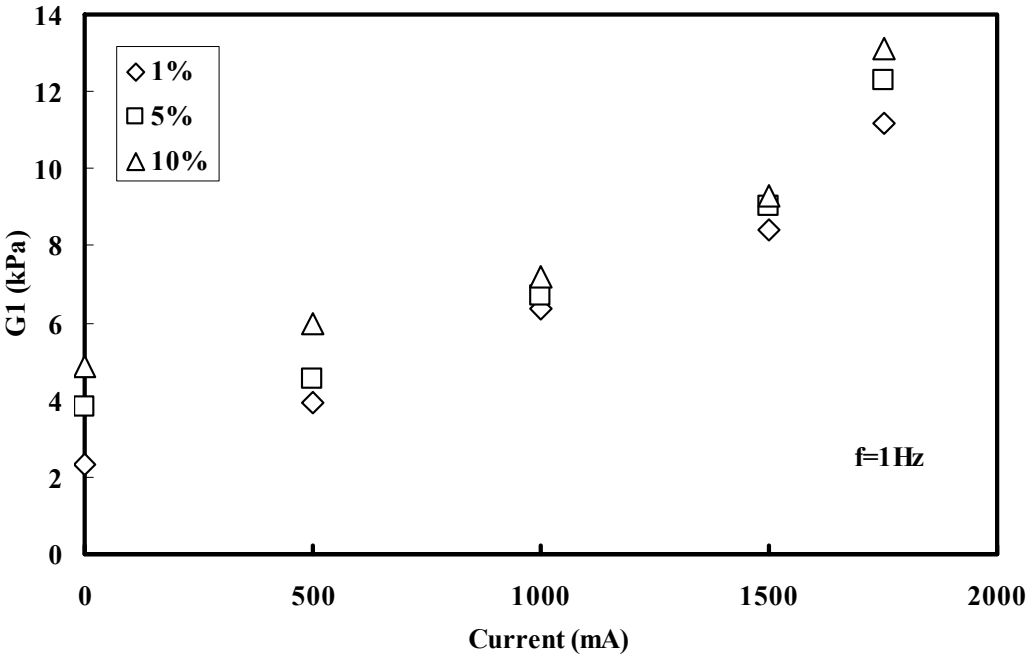

(a)

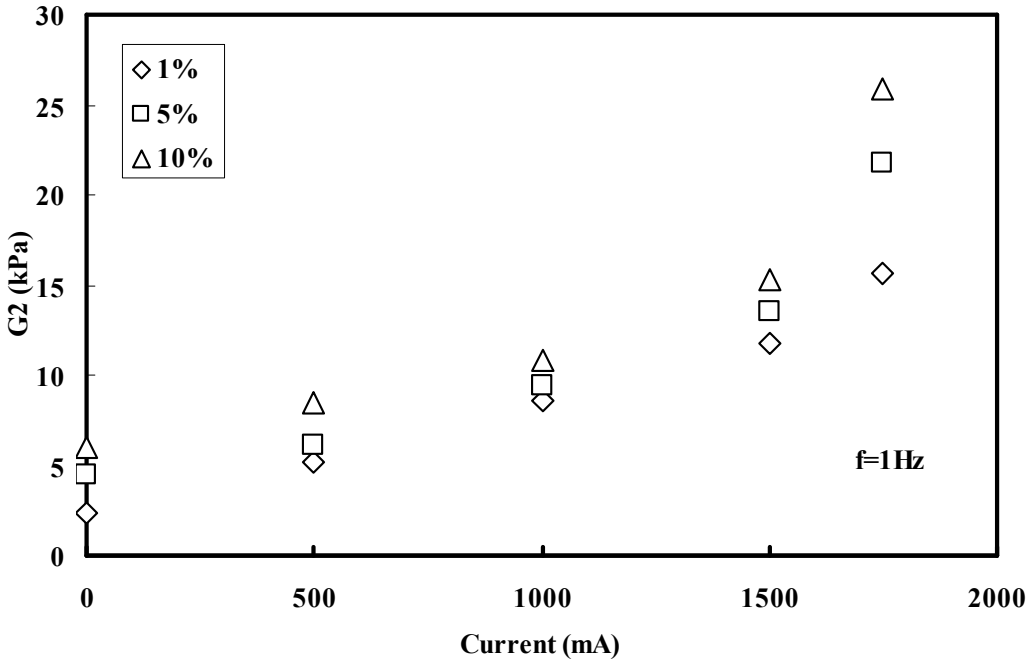

(b)

Figure 3.10: The relationship of current inputs with the storage and loss modulus: (a) Storage modulus (G_1). (b) Loss modulus (G_2).

On the other hand the effect of frequency on the storage modulus (G_1) and loss modulus (G_2) were shown in figure 3.11. We find that when an MRE sample was applied at the same amplitude of strain input, both the storage modulus (G_1) and loss modulus (G_2) increased steadily with increasing frequency inputs.

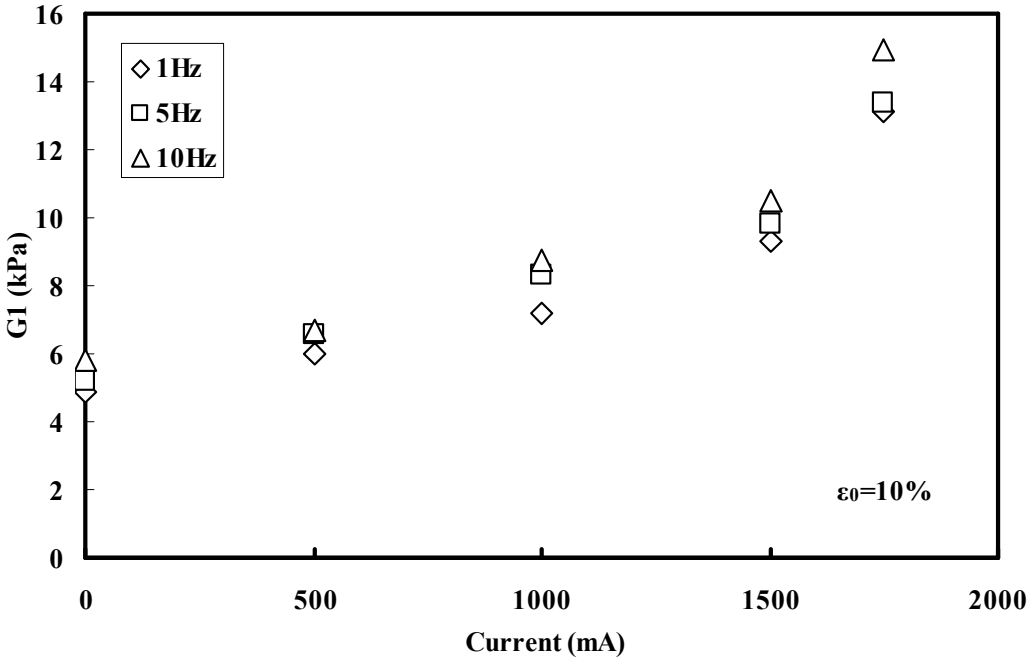

(a)

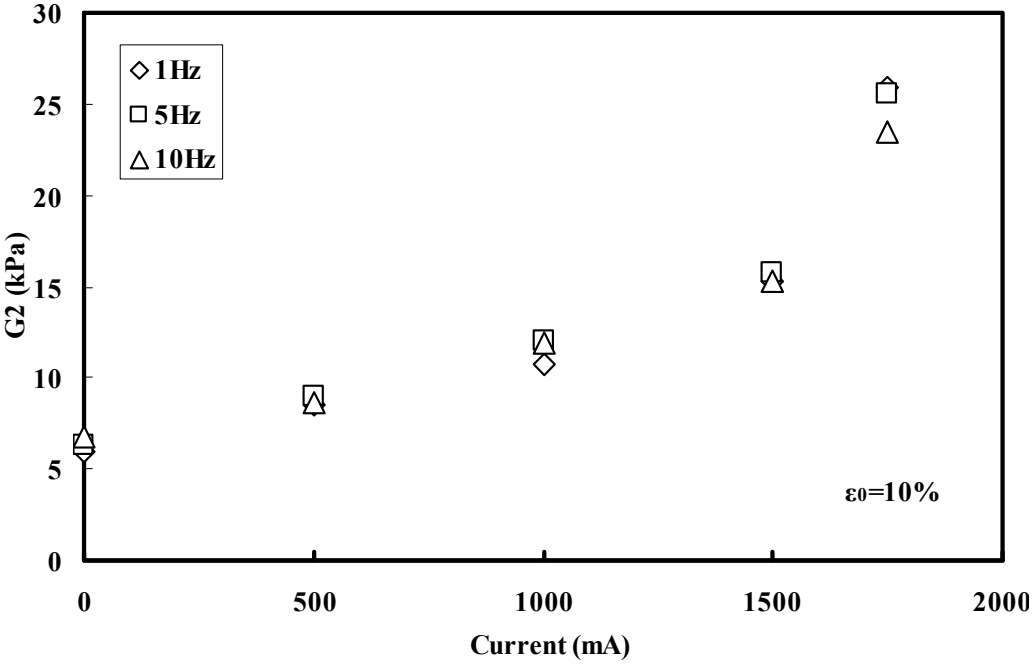

(b)

Figure 3.11: The relationship of frequency inputs with the storage and loss modulus: (a) Storage modulus (G_1). (b) Loss modulus (G_2).

3.5 CONCLUSION

In this chapter the steady state and dynamic state characteristics of MRE materials were studied experimentally. A four-parameter viscoelastic model was proposed to describe the performance of MR elastomers. When the parameters of the four-parameter viscoelastic model were identified and compared there was a tendency to increase with the current. The strain amplitude and frequency were changed for different cases and the results from the experiments and those predicted by the model matched very well except where the strain amplitude inputs were over 50%. Thus the four-parameter viscoelastic model can represent the MRE performance affectively.

CHAPTER 4

PHENOMENOLOGICAL MODEL OF MRE BEARINGS

4.1 INTRODUCTION

This chapter presents the experimental and modelling study of MRE bearings. A multi-layer MRE bearing was fabricated and its mechanical performance under harmonic loadings at various magnetic fields was tested experimentally. The damping and stiffness of MRE bearings were also discussed. A four-parameter phenomenological model was proposed to describe the performance of MRE bearings. The link between MRE materials and MRE based devices were discussed.

4.2 EXPERIMENTAL

4.2.1 Design and fabrication of MRE bearings

In this project a scaled MRE bearing was fabricated. The dimensions are given in figure 4.1. The bearing consists of 6 - 6mm thick MRE bearings. The bearing was ϕ90mm× 43mm and had a 45mm diameter gap in the centre. Each layer was separated by a 1mm thick steel plate. The MRE material was fabricated with the same weight ratio of components as discussed in Chapter 3. The core supports the bearing and an electro-magnetic coil was used to generate a magnetic field.

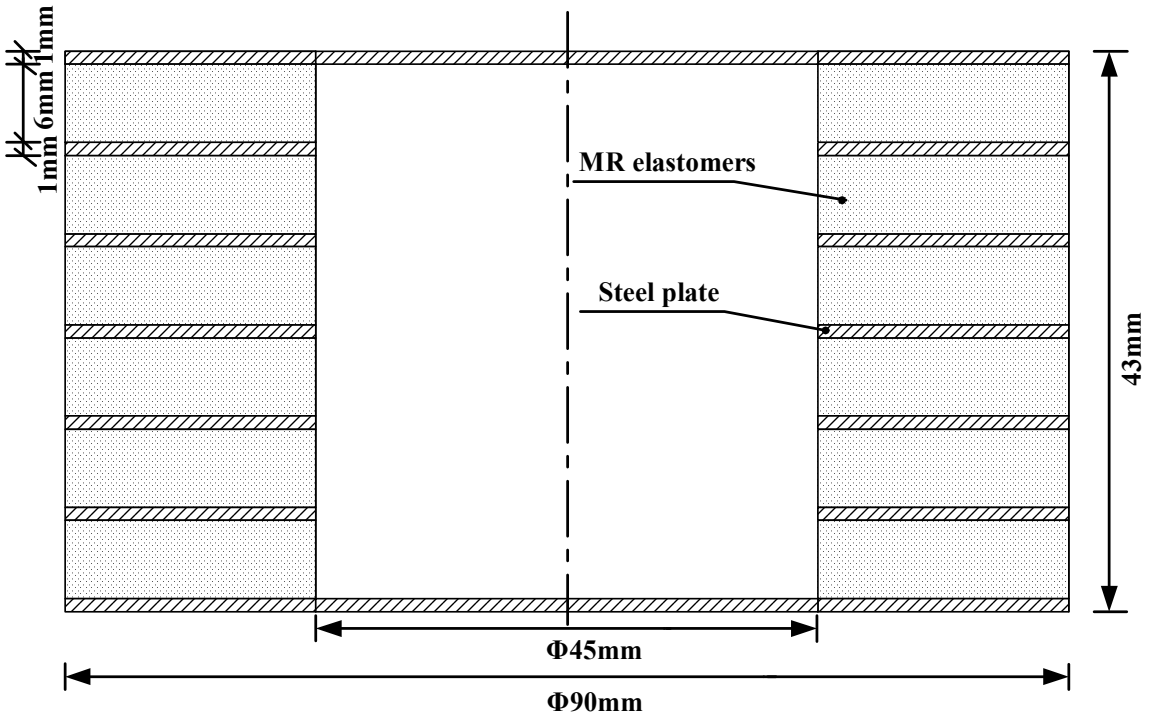

Figure 4.1: Schematic cross-section of the MR elastomers bearing

4.2.2 Experimental setup

The purpose of this experiment is to characterise the dynamic performance of the MRE device. Its equivalent stiffness and damping properties will be studied experimentally. A schematic of the experimental setup was shown in figure 4.2. In the experiment the MRE device was installed in an electro-magnet (S&T 139802) which can generate varying magnetic fields. A force sensor (CA-YD-106 53317) was placed on the MREs device to measure any changes in the force on it. A sensor (CA-YD-106 50798 & 50837) was used to measure displacement at different magnetic fields and an electro-magnetic shaker (SINOCERA JZK-5) was used to generate excitation to it. The electro-magnetic shaker was controlled by computer connected to a DAQ board (SCB-68). LABVIEW software was used to program the excitation interface and a Tesla-meter (IMADA HT201) to measure different magnetic flux. A photograph of this experimental setup was shown in figure 4.3.

In this study a harmonic loading was applied to the MRE bearing. The amplitude and frequency selected were 5mm and 1Hz, respectively. Five different magnetic fields, 0,

100, 200, 300 and 400mT were selected. The force and displacement responses were recorded.

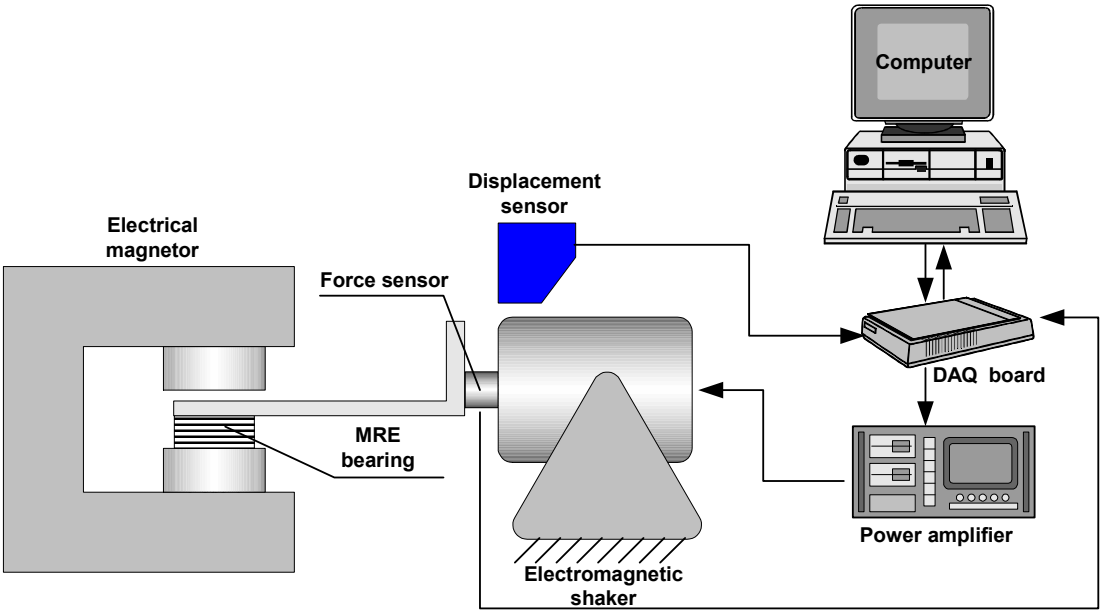

Figure 4.2 Schematic of experiment setup for MRE devices

Figure 4.3 Photograph of experiment setup for MRE devices

4.2.3 Results and discussion

The force-displacements from the experimental studies which were shown in figure 4.4 forms elliptical loops, similar to the study on MRE materials. As the magnetic field increases, so too does the area of the loops, which again proves that the damping capability of MRE increases steadily.

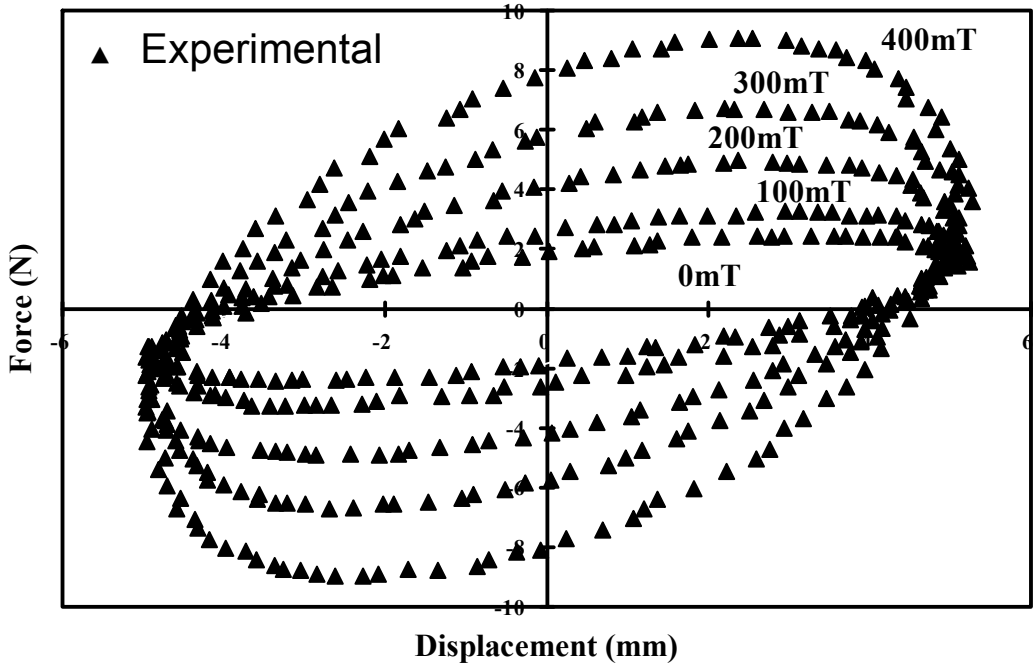

Figure 4.4 Relationship of displacement and force for the MRE devices

The non-linear force-deformation characteristic of the isolator can be represented by an equivalent linear model through effective elastic stiffness and viscous damping [47]. The linear force developed in the isolation system is expressed as equation (4.1)

$$f_b = k_{eff} x_b + c_{eff} \dot{x}_b \tag{4.1}$$

where k_{eff} is the effective stiffness; c_{eff} is the effective viscous damping constant.

Here, the equivalent linear elastic stiffness for each loop was calculated from a force-deformation curve obtained experimentally from the isolator and expressed mathematically as equation (4.2)

$$k_{eff} = \frac{F^{+} - F^{-}}{\Delta^{+} - \Delta^{-}} \tag{4.2}$$

where F^+ and F^- are the positive and negative forces at test displacements Δ^+ and Δ^-, respectively. Thus k_{eff} is the slope of the peak-to-peak values of the hysteresis loop.

The equivalent linear elastic stiffness for each cycle of loading is calculated from obtained force-deformation curve of MREs. The effective viscous damping coefficient of the isolator unit calculated for each cycle of loading is specified as

$$c_{eff} = \frac{E_{loop}}{\pi \omega_{eff} A^2} \tag{4.3}$$

where A is the test displacement amplitude, E_{loop} is the energy dissipation per cycle of loading and ω_{eff} is the angle frequency.

The relationships between the effective stiffness and effective viscous damping constant with the external magnetic flux density were identified from the experimental results, as shown in figure 4.5 (a) and (b). With an increase in the external magnetic flux density both the effective stiffness and viscous damping constant both tend to increase.

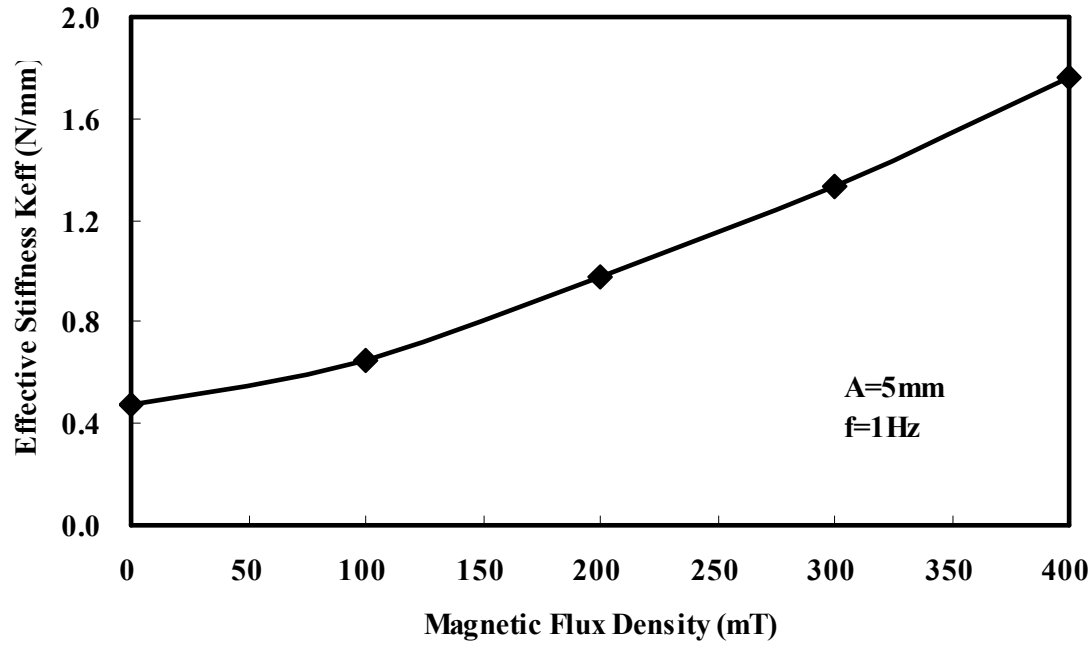

(a)

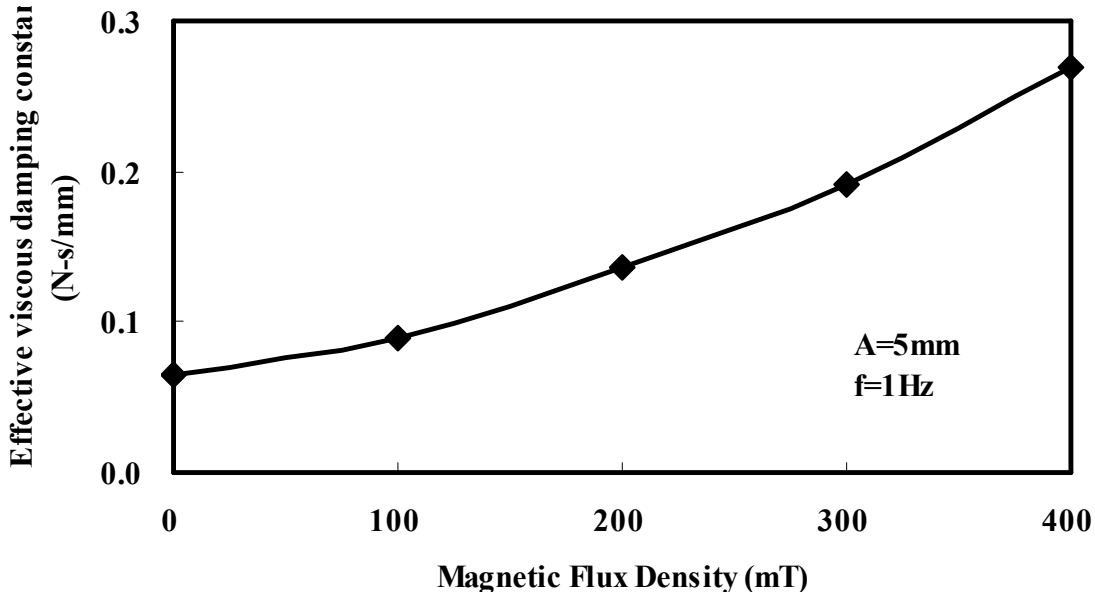

(b)

Figure 4.5 Relationship of effective stiffness and effective viscous damping constant with external magnetic flux density: (a) Effective stiffness; (b) Effective viscous damping constant.

For example, the effective stiffness changed from 0.47N/mm to 1.76N/mm when the external magnetic field changed from 0mT to 400mT. This approximate 4 fold increase in effective stiffness was generated. For the effective viscous damping constant it changed from 0.07 N-s/mm to 0.27 N-s/mm when the external magnetic field changed

from 0mT to 400mT. The effective viscous damping constant also increased about 4 times. This character was consistent in the study of MRE materials.

4.3 PHENOMENOLOGICAL MODEL

4.3.1 Modelling analysis

In figure 4.4 the loops of displacement and force not only increase the slope of the main axis, they also increase the size of ellipses. Similar to the modelling MRE material, a four-parameter viscoelastic phenomenological model was used to describe the character of an MRE device. Figure 4.6 shows the plot of the four parameter viscoelastic model for the MRE device.

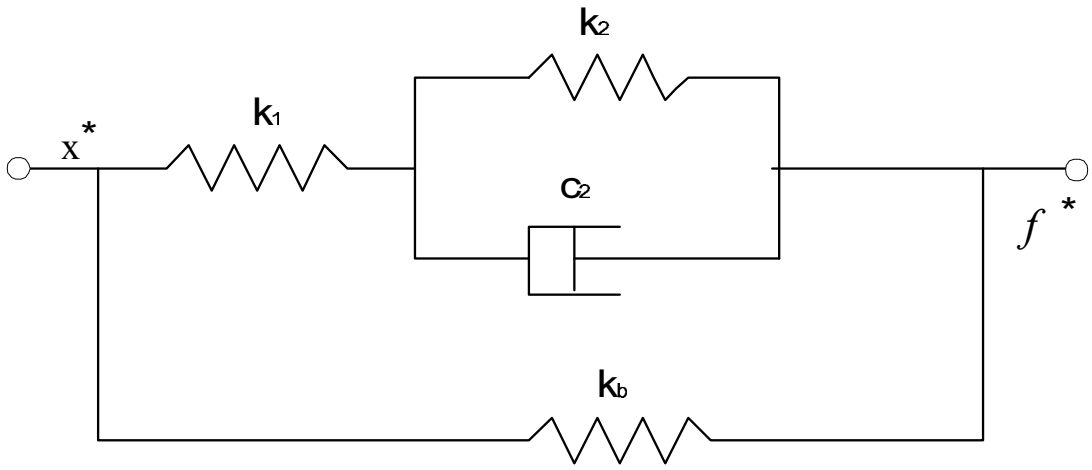

Figure 4.6: The four-parameter viscoelastic model for the MRE device

In this model k_1, k_2 and c_2 for a standard solid and k_b is placed viscoelastic theory. x^* and f^* are represented as inputs displacement and outputs force, respectively. The relationship of displacement and force can be represented as:

$$(1+k_2/k_1)f^*+c_2\dot{f}^*/k_1=(k_b+k_bk_2/k_1+k_2)x^*+c_2(1+k_b/k_1)\dot{x}^* \qquad (4.4)$$

Where k_1, k_2 and c_2 are the three parameters in the Kelvin-Voigt model respectively, k_b is the stiffness of spring which is connected parallel to the Kelvin-Voigt model.

Because the MRE device behaves with linear viscoelastic properties, the force-displacement relationship is given by

$$f^* = K^* x^* = (K_1 + iK_2)x^* \tag{4.5}$$

$$\dot{f}^* = K^* \dot{x}^* \tag{4.6}$$

Suppose the input displacement x^* is harmonic, which is given by

$$x^* = x_0 e^{i\omega t} \tag{4.7}$$

Where ω and x_0 are angle frequency and amplitude of the displacement, respectively. By substituting equations (4.5), (4.6) and (4.7) into (4.4), the real and imaginary parts of the complex stiffness K^* can be expressed as

$$K_1 = \frac{(k_1k_b + k_2k_b + k_1k_2)[(k_1 + k_2)^2 + c_2^2\omega^2] + c_2^2\omega^2k_1^2}{(k_1 + k_2)[(k_1 + k_2)^2 + c_2^2\omega^2]} \tag{4.8}$$

$$K_2 = \frac{c_2\omega k_1^2}{[(k_1 + k_2)^2 + c_2^2\omega^2]} \tag{4.9}$$

Also the displacement is supposed to be a harmonic input again so the steady-state response of the displacement can be obtained as

$$f(t) = x_0\sqrt{K_1^2 + K_2^2}\sin(\omega t + \phi) \tag{4.10}$$

where ϕ is the phase angle difference between the input and output, which can be calculated as $\phi = \tan^{-1}(K_2/K_1)$.

4.3.2 Parameter Identification

The four parameter viscoelastic model for the MRE device also includes four parameters, i.e. k_b, k_1, k_2, c_2. The model uses displacement as an input, calculates the modulus K_1 and K_2 needed for the model, and then gives the force, given by the equation (4.10). The four parameters are estimated using the least squares method to minimise any error between the model-predicted force of Fm and the experimental result of Fe. The error in the model is represented by the objective function J given by

$$J = \sum_{i=1}^{N} (Fm_i - Fe_i)^2 \tag{4.11}$$

where N is the experimental number of one loop. Fm is the force value as predicted by equation (4.11). This optimisation was also done with the MATLAB optimisation function.

We can now identify a group of four parameters for each ellipse loop from the experimental results. Table 4.1 shows the values of four parameters due to different magnetic flux density inputs.

Table 4.1 Four parameters at different magnetic flux density inputs

B (mT)	k_b (N/mm)	k_1 (N/mm)	k_2 (N/mm)	c_2 (N-s/mm)
0	0.40	53.04	0.045	0.075
100	0.61	59.97	0.048	0.114
200	0.80	63.00	0.050	0.159
300	1.08	65.38	0.053	0.229
400	1.27	67.85	0.056	0.283

Then the relationship of these four parameters depending on different magnetic flux density inputs can be shown in figure 4.7, respectively.

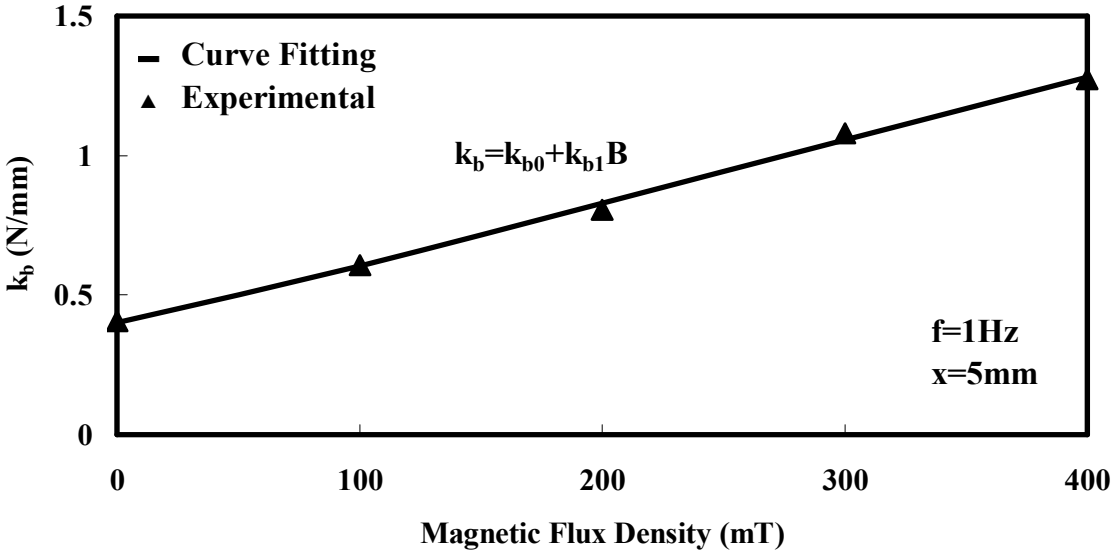
1.5
1
0.5
0
k_b (N/mm)
Curve Fitting
Experimental
$k_b=k_{b0}+k_{b1}B$
f=1Hz
x=5mm
0
100
200
300
400
Magnetic Flux Density (mT)

(a)

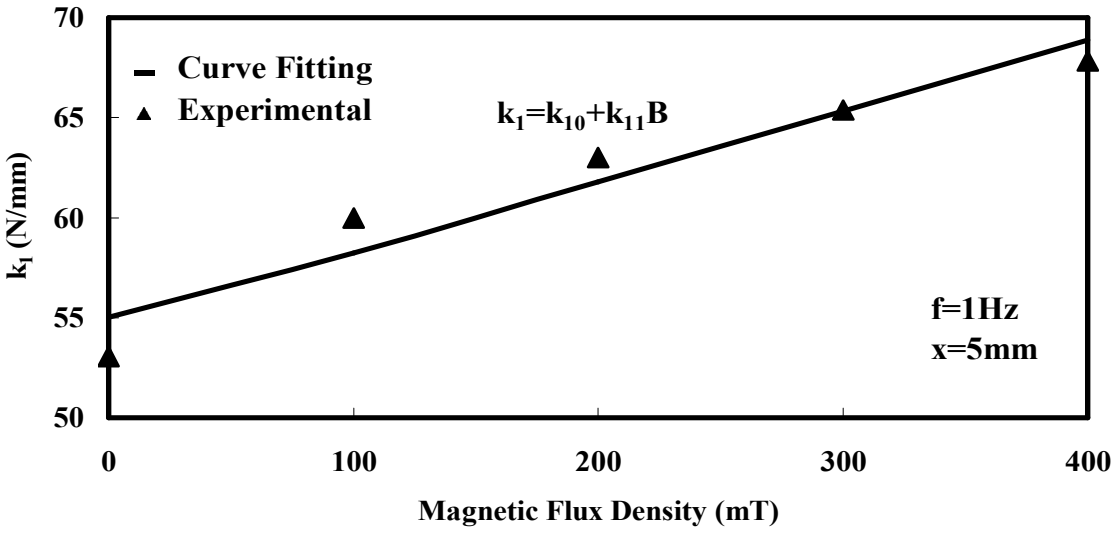
70
65
60
55
50
k_1 (N/mm)
Curve Fitting
Experimental
$k_1=k_{10}+k_{11}B$
f=1Hz
x=5mm
0
100
200
300
400
Magnetic Flux Density (mT)

(b)

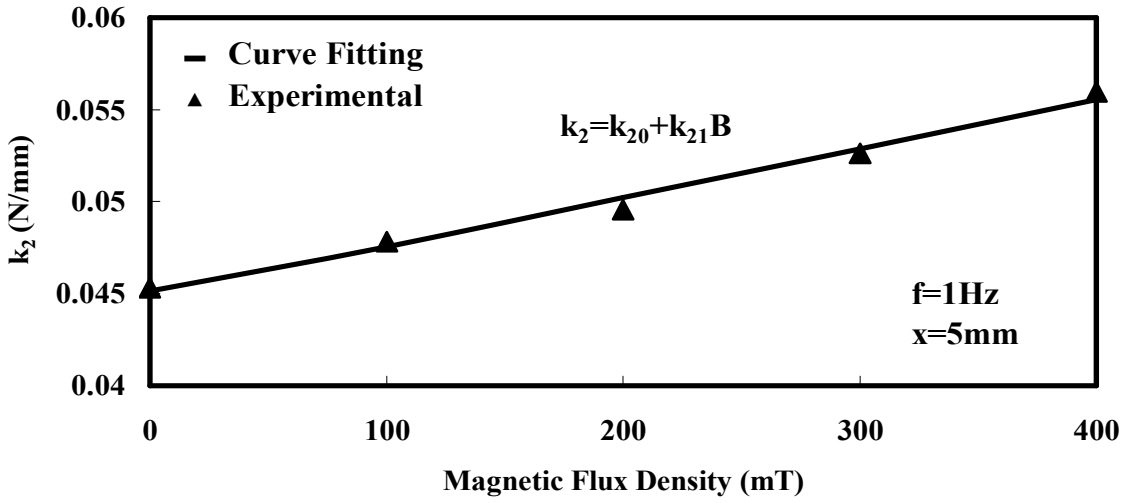

(c)

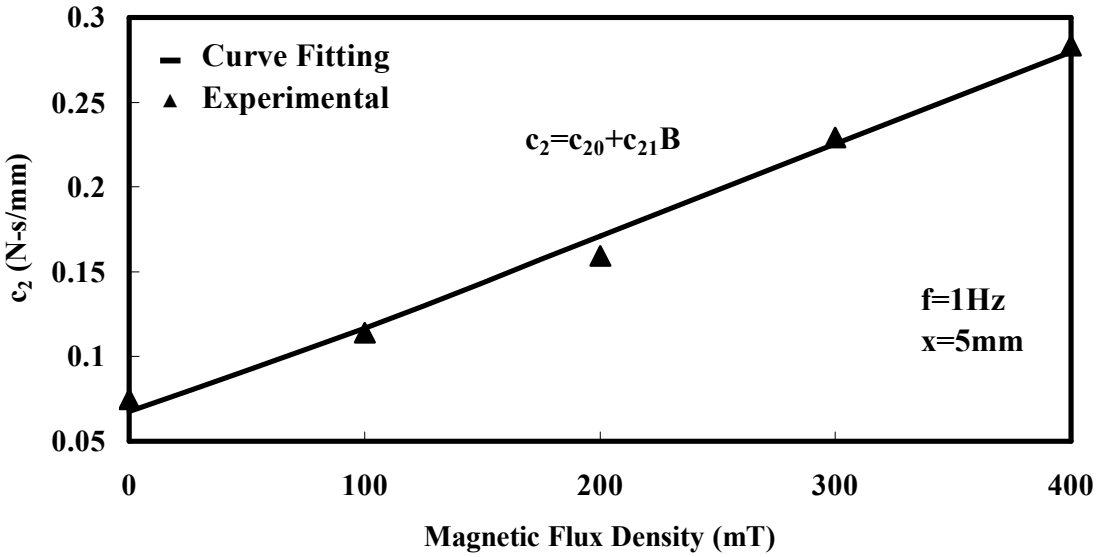

(d)

Figure 4.7: The relationship of four parameters with magnetic flux density inputs. (a) Experimental results and curve fitting results of k_b (b) Experimental results and curve fitting results of k_1 (c) Experimental results and curve fitting results of k_2 (d) Experimental results and curve fitting results of c_2

Figure 4.7 shows the four parameters of k_b, k_1, k_2 and c_2 identified at various magnetic flux levels. Also, the linear curve fitting was applied to all these four parameters. The four parameters for each magnetic flux density can be determined from the curve fitting and therefore the four parameters of the viscoelastic model for the MRE device can all

be expressed as linear function of the input magnetic flux density, as shown in figure 4.7. The relevant parameters for different functions are listed in Table 4.2 below. Similarly, expressions of the four parameters of viscoelastic model for the MRE device can be shown in equation 4.12

$$\begin{cases} k_b = k_{b0} + k_{b1}B \\ k_1 = k_{10} + k_{11}B \\ k_2 = k_{20} + k_{21}B \\ c_2 = c_{20} + c_{21}B \end{cases} \tag{4.12}$$

where B is the external magnetic flux density inputs. The relationship of magnetic flux density and current intensity can be shown as the table in Appendix C.

Table 4.2: Identification of the function parameters for the viscoelastic model

No.	Parameters of Function	Identification Value
1	k_{b0} (N/mm)	0.3926
2	k_{b1} (N/(mm mT))	0.0022
3	k_{10} (N/mm)	54.8437
4	k_{11} (N/(mm mT))	0.0350
5	k_{20} (N/mm)	0.0450
6	k_{21} (N/(mm mT))	2.61E-05
7	c_{20} (N-s/mm)	0.0658
8	c_{21} (N-s/(mm mT))	0.0005

4.3.3 A comparison between experimental and model

As with the MRE materials, a comparison between the results predicted by the model and the experimental results were conducted to verify the effectiveness of the four-parameter viscoelastic model. Figure 4.8 shows the comparison between the experimental results and results from the analytical model. These hysteresis loops effectively describe the behaviour of the MRE device. Based on the data collected, the four parameter viscoelastic model can also be used to analyse the characteristics of the MRE device. The loops of the four parameter viscoelastic model and the experimental

hysteresis loops match very well.

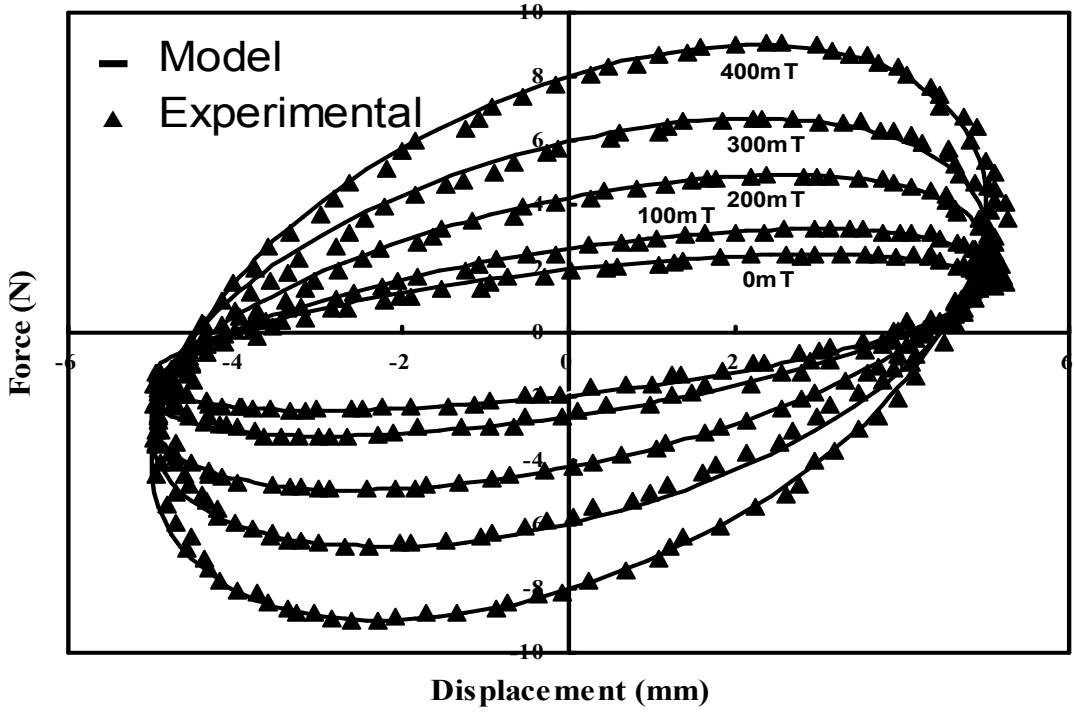

Figure 4.8 Comparison of experimental results and analytical model results

4.3.4 Discussion of the MRE device

The complex stiffness reflects the effective stiffness k_{eff} and equivalent viscosity damping coefficient c_{eff} of the structure [48]. From equation (4.5) the real part (K_1) of the MRE device is equal to the effective stiffness of the device, and the ratio of the imaginary part and real part (K_2/K_1) is related to the equivalent viscosity damping coefficient of structure. The relationship of this ratio and equivalent viscosity damping coefficient can be expressed as

$$C_{eff} = \eta \frac{k_{eff}}{\omega} \tag{4.13}$$

where k_{eff} is the effective stiffness of structure, ω is the frequency input of structure and η is damping loss factor for structure which is expressed as

$$\eta = \frac{K_2}{K_1} \tag{4.14}$$

With the four parameters now identified the real part (K_1) and the imaginary part (K_2) of four-parameter viscoelastic model can be illustrated with the magnetic flux density inputs. Figure 4.9 shows the relationship of the real part and the imaginary part with the magnetic flux density inputs.

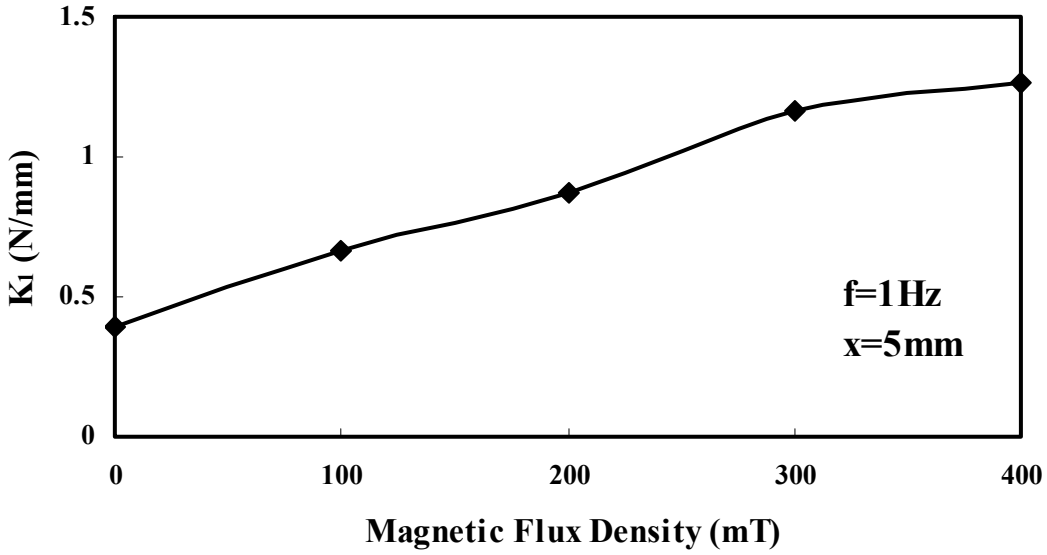

(a)

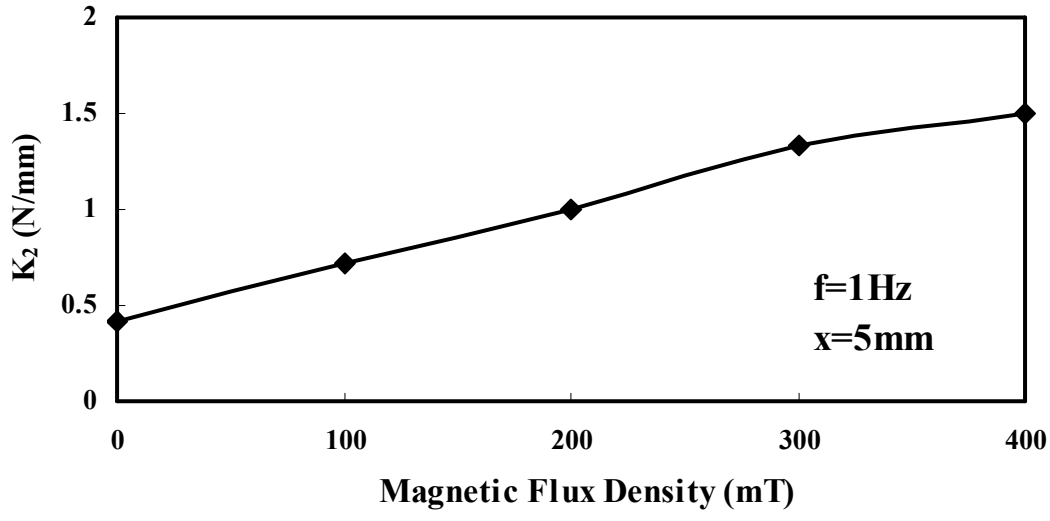

(b)

Figure 4.9: The relationship of the real part and the imaginary part with magnetic flux density inputs. (a) Real part K_1 (b) Imaginary part K_2

Thus, from figure 4.9 the real part of the MRE device increases from 0.38N/mm to

1.29N/mm with the magnetic flux density increasing from 0mA to 1750mA. This change was increased about 3.4 times of the initial stiffness. For the imaginary part of the MRE device the value increases from 0.40 N/mm to 1.49 N/mm with increasing magnetic flux density inputs. This is also about 3.7 times of the initial value, which means the equivalent viscosity damping coefficient c_{eff} of the MRE device increases about 4 times with increasing magnetic flux density inputs. This finding is similar to the results obtained from the effective stiffness and damping processes (section 4.2).

Obviously, the four-parameter viscoelastic model is an effective model for describing the characteristics of the MRE device even though it is a scaled model due to experimental limitations. Thus, although the change of effective stiffness and the equivalent viscosity damping coefficient is significant, the effective stiffness of the MRE device was too weak to be used on a building structure. In order to achieve the effects on a scaled building structure, a large MRE bearing will be constructed for future experiments.

4.4 CONCLUSION

In this chapter, the variable stiffness and variable damping coefficient of the MR device were presented based on the experimental and modelling development. The elliptical loops obtained by experiments on the MR device enabled the effective stiffness and the effective viscous damping coefficient to be identified with application of four-parameter viscoelastic model. By using curve fitting the four parameters for each magnetic flux density input were identified. The effectiveness of the four-parameter viscoelastic model was again verified by a comparison between the experimental and predicted results of the MRE device.

CHAPTER 5

SIMULATED EVALUATION OF AN MRE BEARING FOR STRUCTURAL CONTROL

5.1 INTRODUCTION

This chapter presents a simulated evaluation of an MRE bearing installed in a building model under external ground excitations. There are two kinds of ground excitation data used in this simulation. One is the El Centro-north-south component of the 1940 Imperial Valley, Calif. The other is the Northbridge-north-south component of the 1994 Northbridge Earthquake (magnitude 6.8) recorded at the Sylmar County Hospital parking lot in Sylmar, Calif. Three controllers, passive on, passive off and bang-bang control strategy, were used to compare the response of each storey with and without control.

5.2 THREE STOREY BUILDING MODEL INCORPORATING AN MRE BEARING

5.2.1 Model of multi-storied structures

Considering a general building structure with n-degree-of-freedom, as shown in figure 5.1, the building structure is modelled as a linear structure with a lumped mass-spring system. Suppose that the building structure is subjected to a seismic ground acceleration, which is a horizontal effect, expressed as $\ddot{x}_g(t)$.

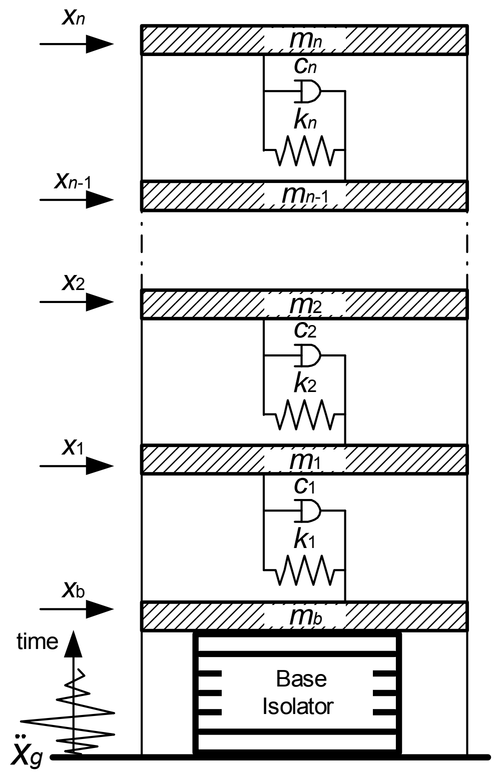

Figure 5.1 Idealised structural model

By considering the equilibrium of forces for each degree of freedom, the governing equations of motion for an n-degree-of-freedom structure can be obtained by the theory of system dynamics. It is assumed that the displacements (x_i), velocities ($\dot{x}_i$) and ground acceleration ($\ddot{x}_g(t)$) can be measured in real-time by sensors for each storey. Governing equations of motion for structure are derived as follows:

$$\begin{aligned} &m_b\ddot{x}_b + (c_b + c_1)\dot{x}_b - c_1\dot{x}_1 + (k_b + k_1)x_b - k_1x_1 + F_{Isolator} = -m_b\ddot{x}_g(t), \\ &m_1\ddot{x}_1 - c_1\dot{x}_b + (c_1 + c_2)\dot{x}_1 - c_2\dot{x}_2 - k_2x_b + (k_1 + k_2)x_1 - k_2x_2 = -m_1\ddot{x}_g(t), \\ &\qquad\qquad\qquad\qquad\qquad \ldots\ldots \\ &m_n\ddot{x}_n - c_n\dot{x}_{n-1} + c_n\dot{x}_n - k_nx_{n-1} + k_nx_n = -m_n\ddot{x}_g(t) \end{aligned} \tag{5.1}$$

where m_n, x_n are the mass, displacement of the n^{th} storey with respect to the ground. k_n, c_n are the elastic stiffness coefficient, viscous damping coefficient for the n^{th} storey. m_b, k_b, c_b are the mass of the MRE bearing, the original stiffness and damping coefficient of the MRE bearing without control current. $F_{isolator}$ is the control force developed in the MRE isolator which can be predicted by its mathematical model.

By using the matrix-vector notation the system of equations given above in discrete form can also be expressed as

$$\mathrm{M}\ddot{\mathrm{X}}(t) + \mathrm{K}\mathrm{X}(t) + \mathrm{C}\dot{\mathrm{X}}(t) = -\mathbf{m}\ddot{x}_g(t) + \mathbf{L}\cdot \mathrm{F}_{\mathrm{Isolator}} \tag{5.2}$$

where $\mathrm{X}(t)=[x_1,\ldots, x_n]^{\mathrm{T}}$ is the n-dimensional response vector denoting the displacements (here T indicates the transpose of vector and matrix). M, C and K are (n+1×n+1)-dimensional positive-definite matrices corresponding to the mass, viscous damping and the stiffness of the structure, respectively, $\mathbf{m}=-[\, m_{\mathrm{b}}, m_1,\ldots,m_n]^{\mathrm{T}}$. L is the MRE bearing location vector and $\mathbf{L}=[-1,0,0\ldots0]^{\mathrm{T}}$ for the case of base-isolated building. The matrices M, K, C are mass, stiffness, and damping matrices.

5.2.2 A three-storied benchmark model incorporating an MRE bearing

Dyke et al. [37, 49, 50, 51] studied the response of a three-storey benchmark building incorporating an MRF damper. In this study the same three-storey building model will be used to study an MRE bearing. The MR elastomers device was rigidly connected between the ground and the first floor of the structure. A schematic of the three storied building model incorporating an MRE bearing is shown in figure 5.2(a).

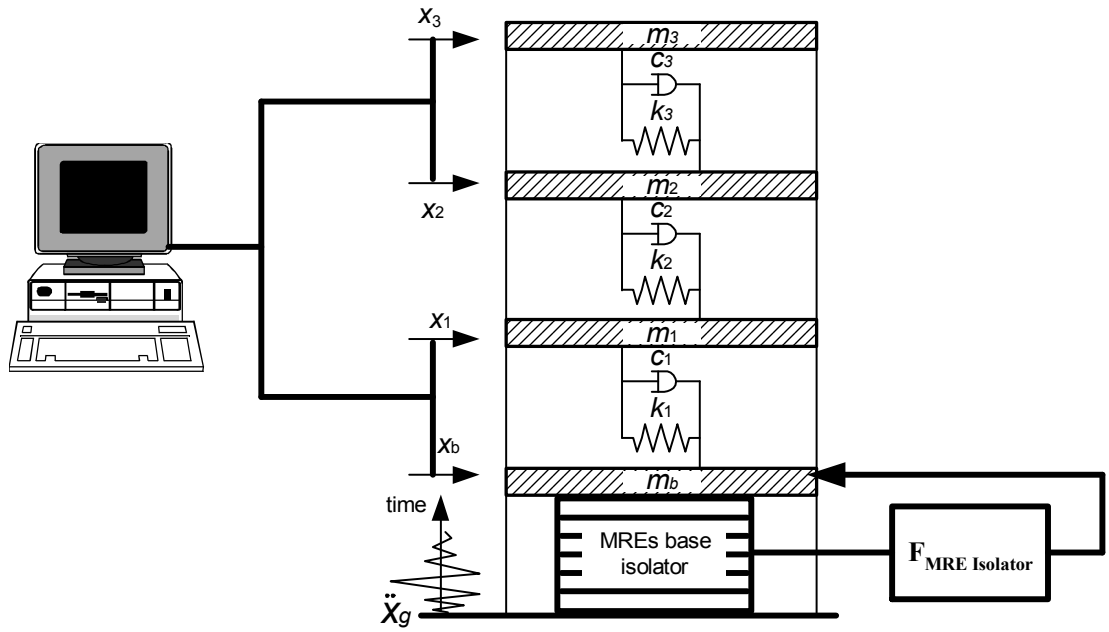

(a)

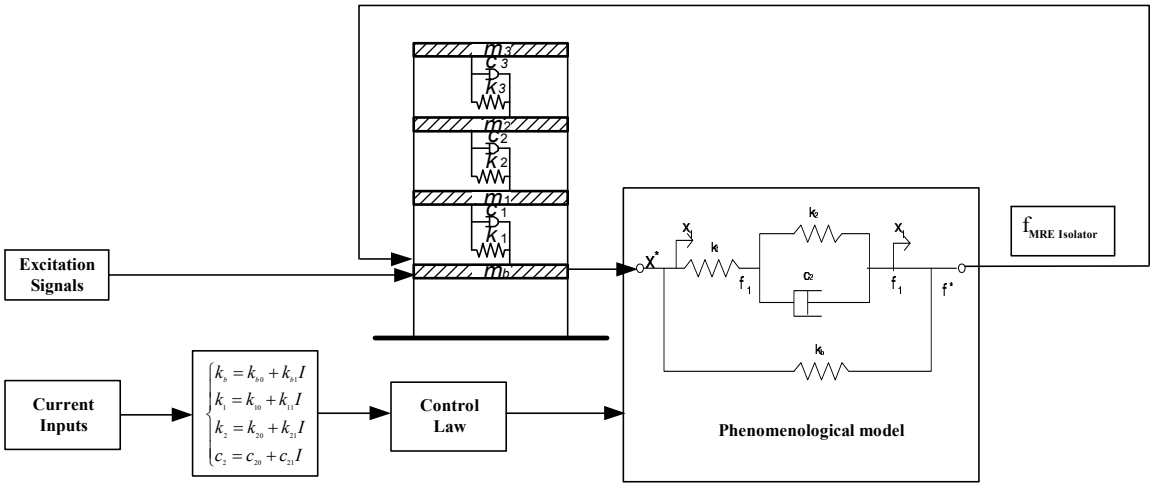

(b)

Figure 5.2 Schematic of a three storied building model incorporating an MRE bearing: (a) Schematic of MRE bearing using in a three storied building (b) Block diagram of simulation of MR elastomers.

As shown in figure 5.2(a), the control force of the MRE bearing was generated by the displacement of an MRE bearing installed on the base floor and the current applied on the MRE bearing. Currents applied to an MRE bearing can be directly changed by control law. With the displacement input and current input of the MRE bearing, the desired control force can be produced to structurally control the building. This control

force is directly applied to the ground floor of the building. A typical block diagram of the three-storey building model incorporating an MRE bearing is shown in figure 5.2(b). The simulation was implemented with MATLAB SIMULINK, as shown in Appendix D.

A diagram of the system simulation for the three-storey building is shown in figure 5.2(b). This model is a four-degree-of-freedom (4DOF) system because the ground floor is also included. All the parameters for a three-storey fixed-base building were used the same as the structural parameters [37, 49, 50] which were listed in Table 5.1.

Table 5.1. Structural model parameters [37, 49, 50]

Level	Floor mass (kg)	Stiffness coefficient (kN/m)	Damping coefficient (kNs/m)
Isolator	m_0=62.65	k_0=1.31	c_0=0.04
1st	m_1=62.65	k_1=104.81	c_1=0.39
2nd	m_2=62.65	k_2=88.19	c_2=0.27
3rd	m_3=62.65	k_3=85.19	c_3=0.25

With the parameters shown in table 5.1, the matrices M ($[m_b\ m_1\ m_2\ m_3]$), K ($[k_b\ k_1\ k_2\ k_3]$) and C ($[c_b\ c_1\ c_2\ c_3]$) in the equation (5.2) are listed below.

$$M = \begin{bmatrix} 62.65 & 0 & 0 & 0 \\ 0 & 62.65 & 0 & 0 \\ 0 & 0 & 62.65 & 0 \\ 0 & 0 & 0 & 62.65 \end{bmatrix} \text{ kg}$$

$$K = \begin{bmatrix} 106.12 & -104.81 & 0 & 0 \\ -104.81 & 193 & -88.19 & 0 \\ 0 & -88.19 & 173.38 & -85.19 \\ 0 & 0 & -85.19 & 85.19 \end{bmatrix} \text{ (kN/m)}$$

$$C = \begin{bmatrix} 0.44 & -0.39 & 0 & 0 \\ -0.39 & 0.66 & -0.27 & 0 \\ 0 & -0.27 & 0.52 & -0.25 \\ 0 & 0 & -0.25 & 0.25 \end{bmatrix} \text{ (kNs/m)}$$

5.3 SIMULINK IMPLEMENTATION AND ANALYSIS

The simulation work of a three-storey building structure and the external seismic excitations and control laws should be determined. In this study two different external excitations and three controllers for the three-storey building model incorporating an MRE bearing on the base floor were investigated.

5.3.1 External seismic excitations

To investigate the response of the building installed with an MR elastomers isolator, actual seismic data were applied in this simulated progress. Basically, the effective ground excitations are the data varied with time. These external excitations are always combined with the function of ground acceleration and time.

The isolated structures considered here were excited by a suite of ground motions that are intended to encompass both moderate and severe events. For moderate events the El Centro-north-south component of the 1940 Imperial Valley, Calif. earthquake (magnitude 7.1) recorded at Imperial Valley Irrigation District substation in El Centro, Calif., was simulated, and for severe events the Northbridge-north-south component of the 1994 Northbridge Earthquake (magnitude 6.8) recorded at the Sylmar County Hospital parking lot in Sylmar, Calif, was simulated.

These kinds of seismic record data are considered as a record of any kind of historical

earthquake, such as El Centro NS, Northbridge, and Kobe [52]. We selected a frequency period from 0s to 5s as the recorded period. The scaling factors for these two earthquakes were 120%. During this time the amplitude of ground excitation was the most significant part of the recorded period. Typical charts of the ground acceleration with time for El Centro NS and Northbridge are shown in Figure 5.3(a and b).

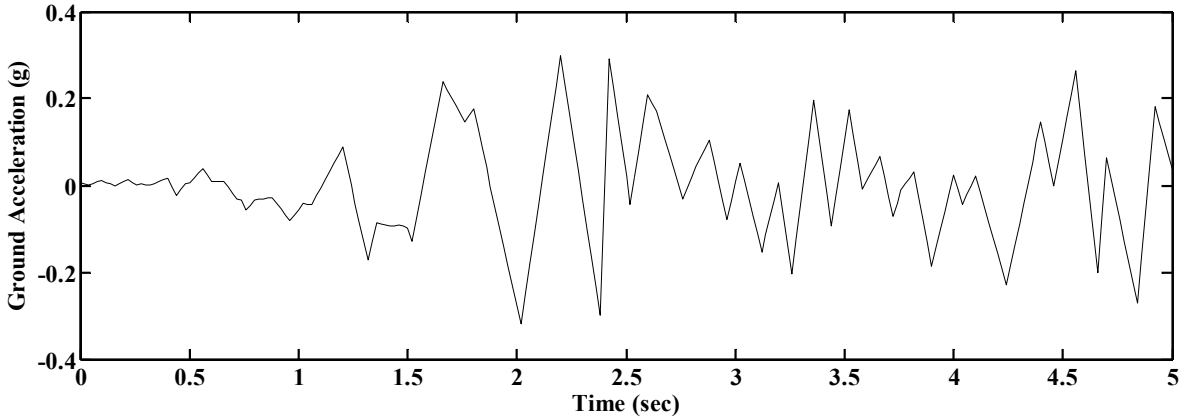

(a)

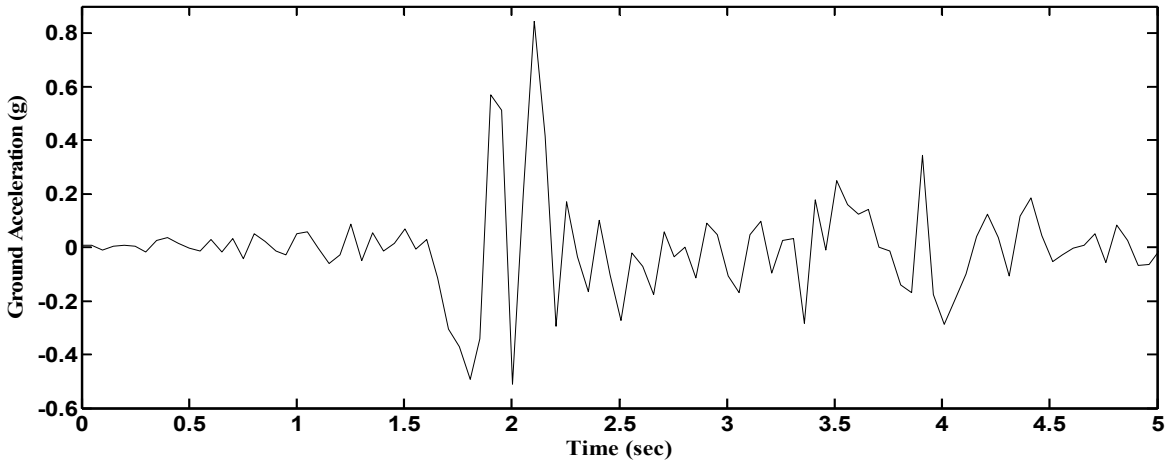

(b)

Figure 5.3 Time-scaled ground acceleration of a typical seismic excitation record. (a) Time-scaled NS component of the ground acceleration for El Centro earthquake. (b) Time-scaled NS component of the ground acceleration for Northbridge earthquake.

Additionally, the earthquakes are scaled by several magnitudes to better understand the effectiveness of the isolation strategies for different strength earthquakes. Moderate records are scaled from 0.5 to 2.0 times the historical record and severe ones from 0.5 to 1.5. Although magnifying the severe earthquakes might seem unnecessary, the results using 1.5 times the historical records are included to show the behaviour of different damping devices under extreme, but conceivable, events [53].

5.3.2 Three controllers

There are many conventional control logics used for applying MR materials but in this study we selected the passive off, passive on, and Bang-bang control methods to compare the effects of the MR elastomers device.

A: Passive off control logic

Two cases were considered in this study in which an MRE bearing was used in a passive mode. The first was designated as passive-off which means that the command current to the MR elastomers device was always held at 0 A. The MR elastomers device is unable to work out its MR effect because there is no current supplied on MR elastomers, it's just like it was switched off.

B: Passive on control logic

In the second passive case the current to the MR elastomers device was held at the maximum current level anytime and was denoted as passive-on. That means that the MR elastomers device was always charged to the maximum current inputs, as if it was switched on. This device can work out its MR effect without any intervals.

C: Bang-bang control logic

Kobori [54] described the seismic structural response process using the asymptotic motion equation (5.3). This control strategy based on non-resonance theory was used to control the isolator of MR fluid and MR elastomers [55].

$$\{\ddot{x}(t)\} = [E(t)](\{\mathrm{SF}(t)\} + \{\mathrm{RF}(t-\Delta t)\})$$

$\{\ddot{x}(t)\}$: Seismic structural response

$[E(t)] = f(M(t), C(t), K(t))$: Transfer function

$[\mathrm{SF}(t)] = f(M(t), \ddot{y}(t))$: Instantaneous seismic force

$$[RF(t-\Delta t)] = f(M(t), C(t), K(t), \ddot{x}(t-\Delta t), \dot{x}(t-\Delta t), x(t-\Delta t)]$$: Instantaneous resonant force (5.3)

The time-varying transfer function [*E*(t)] implies a dynamically controllable property in the seismic response control system. This isolator aims to reduce the current response by altering the stiffness in [*E*(*t*)], i.e. to avert resonance under any excitation. By altering its parameters the system can avoid the build-up of dominant periodic components of excitation, and therefore the input energy to the system and its response can be reduced. Kobori suggested a control algorithm to shift the building frequencies as far away as possible from the disturbance dominant frequencies. The main idea of the algorithm was that the stiffness of the system should be increased if the product of drift $x(t)$ and velocity $\dot{x}(t)$ is positive, i.e. if $x(t)$ and $\dot{x}(t)$ are in the same direction. If $x(t)$ and $\dot{x}(t)$ are opposite to each other then the stiffness should be decreased. For this simple control algorithm the long calculation of feed back signals can be avoided and real time control can be obtained easily. In this study the control was designed as

$$I(t) = \begin{cases} I_{\max} & x_b(t)\dot{x}_b(t) > 0 \\ I_{\min} & x_b(t)\dot{x}_b(t) \le 0 \end{cases} \quad (5.4)$$

where *I(t)* was the control signal. I_{max} was the maximum value of the input current and while I_{min} was the minimum value of the input current.

In this control logic the switch of current supplier depended on the product of drift $x(t)$ and velocity $\dot{x}(t)$ on the ground floor. If this product was greater than zero, which meant that the deformation drift and velocity of the ground floor were both in the same direction, the current supplier for the MRE bearing should apply maximum current to the device. Otherwise, when this product is equal to or less than zero, the current supplier will switch off and apply minimum current to the device. On this assumption we can develop the simulation based on this control logic in the MATLAB SIMULINK program. The bang-bang control logic schematic is shown in figure 5.4.

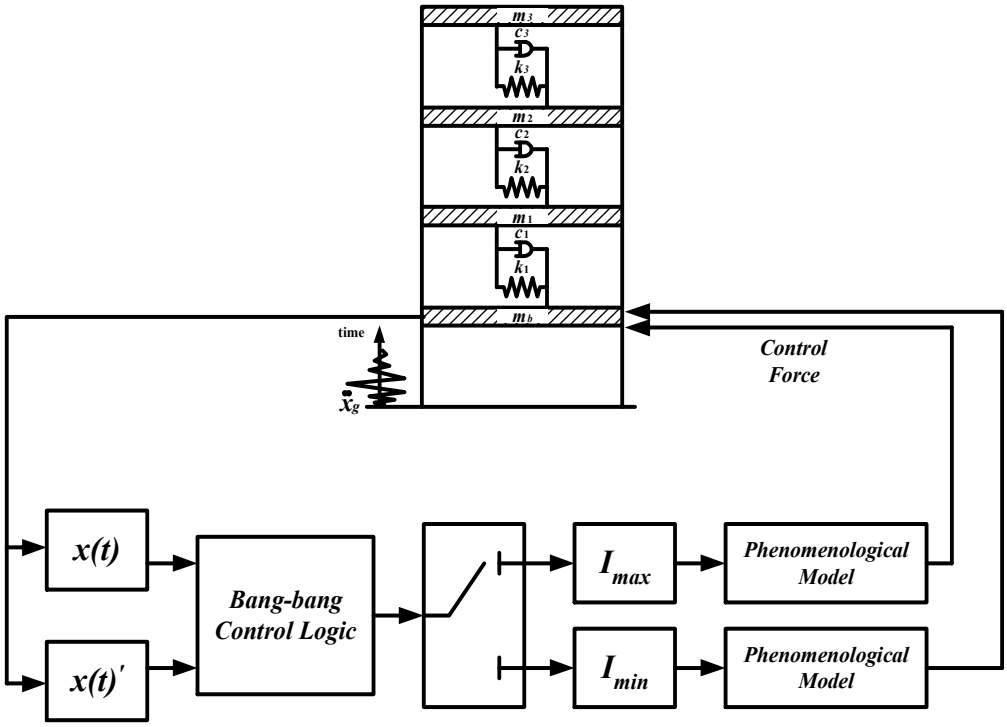

Figure 5.4 The bang-bang control logic schematic for the building

5.3.3 Performance evaluation

In this section, three different control logics were used to investigate the displacement and acceleration on each floor of the three storied building. To simulate an MRE device, a four-parameter viscoelastic phenomenological model was used in the program. In order to compare its effectiveness with each control strategy, two kinds of curves including a response with and without control are illustrated. Two recorded ground excitations were used in this simulation, the El Centro NS and Northbridge. The

performance of ground excitation at El Centro NS was compared in this section, while the relevant performance of ground excitation at Northbridge is shown in Appendix E.

Case A: Passive off control logic

With the passive off control logic the current supplier for the MR elastomers device was always switching off which meant that the current input of the four-parameter viscoelastic model was a constant value of 0A. In this case the MR elastomers device can only inherently perform as initial effective stiffness and equivalent viscosity damping coefficient to generate a control force on the building. Figure 5.5a-d shows the displacement for each floor where an MRE device was installed. Figure 5.6 shows the acceleration for each floor where an MRE device was installed.

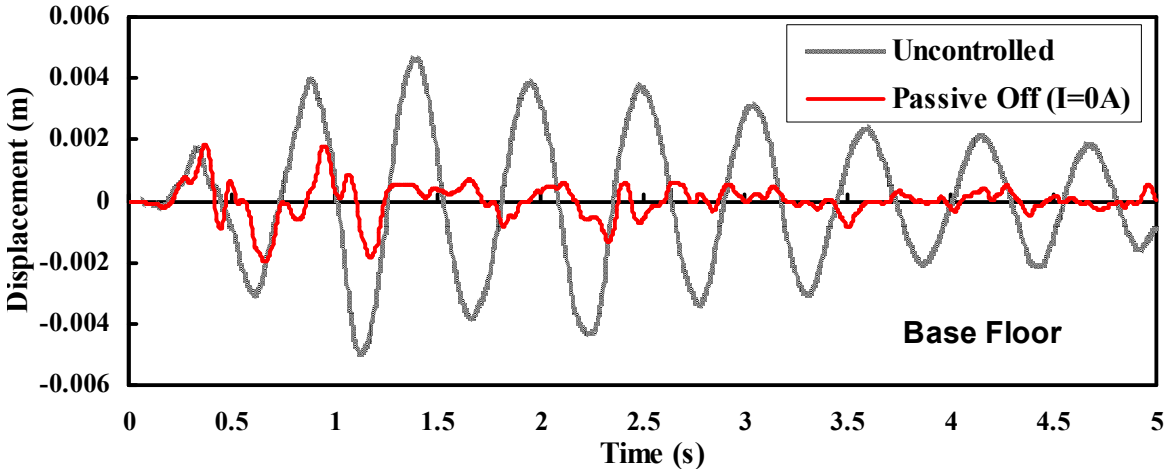

(a)

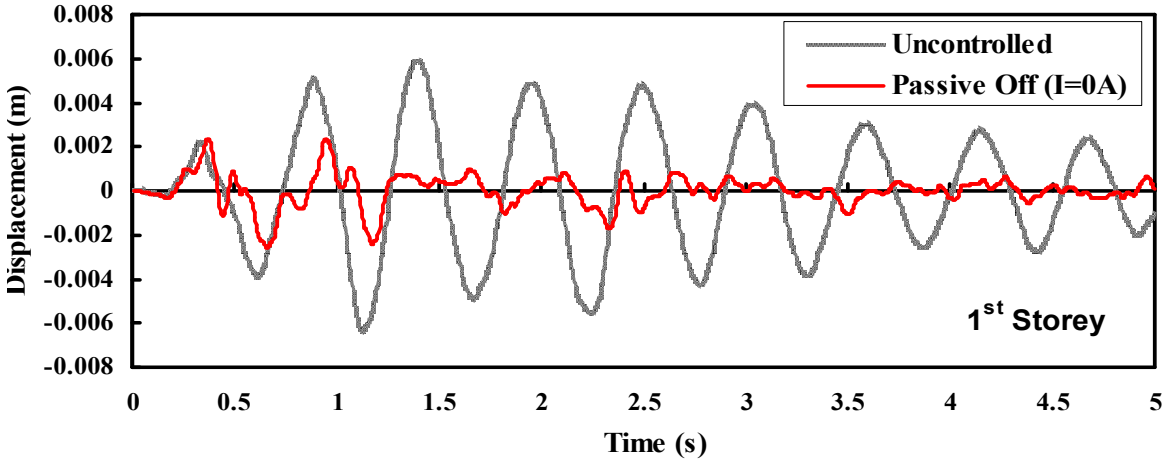

(b)

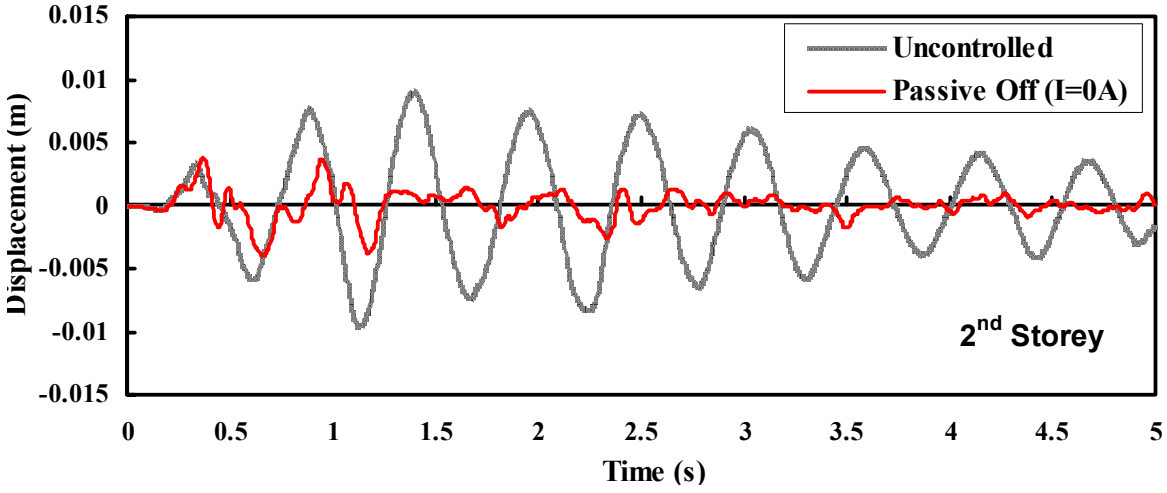

(c)

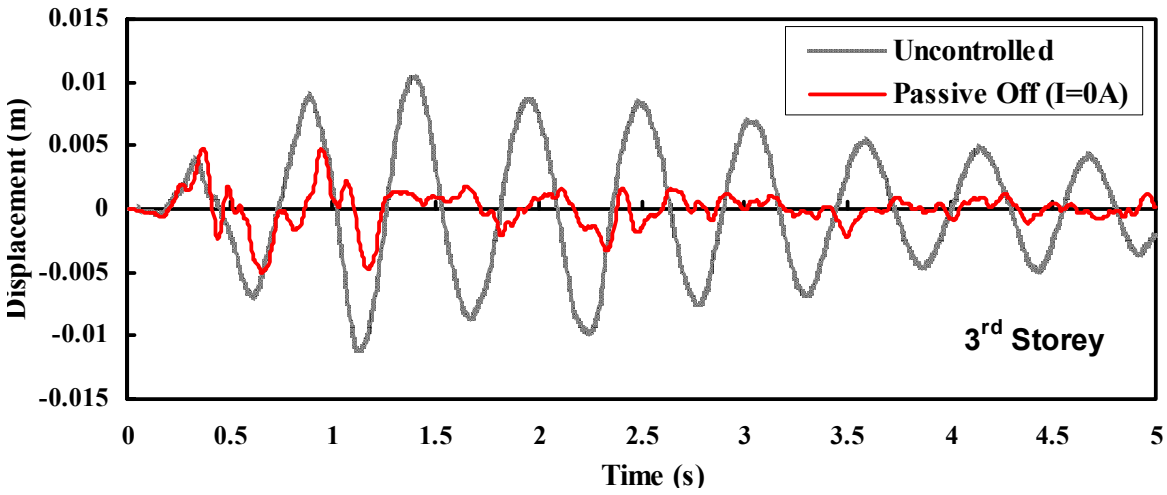

(d)

Figure 5.5 Displacement for each floor with an MRE device for passive off control logic: (a) Displacement of ground floor. (b) Displacement of first floor. (c) Displacement of second floor. (d) Displacement of third floor.

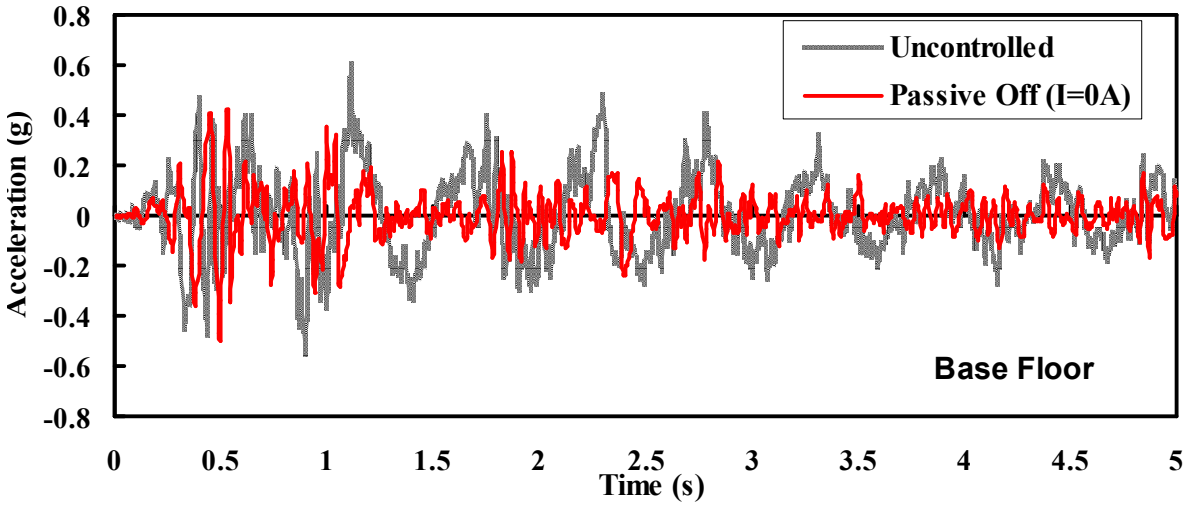
Uncontrolled
Passive Off (I=0A)
Base Floor
Acceleration (g)
Time (s)
0.8
0.6
0.4
0.2
0
-0.2
-0.4
-0.6
-0.8
0
0.5
1
1.5
2
2.5
3
3.5
4
4.5
5

(a)

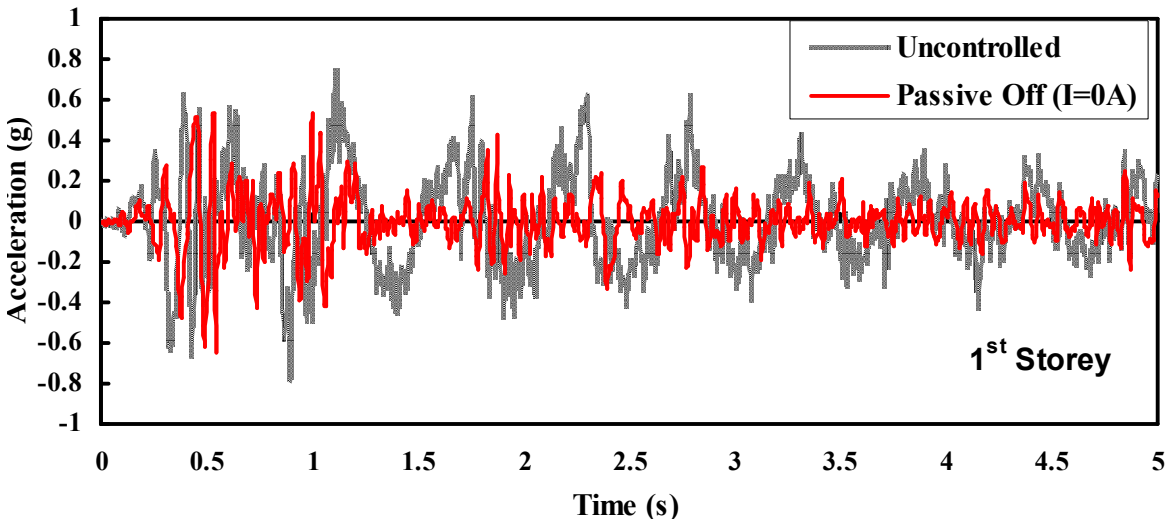
Uncontrolled
Passive Off (I=0A)
1st Storey
Acceleration (g)
Time (s)
1
0.8
0.6
0.4
0.2
0
-0.2
-0.4
-0.6
-0.8
-1
0
0.5
1
1.5
2
2.5
3
3.5
4
4.5
5

(b)

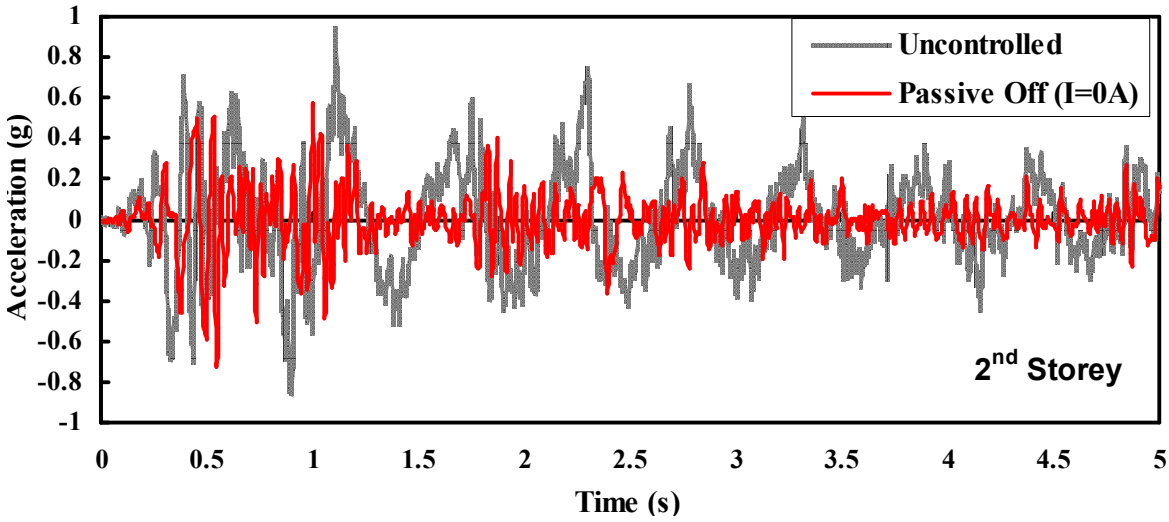

(c)

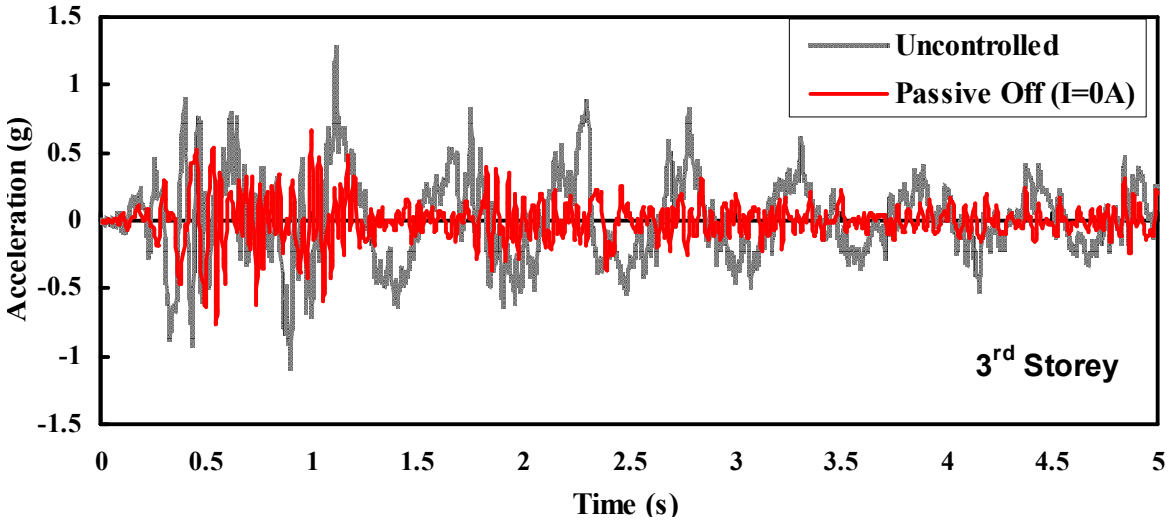

(d)

Figure 5.6 Acceleration for each floor with an MRE device for passive off control logic: (a) Acceleration of ground floor. (b) Acceleration of first floor. (c) Acceleration of second floor. (d) Acceleration of third floor.

The displacement and acceleration of each floor with passive off control logic are shown in figure 5.5 and figure 5.6, respectively. The peak responses due to the EI Centro NS record are listed in table 5.2.

Table 5.2 Peak responses due to the El Centro earthquake (Passive Off)

Response	x_i(mm)				$\ddot{x}_i$ (g)			
Floor	Base	1st	2nd	3rd	Base	1st	2nd	3rd
Uncontrolled	4.6	5.9	8.9	10.4	0.605	0.747	0.943	1.274
Passive-off	1.8	2.4	3.7	4.7	0.424	0.538	0.566	0.650
Reduction (%)	-60.9	-59.3	-58.4	-54.8	-29.9	-28.0	-40.0	-49.0

Table 5.2 shows a reduction in displacement ranging from 54.8% on the 3rd floor to 60.9% on the ground floor and a reduction in acceleration from 29.9% on the ground floor to 49.0% on the 3 rd floor.

Case B: Passive on control logic

With the passive on control logic the current supplier for the MR elastomers device is always switching on, which is opposite to the passive off control logic. This means that the input of the four parameters viscoelastic model is a constant maximum value current. In this case the MR elastomers device can only perform its extreme properties such as maximum effective stiffness and equivalent viscosity damping coefficient to generate a control force on the building. Figure 5.7 shows the displacement for each floor with an MRE device and Figure 5.8 shows the acceleration for each floor with an MRE device.

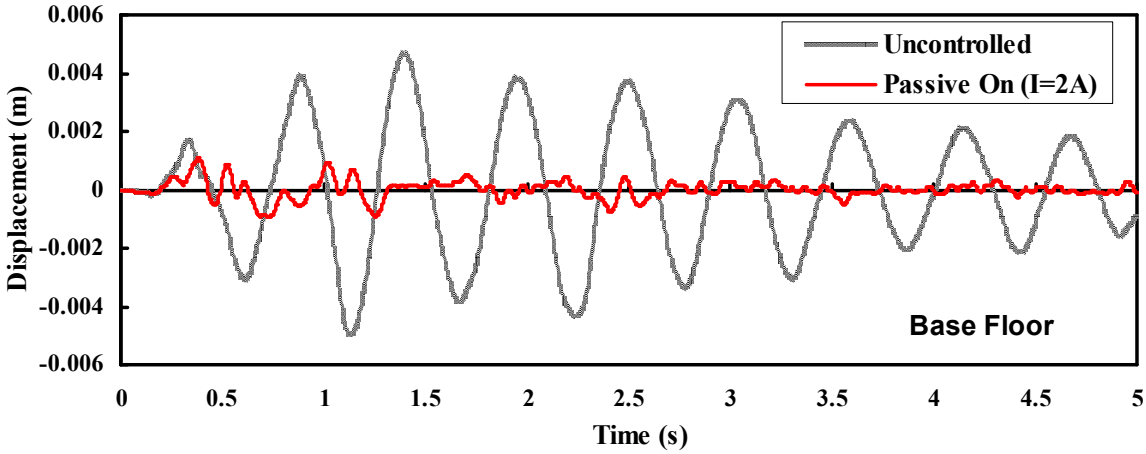
Uncontrolled
Passive On (I=2A)
Base Floor
Displacement (m)
Time (s)
0.006
0.004
0.002
0
-0.002
-0.004
-0.006
0
0.5
1
1.5
2
2.5
3
3.5
4
4.5
5

(a)

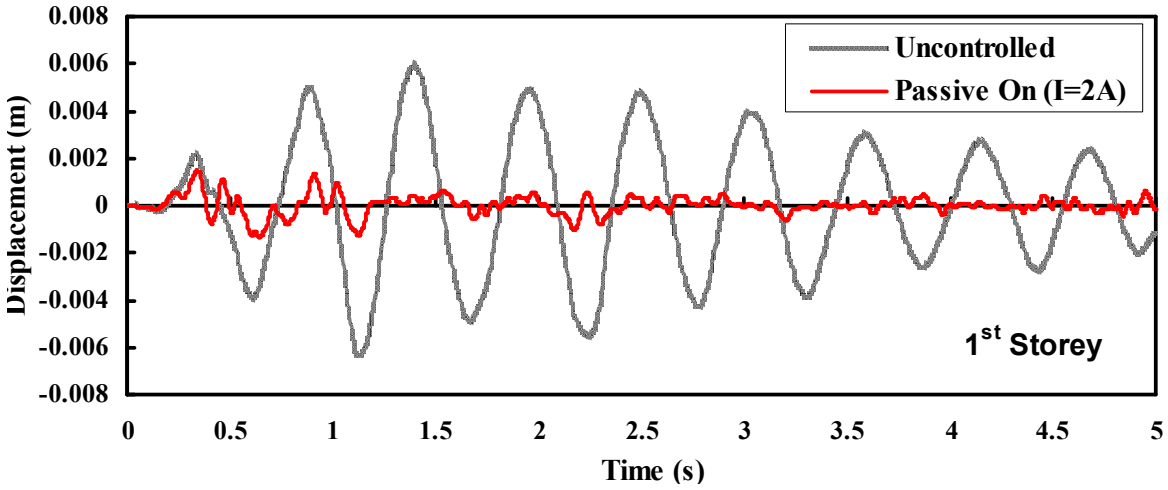
Uncontrolled
Passive On (I=2A)
1st Storey
Displacement (m)
Time (s)
0.008
0.006
0.004
0.002
0
-0.002
-0.004
-0.006
-0.008
0
0.5
1
1.5
2
2.5
3
3.5
4
4.5
5

(b)

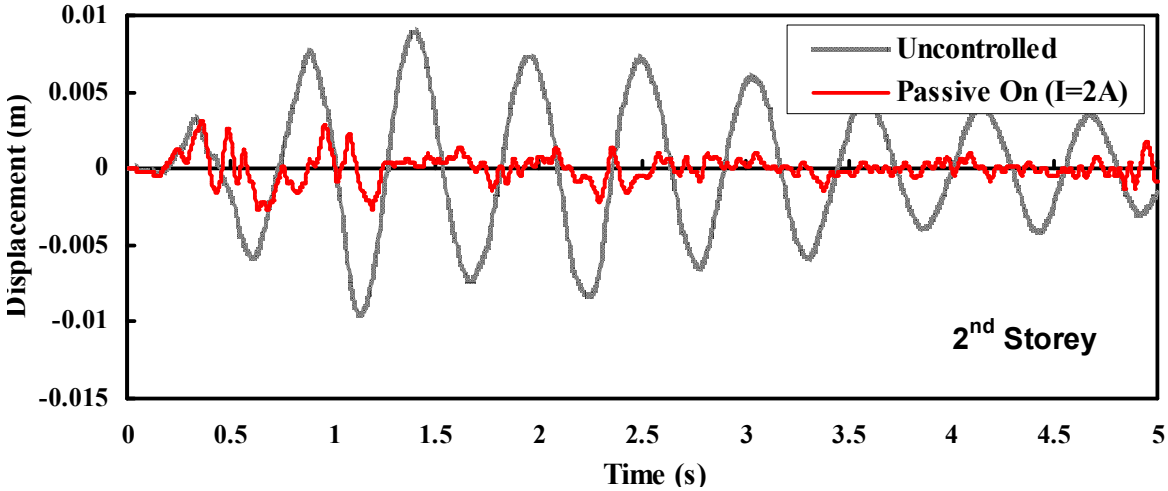
Uncontrolled
Passive On (I=2A)
2nd Storey
Displacement (m)
Time (s)
0.01
0.005
0
-0.005
-0.01
-0.015
0
0.5
1
1.5
2
2.5
3
3.5
4
4.5
5

(c)

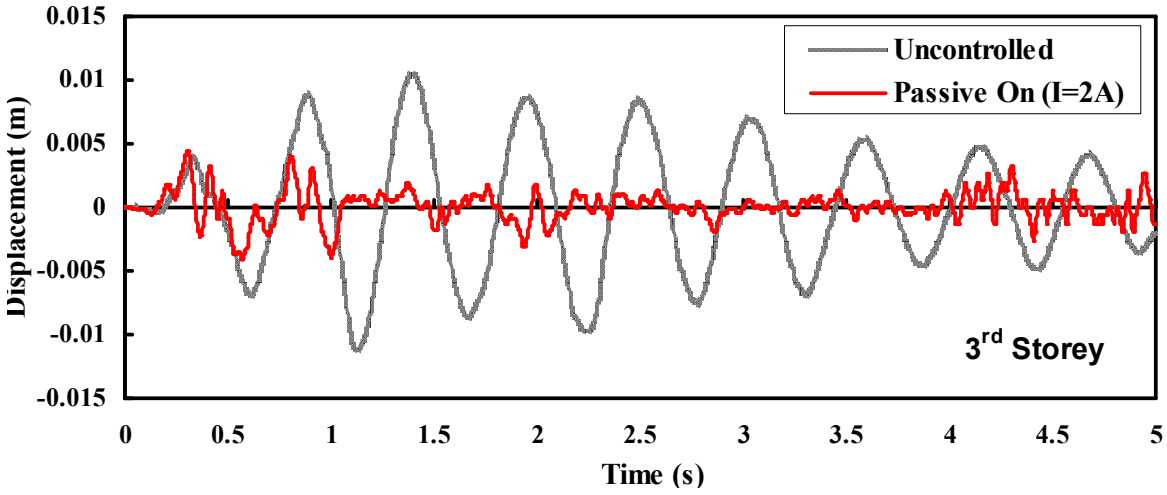

(d)

Figure 5.7 Displacement for each floor with an MRE device for passive on control logic: (a) Displacement of ground floor. (b) Displacement of first floor. (c) Displacement of second floor. (d) Displacement of third floor.

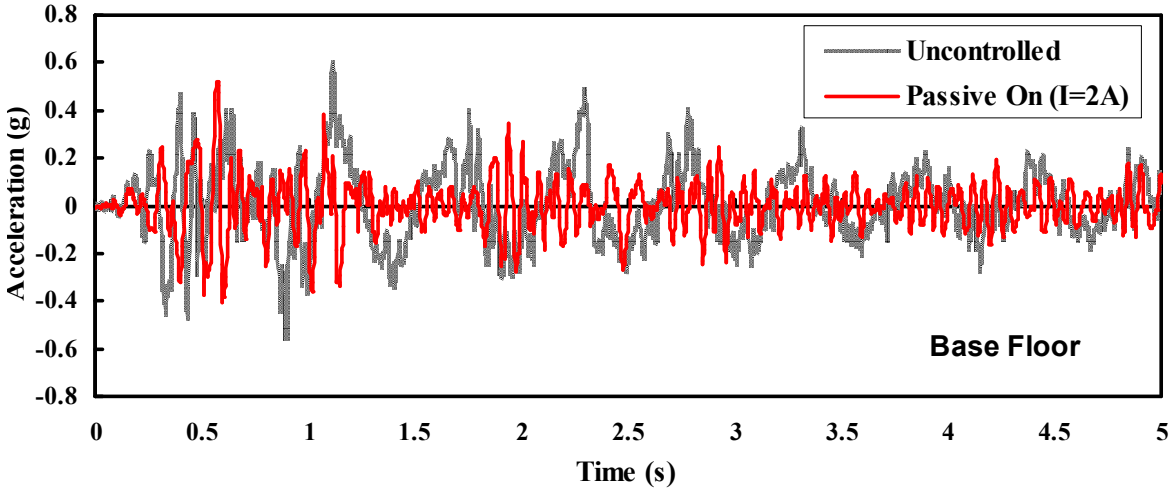

(a)

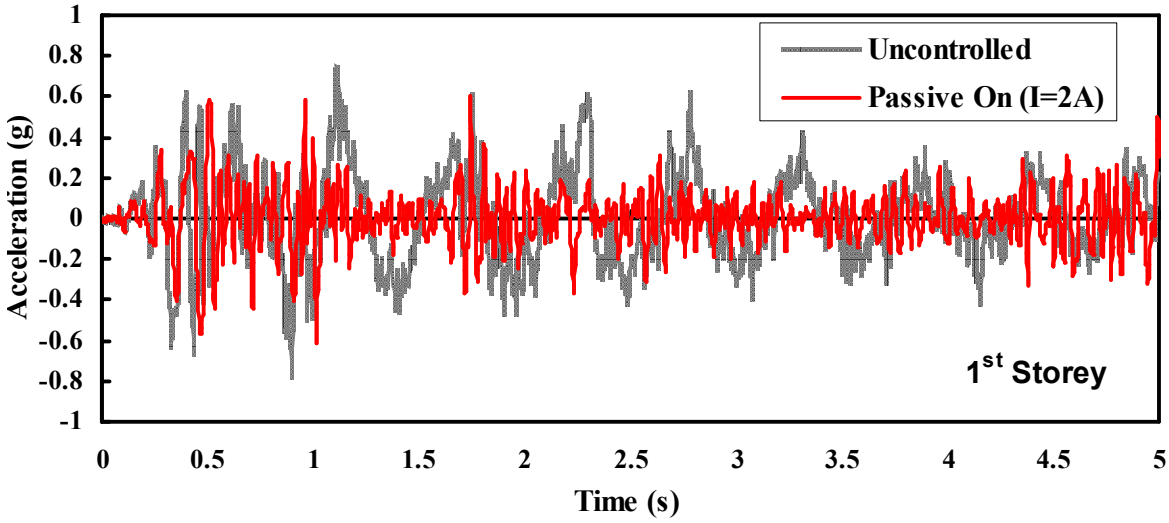
Uncontrolled
Passive On (I=2A)
1st Storey
Acceleration (g)
Time (s)
1
0.8
0.6
0.4
0.2
0
-0.2
-0.4
-0.6
-0.8
-1
0
0.5
1
1.5
2
2.5
3
3.5
4
4.5
5

(b)

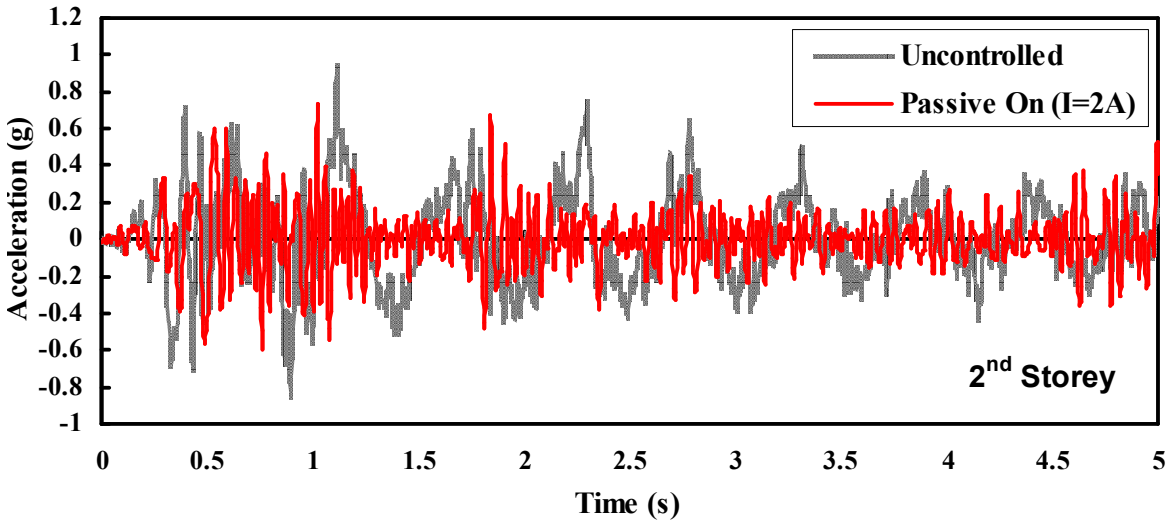
Uncontrolled
Passive On (I=2A)
2nd Storey
Acceleration (g)
Time (s)
1.2
1
0.8
0.6
0.4
0.2
0
-0.2
-0.4
-0.6
-0.8
-1
0
0.5
1
1.5
2
2.5
3
3.5
4
4.5
5

(c)

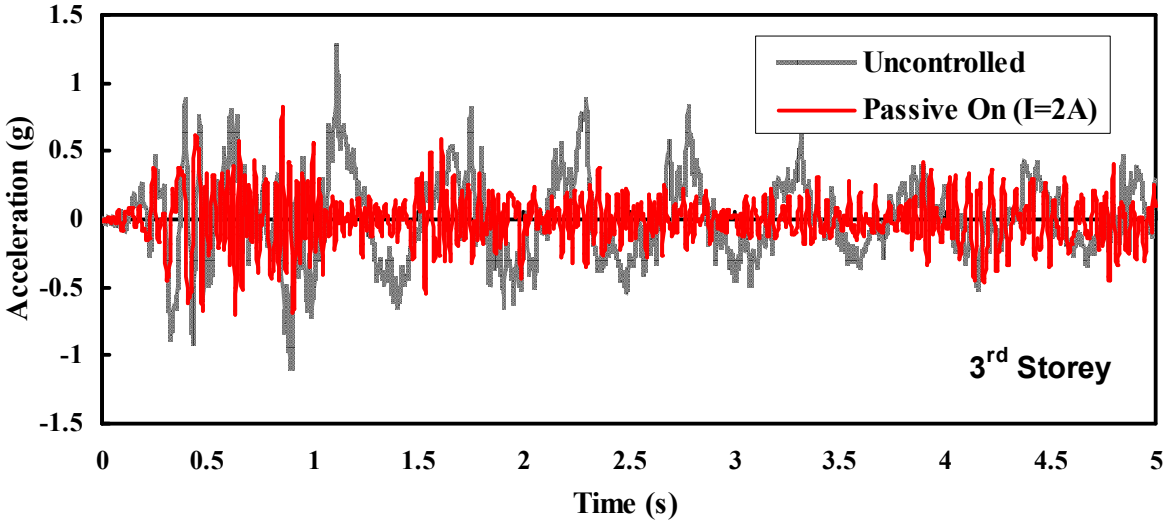

(d)

Figure 5.8 Acceleration for each floor with an MRE device for passive on control logic: (a) Acceleration of ground floor. (b) Acceleration of first floor. (c) Acceleration of second floor. (d) Acceleration of third floor.

The displacement and acceleration for each floor with passive on control logic are shown in figure 5.7 and 5.8. The peak responses due to the EI Centro NS record are listed in table 5.3.

Table 5.3 Peak responses due to the El Centro earthquake (Passive On)

Response	x_i(mm)				$\ddot{x}_i$ (g)			
Floor	Base	1st	2nd	3rd	Base	1st	2nd	3rd
Uncontrolled	4.6	5.9	8.9	10.4	0.605	0.747	0.943	1.274
Passive-on	1.1	1.5	3.1	4.4	0.516	0.607	0.725	0.831
Reduction (%)	-76.1	-74.6	-65.2	-57.7	-14.7	-18.7	-23.1	-34.8

Table 5.3 shows a reduction in displacement ranging from 57.7% on the 3rd floor to 76.1% on the ground floor and a reduction in acceleration from 14.7% on the ground floor to 34.8% on the 3 rd floor.

Case C: Bang-bang control logic

With bang-bang control logic the current supplier for MR elastomers device is sometimes switching on and sometimes switching off, depending on the product of displacement and velocity on the ground floor. This means that the current input of the four parameter viscoelastic model can change at the maximum and minimum. In this case the MR elastomers device can perform its extreme properties and inherent properties while depending on different situations to generate a controlling force on the building. Figure 5.9 shows the displacement for each floor of three storied building incorporating an MRE device. Figure 5.10 shows the acceleration for each floor incorporating an MRE device.

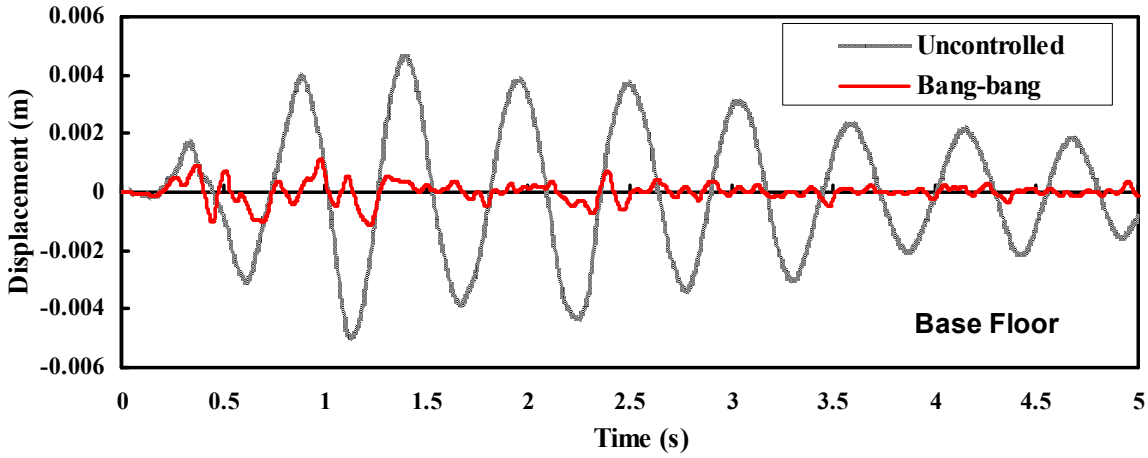

(a)

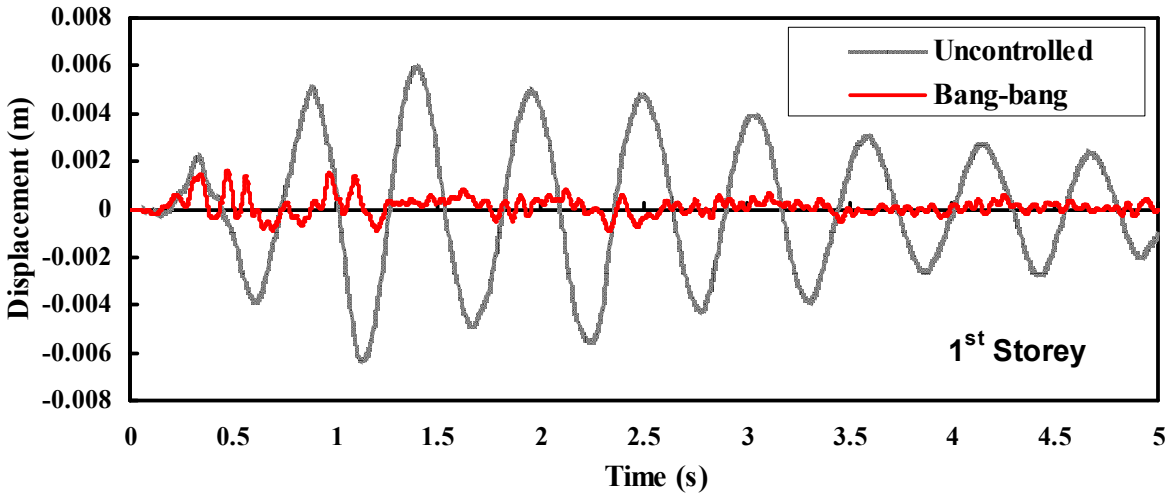
Uncontrolled
Bang-bang
1st Storey
Displacement (m)
Time (s)
0.008
0.006
0.004
0.002
0
-0.002
-0.004
-0.006
-0.008
0
0.5
1
1.5
2
2.5
3
3.5
4
4.5
5

(b)

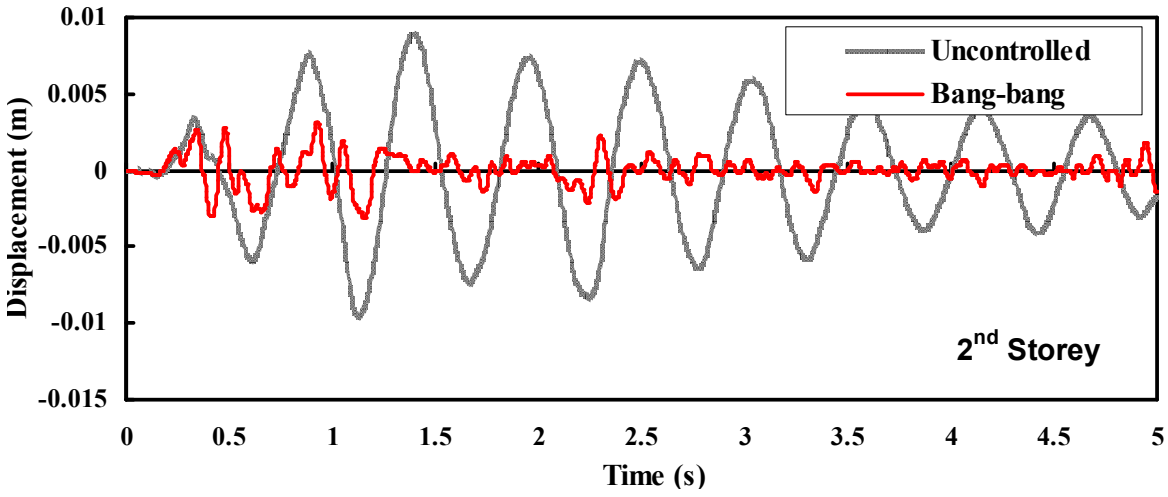
Uncontrolled
Bang-bang
2nd Storey
Displacement (m)
Time (s)
0.01
0.005
0
-0.005
-0.01
-0.015
0
0.5
1
1.5
2
2.5
3
3.5
4
4.5
5

(c)

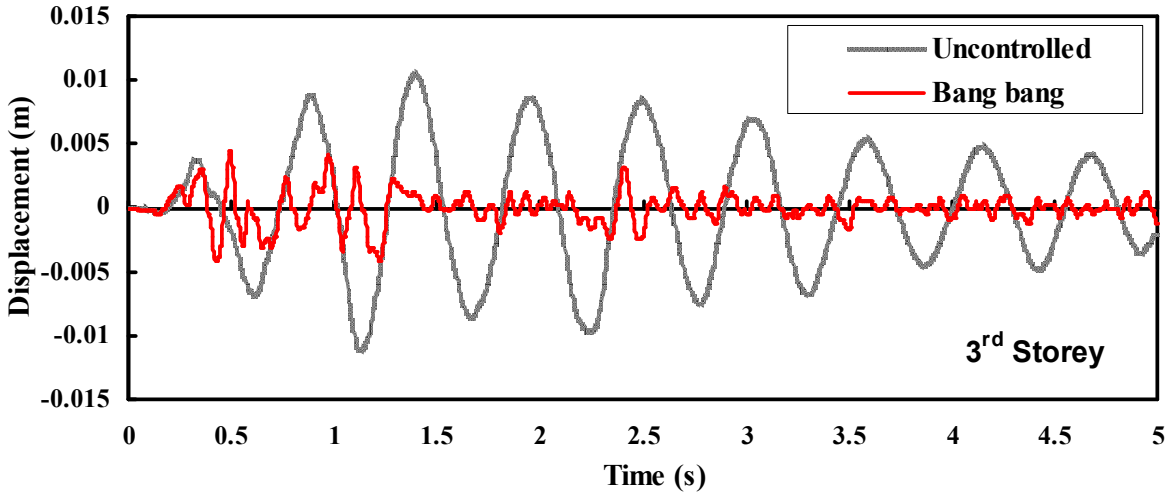

(d)

Figure 5.9 Displacement for each floor with an MRE device for Bang-bang control logic: (a) Displacement of ground floor. (b) Displacement of first floor. (c) Displacement of second floor. (d) Displacement of third floor.

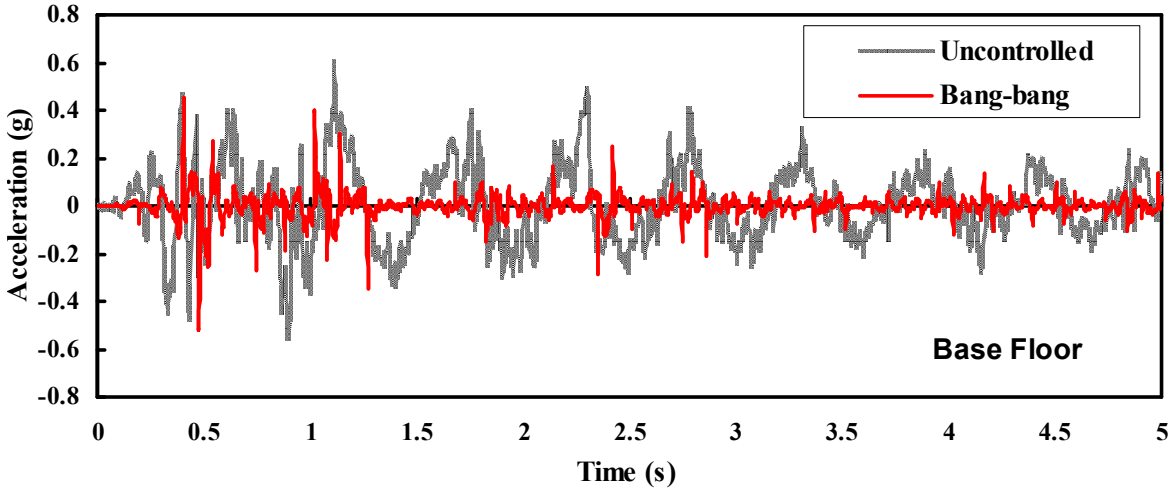

(a)

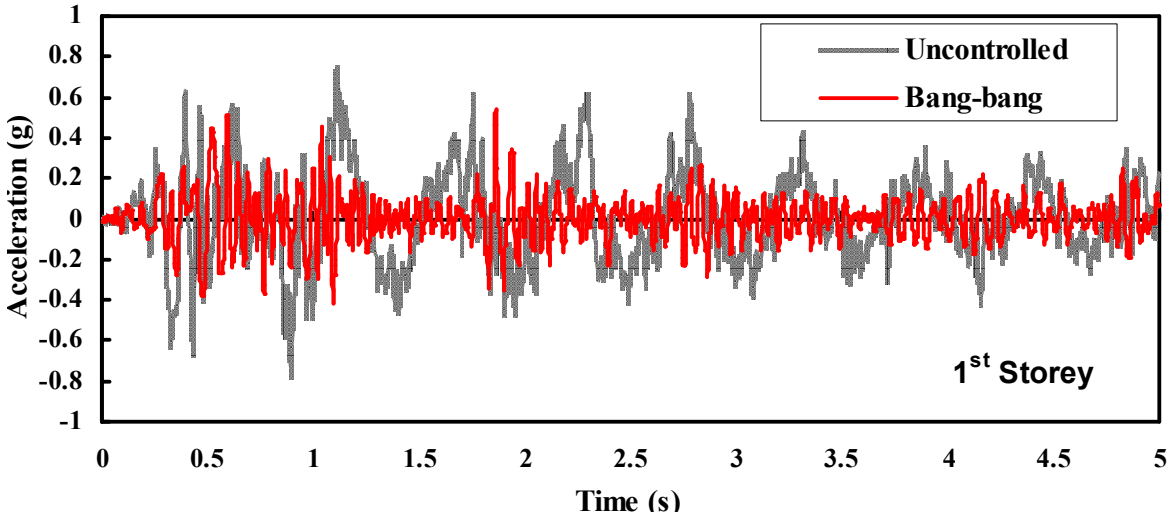
Uncontrolled
Bang-bang
1st Storey
Acceleration (g)
Time (s)
1
0.8
0.6
0.4
0.2
0
-0.2
-0.4
-0.6
-0.8
-1
0
0.5
1
1.5
2
2.5
3
3.5
4
4.5
5

(b)

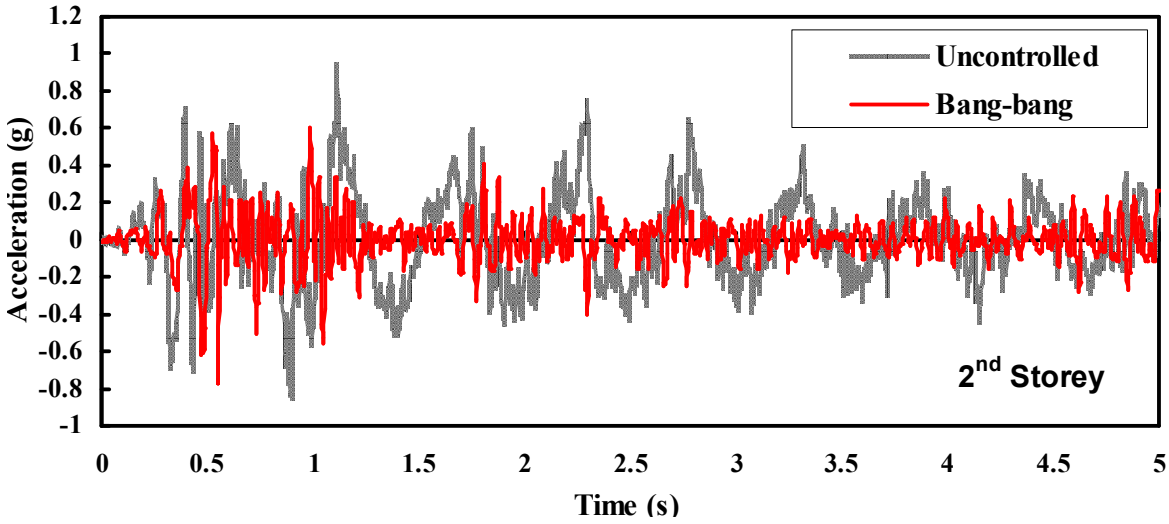
Uncontrolled
Bang-bang
2nd Storey
Acceleration (g)
Time (s)
1.2
1
0.8
0.6
0.4
0.2
0
-0.2
-0.4
-0.6
-0.8
-1
0
0.5
1
1.5
2
2.5
3
3.5
4
4.5
5

(c)

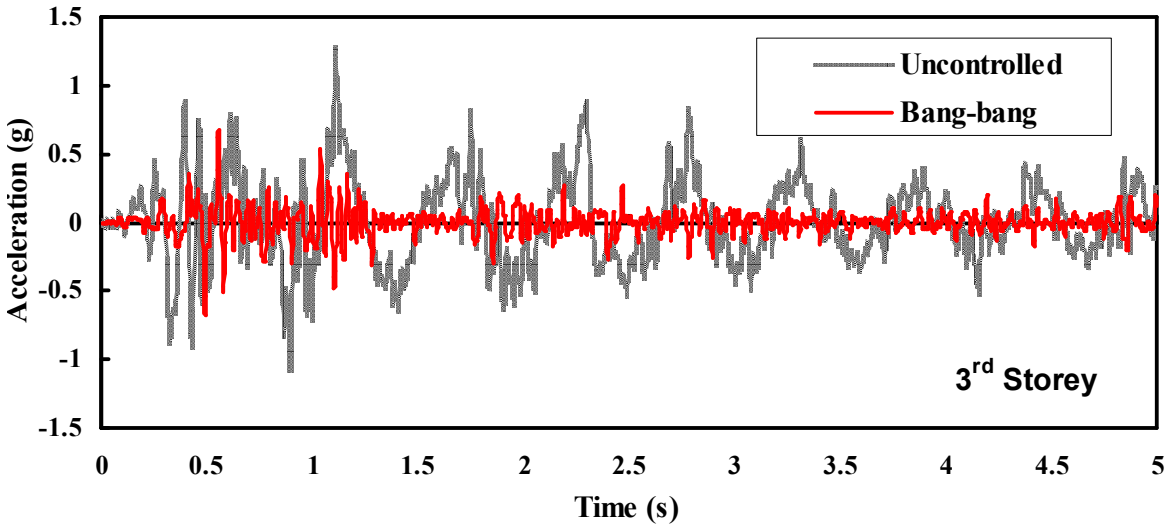

(d)

Figure 5.10 Acceleration for each floor with an MRE device for Bang-bang control logic: (a) Acceleration of ground floor. (b) Acceleration of first floor. (c) Acceleration of second floor. (d) Acceleration of third floor.

The displacement and acceleration for each floor with passive on control logic are shown from figure 5.9 and 5.10. The peak responses due to EI Centro NS record are listed in table 5.4.

Table 5.4 Peak responses due to the El Centro earthquake (Bang-bang)

Response	x_i(mm)				$\ddot{x}_i$ (g)			
Floor	Base	1st	2nd	3rd	Base	1st	2nd	3rd
Uncontrolled	4.6	5.9	8.9	10.4	0.605	0.747	0.943	1.274
Bang-bang	1.1	1.6	3.1	4.4	0.443	0.541	0.603	0.672
Reduction (%)	-76.1	-72.9	-65.2	-57.7	-26.8	-27.6	-36.1	-47.3

Table 5.4 shows a reduction in displacement ranging from 57.7% on the 3rd floor to 76.1% on the ground floor and a reduction in acceleration from 26.8% on the ground floor to 47.3% on the 3 rd floor.

5.3.4 Discussion

Three control logics, passive off, passive on and bang-bang control logic were used in this simulated evaluation process. The displacement and acceleration for each floor with these three control strategies are shown from figure 5.5 to 5.10. The peak responses due to El Centro NS record are listed in table 5.5.

Table 5.5 Peak responses due to the El Centro earthquake

	Floor	Uncontrolled	Passive-off		Passive-on		Bang-bang control	
x_i (mm)	Base	4.6	1.8	-60.9%	1.1	-76.1%	1.1	-76.1%
	1st	5.9	2.4	-59.3%	1.5	-74.6%	1.6	-72.9%
	2nd	8.9	3.7	-58.4%	3.1	-65.2%	3.1	-65.2%
	3rd	10.4	4.7	-54.8%	4.4	-57.7%	4.4	-57.7%
$\ddot{x}_i$ (g)	Base	0.605	0.424	-29.9%	0.516	-14.7%	0.443	-26.8%
	1st	0.747	0.538	-28.0%	0.607	-18.7%	0.541	-27.6%
	2nd	0.943	0.566	-40.0%	0.725	-23.1%	0.603	-36.1%
	3rd	1.274	0.650	-49.0%	0.831	-34.8%	0.672	-47.3%

Here the passive systems are able to achieve a reasonable reduction in the structural response of each floor. The displacement on each floor of the passive on system is better than those of the passive off system but the acceleration of the passive on system is often larger than the passive off system. For instance, the acceleration of the ground floor and third floor in the passive on system are about 21.7% and 27.8% larger than the passive off system, respectively. These increasing levels of acceleration are disadvantageous for the building structure. This finding demonstrates that using a passive device capable of generating large control forces is not always the best approach.

The results of displacement and acceleration by using the Bang-bang control logic

indicate that the semi-active control system was much better at reducing the structural displacement and acceleration than the passive systems. At each level in the building, the bang-bang controller was able to reduce the displacement and floor accelerations much better than the passive on systems. The bang-bang controller reduced the structural response in the excitation of El Centro NS record very well. Almost similar results were obtained when the external excitation was the Northbridge record. The table of peak responses from the Northbridge record earthquake are listed in Appendix E. Although the bang-bang controller was not always able to reduce the displacement as well as the passive on system it can help the structure reduce acceleration on each floor. The response of the bang-bang controller to acceleration on the first and third floors was 16.5% and 23.7% smaller than the passive on system, respectively. This control logic can effectively reduce both the displacement and acceleration for each floor of the building.

5.4 CONCLUSION

In this chapter the three-storey building model was modelled by using the MATLAB SIMULINK program. The four-parameter viscoelastic model was used to simulate an MRE bearing for this structure. Three controllers, passive off, passive on and bang-bang control logic were used to control the MRE device. Based on this simulated model two conventional earthquake data from El Centro NS and Northbridge were used to evaluate this system. A comparison of the displacement and acceleration on each floor proved that these three controllers can effectively reduce the structural responses, albeit the bang-bang controller performed best. This control logic can significantly reduce displacement and also decrease the acceleration. Therefore, in comparison with the passive control system, the semi-active controller is an appropriate approach to structural control.

CHAPTER 6

A COMPARISON BETWEEN THE MRF DAMPER AND MRE ISOLATOR

6.1 INTRODUCTION

This chapter outlines a comparison between an MRF damper and MRE device in structural control. The resultant peak force was selected as a criterion in this evaluation process. The structural response including displacement and acceleration, were evaluated when an MRF damper and an MRE device were incorporated into a three storied building.

6.2 A STUDY OF AN MRF DAMPER

According to Dyke et al [51], an MR fluid damper is one of a number of effective devices which are used to control the structural response in displacement and acceleration. This damper can generate various control forces due to changes in the external magnetic flux density. These sorts of control forces play very important roles in controlling structures.

A Bouc-wen phenomenological model was developed to simulate the characteristics of MR effects for MR fluid dampers [51]. A typical Bouc-wen model with a simple mechanical idealisation is shown in Figure 6.1. This model is the first step in developing an input/output model for an MR fluid damper.

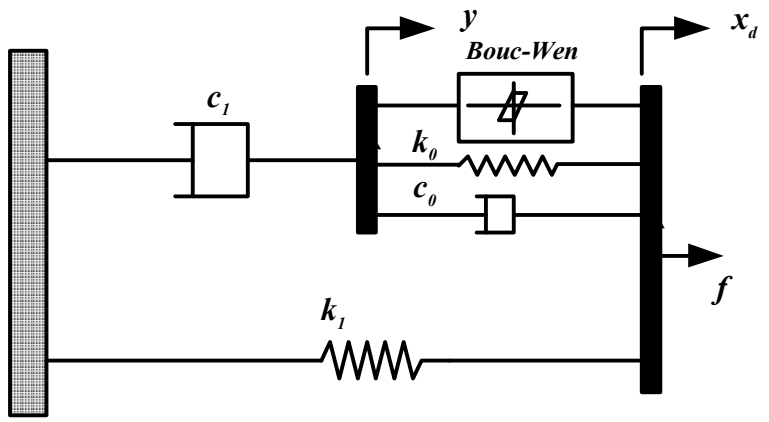

Figure 6.1 A simple mechanical model of an MR damper [51]

The related equations governing the control force *f* predicted by this model are given by

$$f = c_1\dot{y} + k_1(x_d - x_0) \tag{6.1}$$

$$\dot{z} = -\gamma|\dot{x}_d - \dot{y}|z|z|^{n-1} - \beta(\dot{x}_d - \dot{y})|z|^n + A(\dot{x}_d - \dot{y}) \tag{6.2}$$

$$\dot{y} = \frac{1}{c_0 + c_1}\{\alpha z + c_0\dot{x}_d + k_0(x_d - y)\} \tag{6.3}$$

where *z* is an evolutionary variable that accounts for the historic dependence of the response. The model parameters depend on the voltage *v* to the current driver as follows

$$\begin{aligned} \alpha &= \alpha_a + \alpha_b u \\ c_1 &= c_{1a} + c_{1b} u \\ c_0 &= c_{0a} + c_{0b} u \end{aligned} \tag{6.4}$$

where *u* is given as the output of the first-order filter

$$\dot{u} = -\eta(u - v) \tag{6.5}$$

Equation (6.5) is necessary to model the dynamics involved in reaching a rheological equilibrium and driving the electro-magnet in the MR damper [33, 56]. A nominal set of parameters based on the response of the MR damper was obtained in a series of displacement-controlled tests. Then the optimised parameters required to fit the generalised model of the MR fluid damper to the experimental data were determined. One typical set of parameters are given in reference [51]: c_{0a} = 8 N s cm^{-1}, c_{0b} = 6 N s cm^{-1} V^{-1}, k_0 = 50 N cm^{-1}, c_{1a} = 290 N s cm^{-1}, c_{1b} = 5 N s cm^{-1} V^{-1}, k_1 = 12 N cm^{-1}, x_0 =

14.3 cm, $\alpha_a = 100$, $\alpha_b = 450$ V^{-1}, $\gamma = 363$ cm^{-2}, $\beta = 363$ cm^{-2}, $A = 301$, $n = 2$, $\eta = 190$ s^{-1}.

By using the above 14 parameters the force-displacement curves were reconstructed and shown in Figure 6.2, where the amplitude and frequency are 5mm and 2.5Hz, respectively. The relationship between displacement and control force for the MR fluid damper illustrated in figure 6.2 was determined through the MATLAB SIMULINK program. It was found that the peak control forces of the MR fluid damper are -624N at 0V and -1699N at 2.25V.

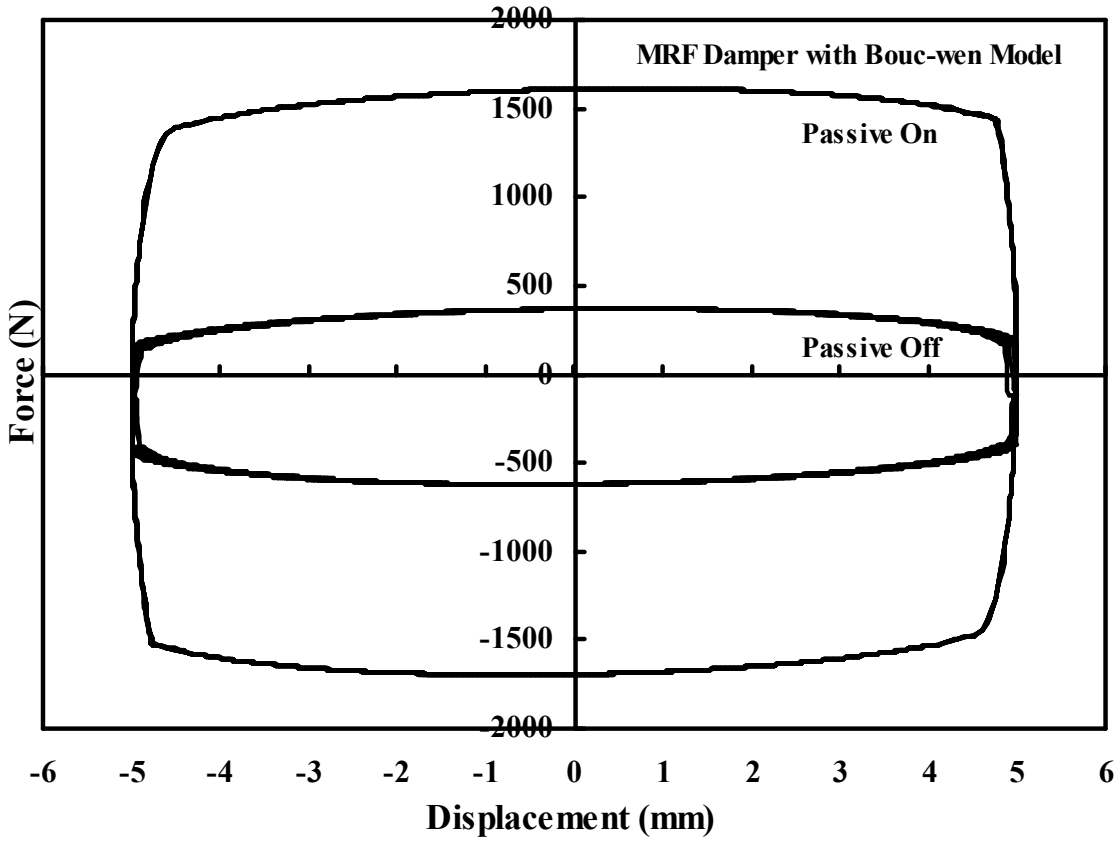

Figure 6.2 The relationship between displacement and force for an MR damper

6.3 SIMULATING AN MRE DEVICE

In order to achieve a peak force equivalent to the MR damper, the same frequency input was applied to the MRE device. From the experimental results given in Chapter 4, the resultant force of the MRE isolator was represented as

$$f(t) = x_0\sqrt{K_1^2 + K_2^2}\sin(\omega t + \phi) \tag{6.6}$$

where ϕ is the phase angle different between the input and the output, which can be calculated as $\phi = \tan^{-1}(K_2/K_1)$.

The damping frequency of the MRF damper is 2.5Hz. To achieve the same frequency input on the MRE device, the curve fitting mathematical method was used to evaluate the related K_1 and K_2 at 2.5Hz frequency input. Linear exploration and the experimental data of 5Hz and 10Hz were used in this study to find the values of K_1 and K_2. The relationship between K_1 and K_2 with different frequency inputs is illustrated in Figure 6.3.

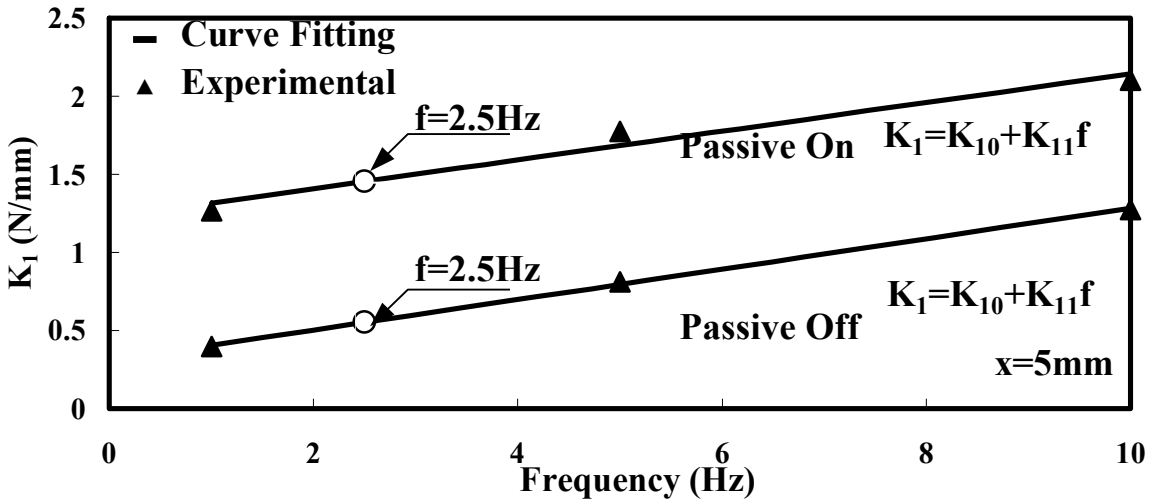

(a)

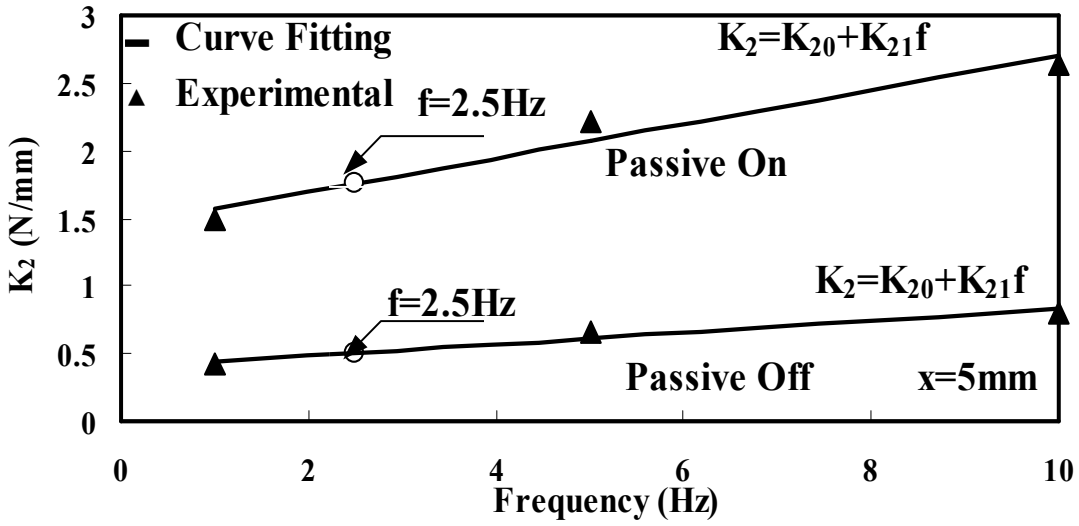

(b)

Figure 6.3 The relationship between K_1 and K_2 with different frequency inputs for an MRE device: (a) K_1 with different frequency inputs. (b) K_2 with different frequency inputs.

The values of K_1 and K_2 at a frequency of 2.5 Hz were found by using the linear exploration method. The parameters (K_{10}, K_{11}, K_{20} and K_{21}) are listed in Table 6.1. The related value of K_1 and K_2 are listed in Table 6.2.

Table 6.1 Parameters of linear exploration for K_1 and K_2

Case	K_{10} (N/mm)	K_{11} (N/mm Hz)	K_{20} (N/mm)	K_{21} (N/mm Hz)
Passive Off	0.3085	0.0973	0.4004	0.0427
Passive On	1.2254	0.0917	1.4455	0.1261

Table 6.2 K_1 and K_2 of MRE device at 2.5 Hz frequency input

Case	K_1 (N/mm)	K_2 (N/mm)	Amplificatory Factor (K)
Passive Off	0.55	0.50	168
Passive On	1.45	1.76	149

With these parameters, the relationship between displacement and force for an MRE device with a frequency input of 2.5Hz are reconstructed and shown in Figure 6.4.

From this chart we find that the peak control forces of the MRE device are -624N at 0A and -1699N at 1.75A. These two peak control forces are the same as the MRF damper.

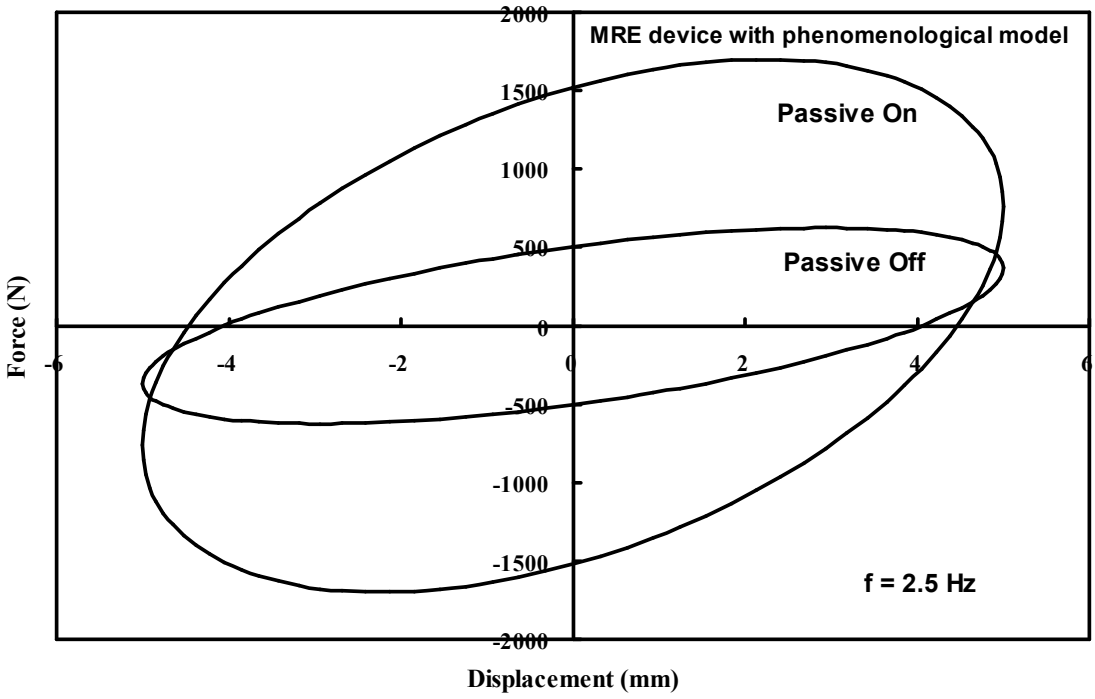

Figure 6.4 The relationship between displacement and force for an MRE device

6.4 PERFORMANCE EVALUATION

6.4.1 Dissipated energy of an MRF damper and MRE device

In order to compare the dissipation energy of an MRF damper and MRE device, the hysteresis loops in Figures 6.2 and 6.4 were combined together for cases of passive off and passive on, respectively. Figure 6.5 shows the combined illustration for the MRF damper and MRE device.

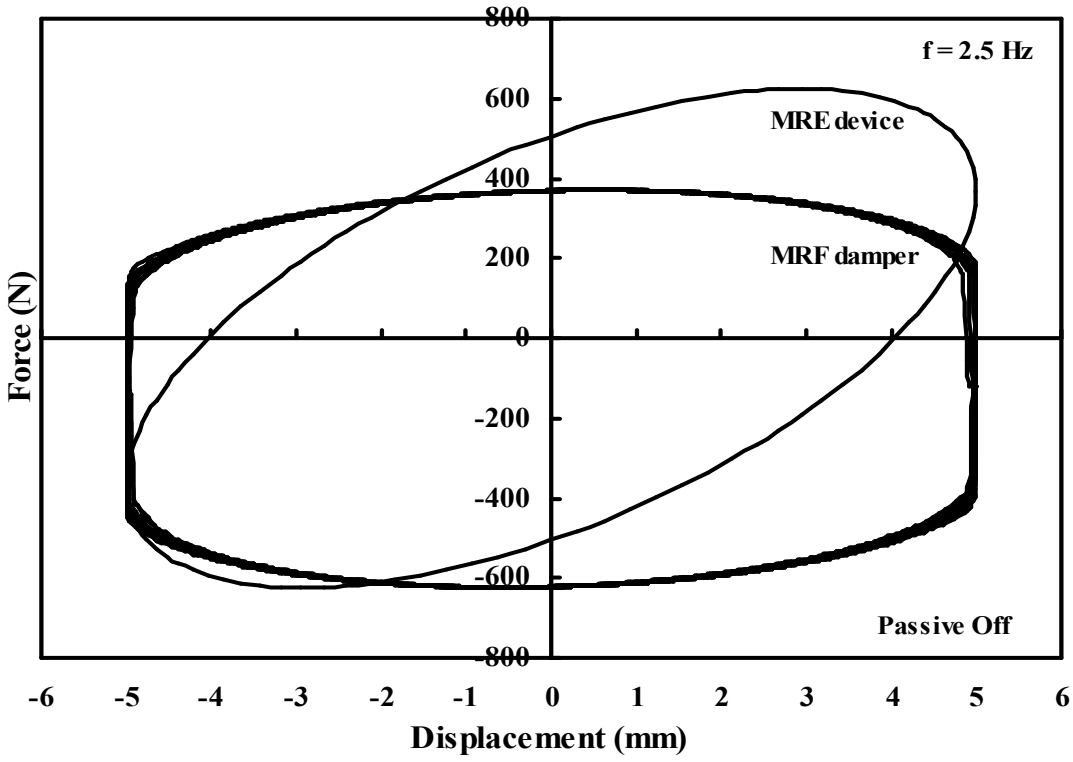

(a)

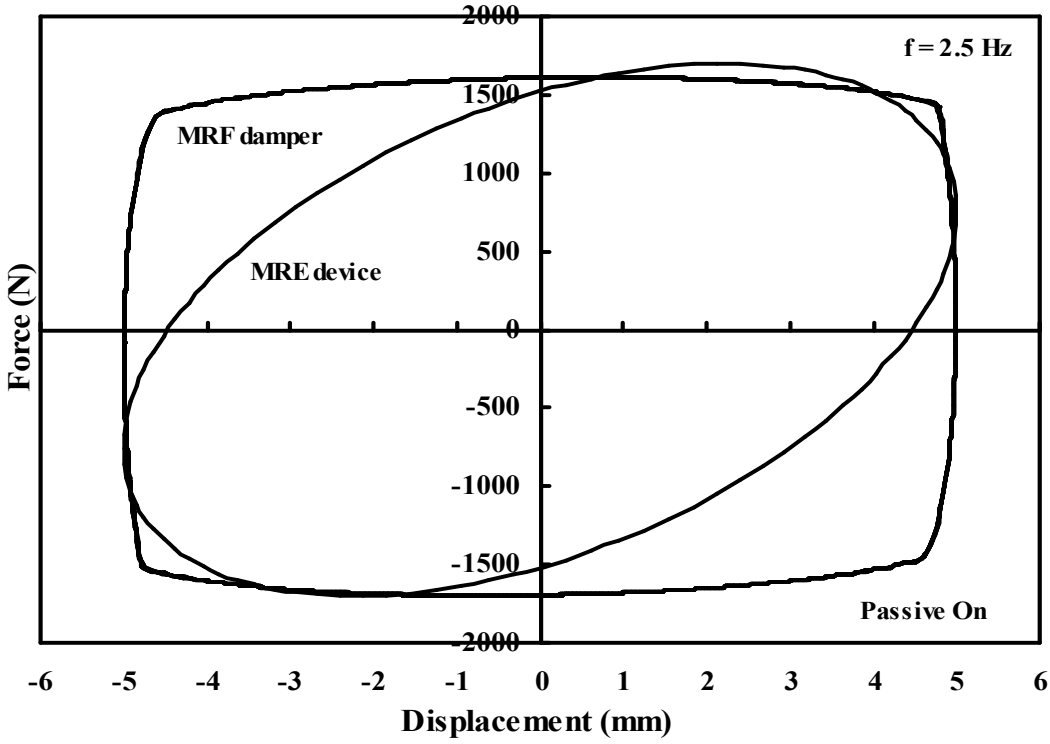

(b)

Figure 6.5 The relationship between displacement and force for an MRF damper and MRE device: (a) Passive off. (b) Passive on.

The dissipation energy of an MRF damper and MRE device were calculated using the finite difference method and the results are listed in Table 6.3.

Table 6.3 Dissipation energy of an MRF damper and MRE device

Case	Energy of MRF (N mm)	Energy of MRE (N mm)	Percentage (%)
Passive Off	9663	8130	-16.0
Passive On	32123	24022	-25.0

6.4.2 Structural responses evaluation

(A) An MRF damper

According to Dyke et al. [51], the peak responses for a three storied benchmark building incorporating an MRF damper were listed in Table 6.4 where the external ground excitation selected was a 120% EI Centro earthquake.

Table 6.4 Peak response due to the El Centro earthquake (MRF)

	Uncontrolled	Passive-off		Passive-on	
x_i(mm)	7.1	2.4	-66.2%	1.3	-81.7%
	10.7	3.6	-66.4%	3.1	-71.0%
	12.5	4.4	-64.8%	4.2	-66.4%
$\ddot{x}_i$ (g)	0.90	0.68	-24.4%	0.94	+4.4%
	1.13	0.73	-35.4%	0.82	-27.4%
	1.53	0.82	-46.4%	0.91	-40.5%

(B) An MRE device

For an MRE device we also applied a ground excitation of a 120% EI Centro earthquake to the building and the peak control forces generated by the MRE device were kept the same as those generated by an MRF damper. The displacement and

acceleration on each floor of the building are illustrated in Figures 6.6 to 6.9 below

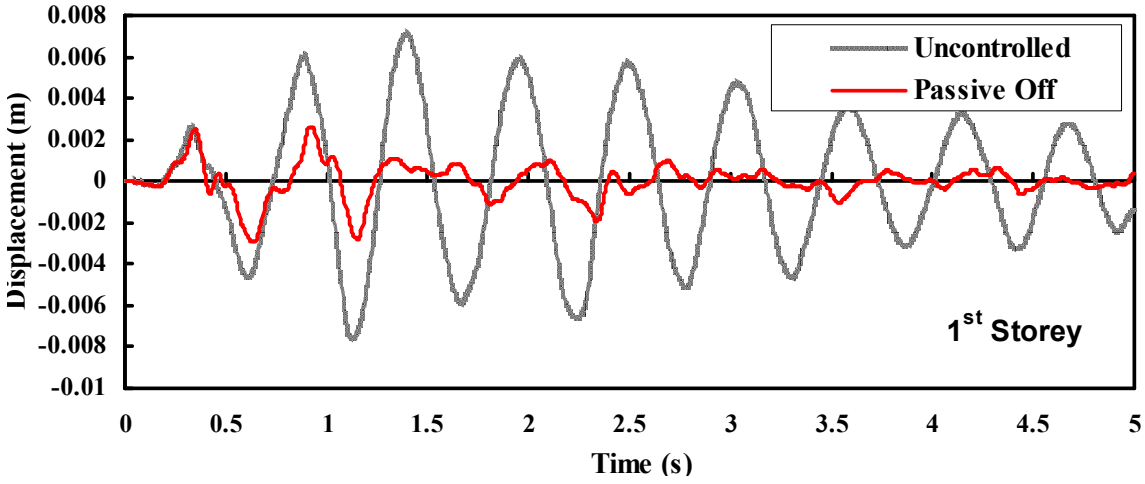

(a)

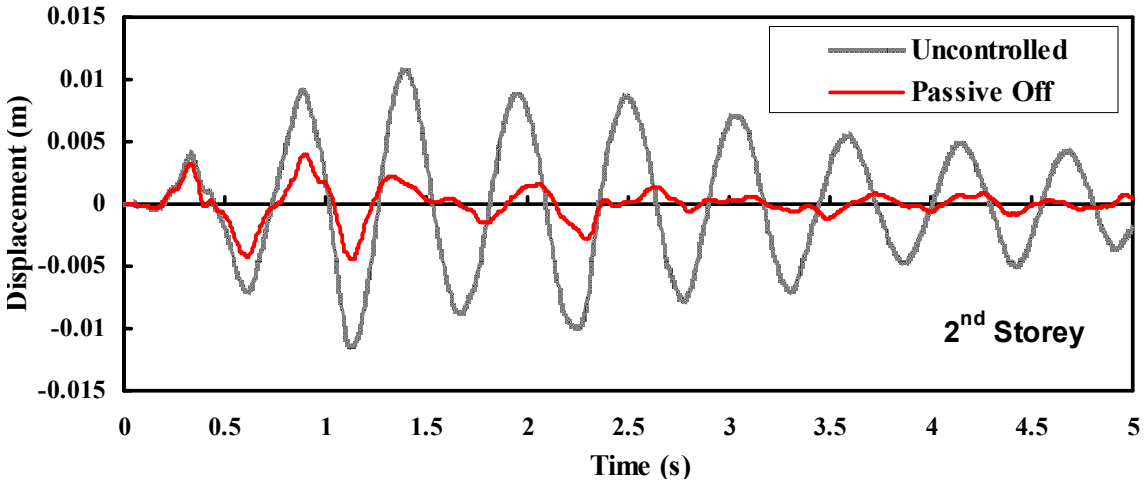

(b)

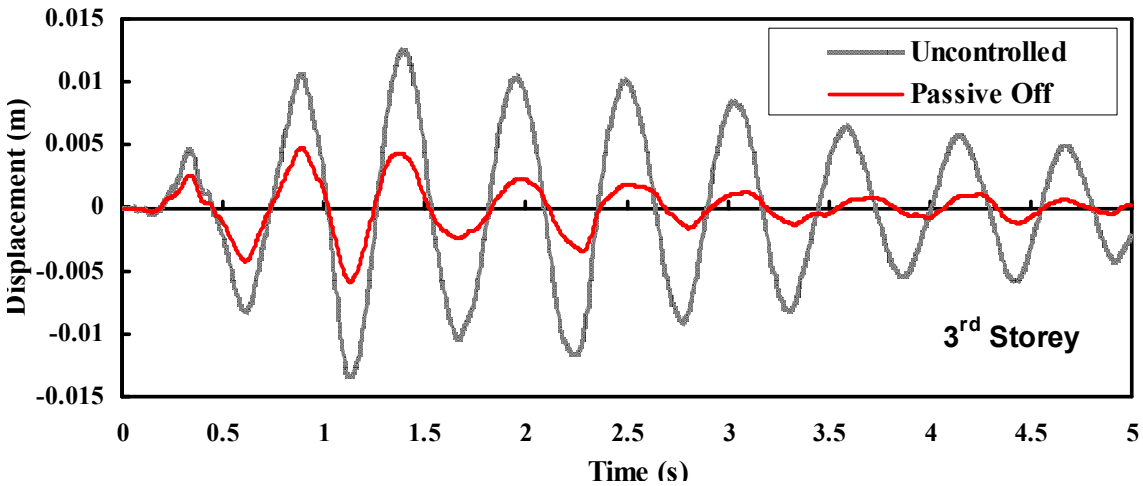

(c)

Figure 6.6 Displacement for each floor with an MRE device for passive off control logic: (a) Displacement of first floor. (b) Displacement of second floor. (c) Displacement of third floor.

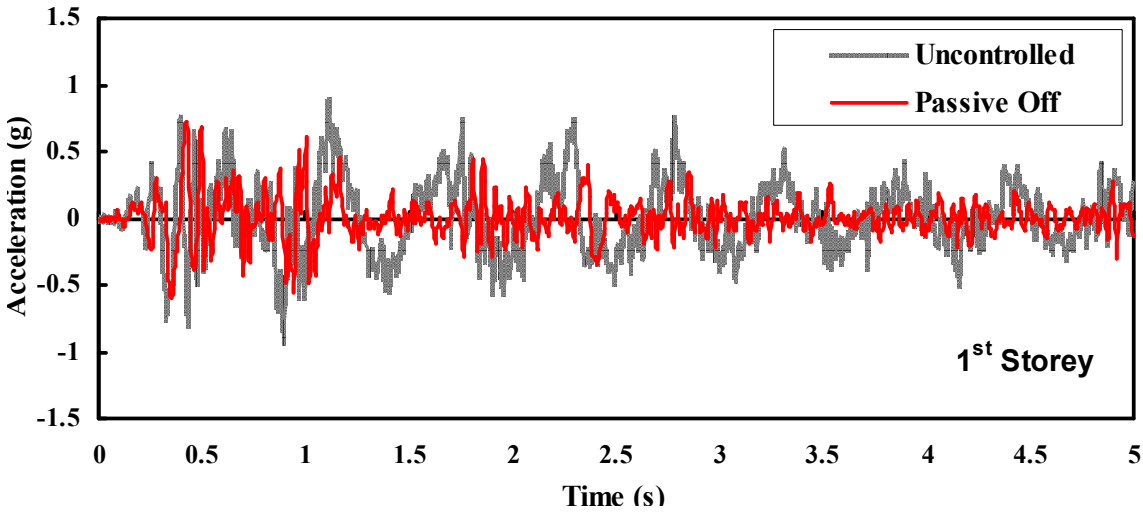

(a)

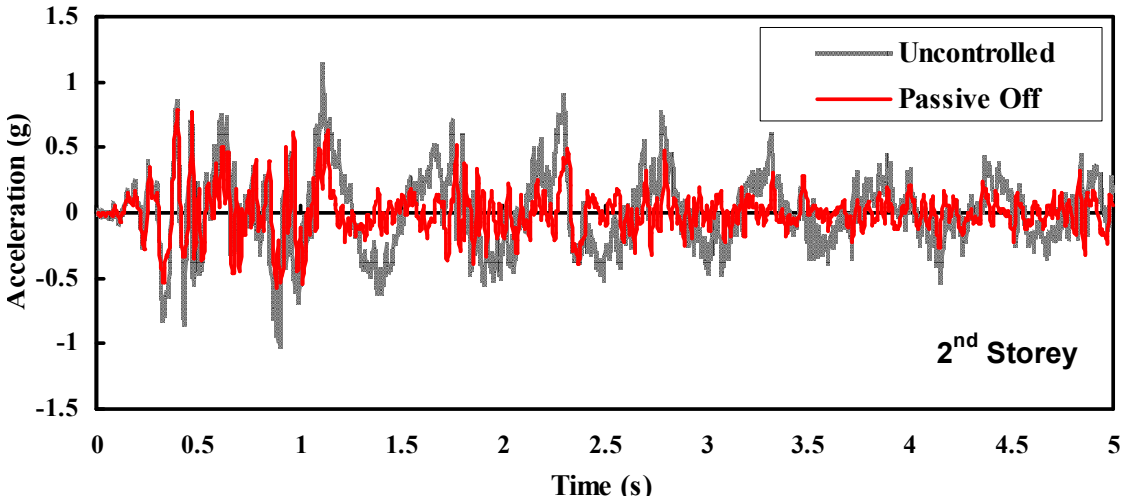

(b)

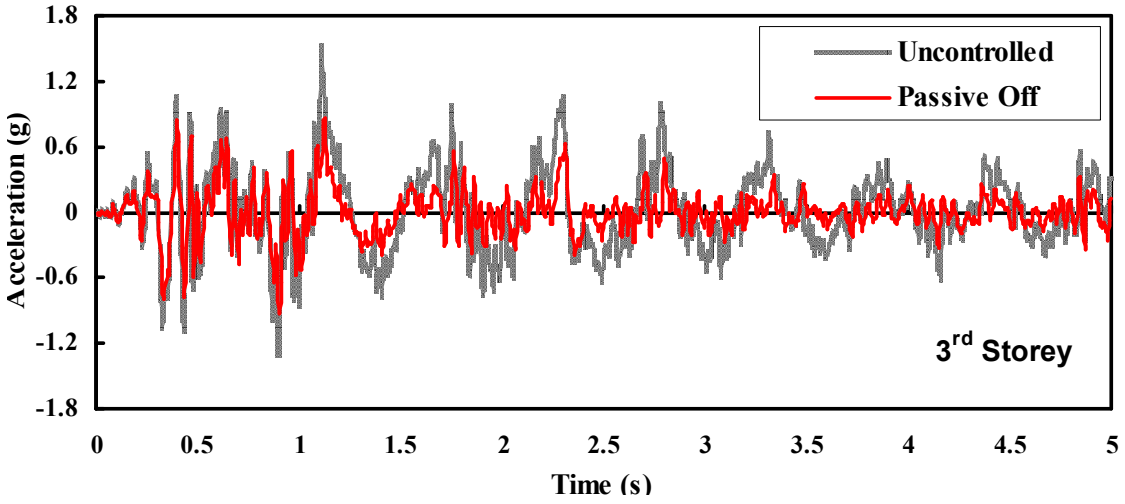

(c)

Figure 6.7 Acceleration for each floor with an MRE device for passive off control logic: (a) Acceleration of first floor. (b) Acceleration of second floor. (c) Acceleration of third floor.

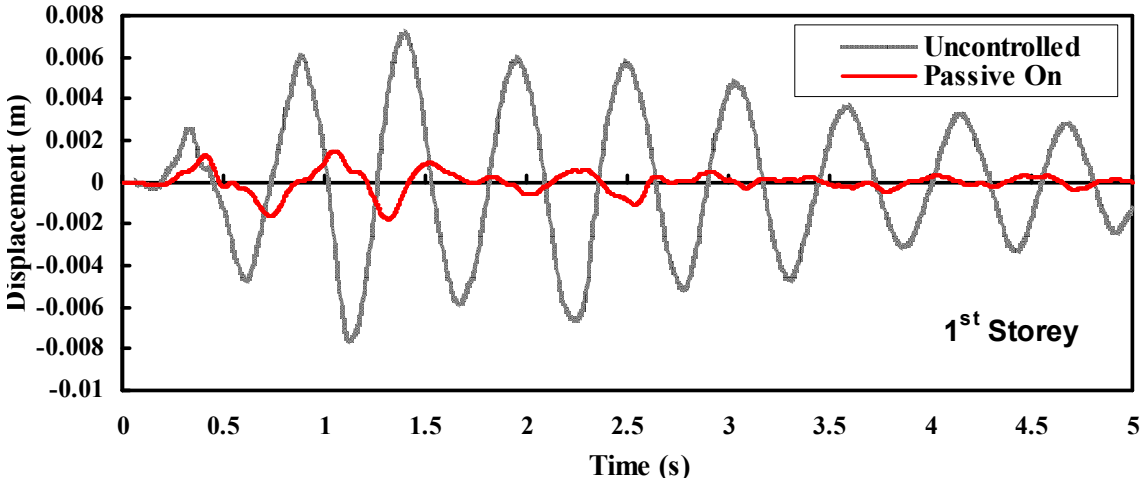
Uncontrolled
Passive On
1st Storey
Displacement (m)
Time (s)
0.008
0.006
0.004
0.002
0
-0.002
-0.004
-0.006
-0.008
-0.01
0
0.5
1
1.5
2
2.5
3
3.5
4
4.5
5

(a)

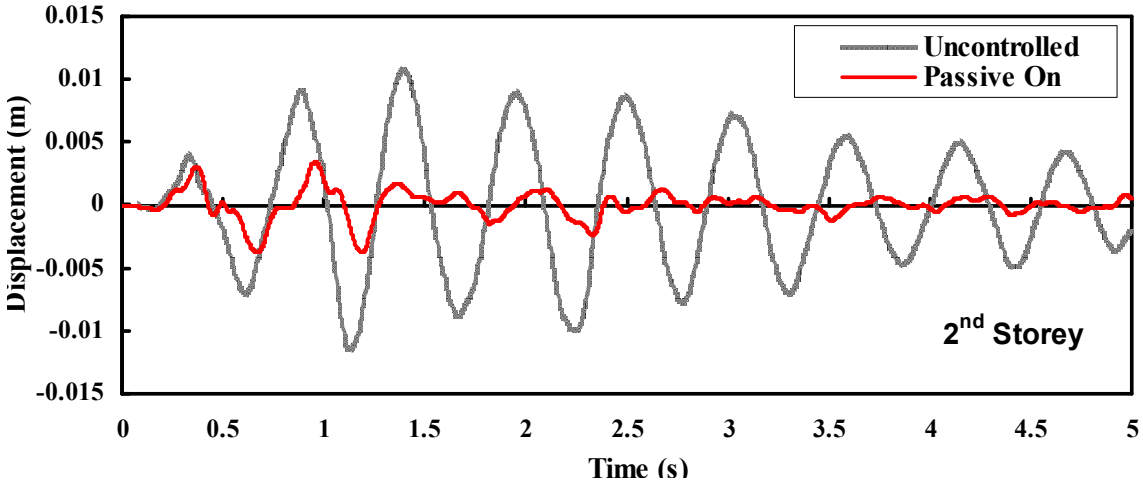
Uncontrolled
Passive On
2nd Storey
Displacement (m)
Time (s)
0.015
0.01
0.005
0
-0.005
-0.01
-0.015
0
0.5
1
1.5
2
2.5
3
3.5
4
4.5
5

(b)

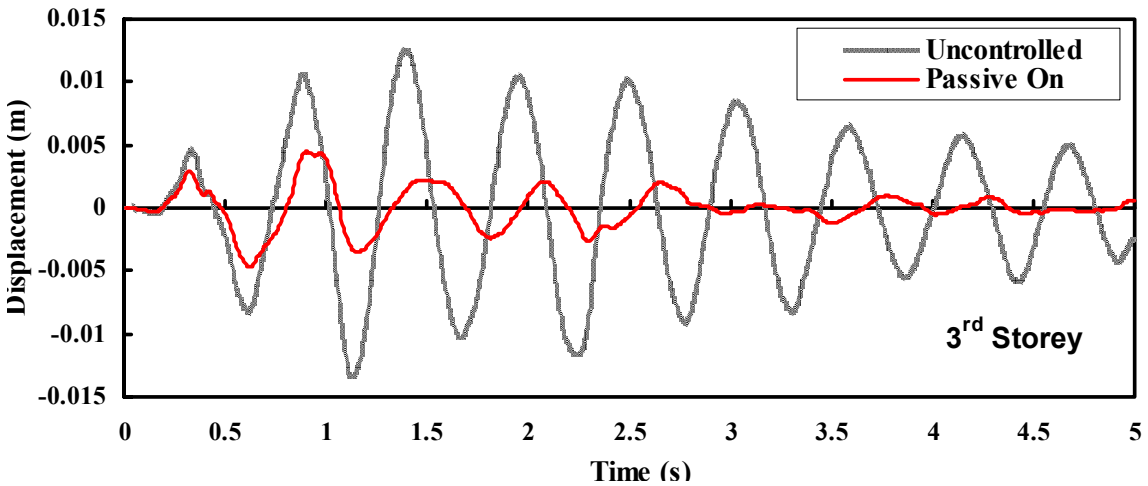

(c)

Figure 6.8 Displacement for each floor with an MRE device for passive on control logic: (a) Displacement of first floor. (b) Displacement of second floor. (c) Displacement of third floor.

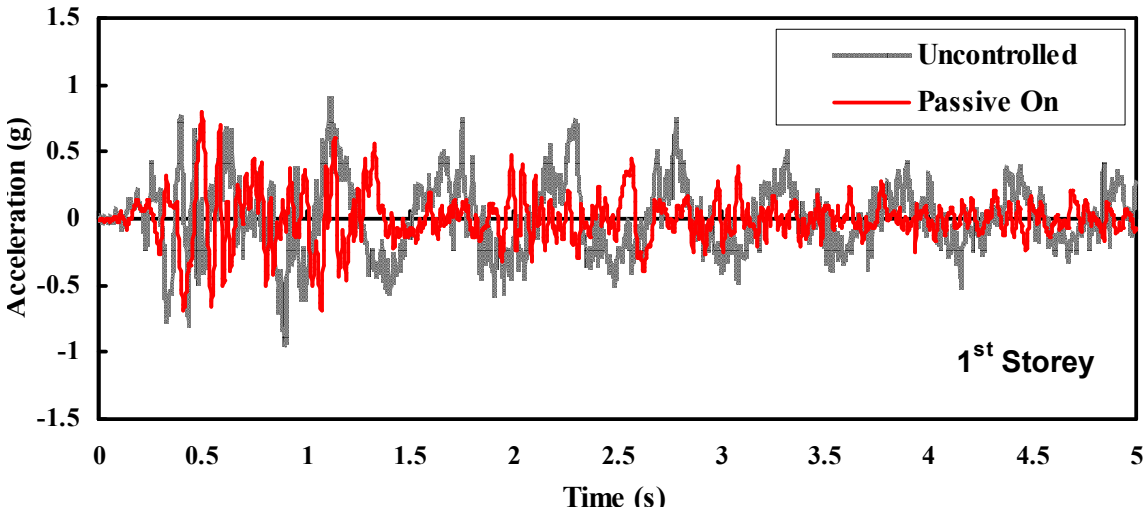

(a)

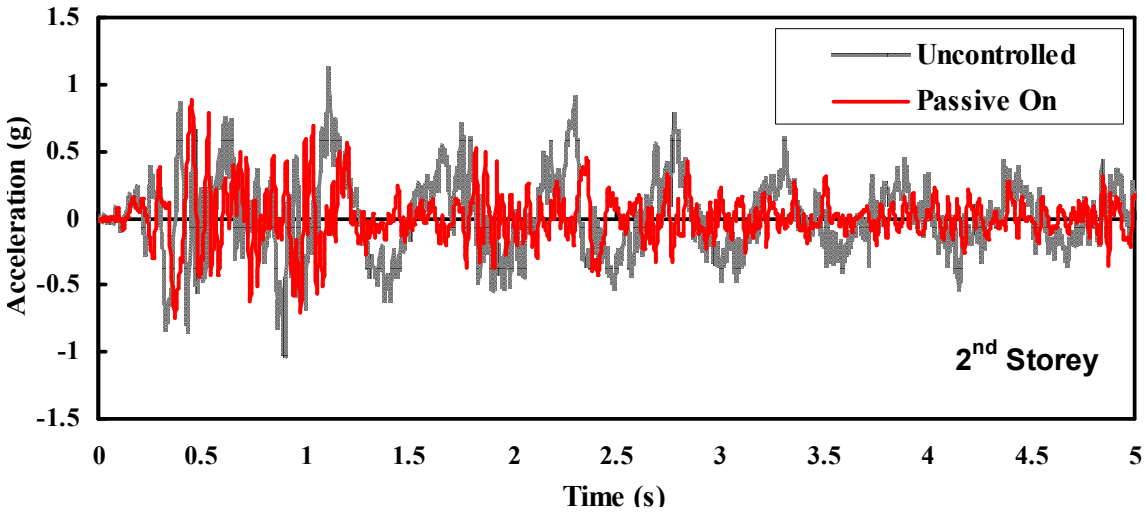

(b)

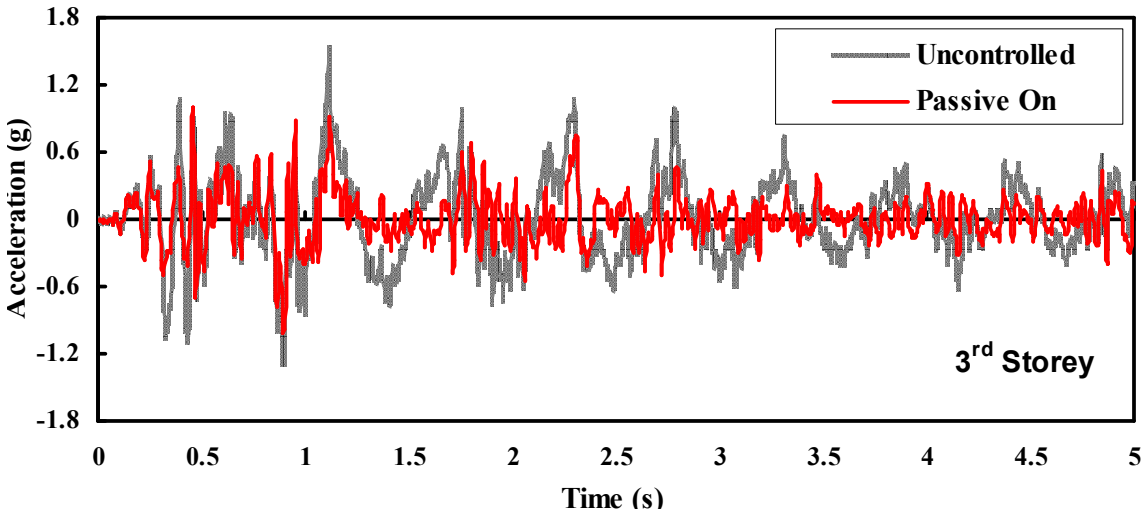

(c)

Figure 6.9 Acceleration for each floor with an MRE device for passive on control logic: (a) Acceleration of first floor. (b) Acceleration of second floor. (c) Acceleration of third floor.

The peak response for a three storied building model incorporating an MRE device is listed in Table 6.5.

Table 6.5 Peak response due to the El Centro earthquake (MRE)

	Floor	Uncontrolled	Passive-off		Passive-on	
x_i(mm)	1st	7.1	2.6	-63.4%	1.5	-78.9%
	2nd	10.7	4.0	-62.6%	3.4	-68.2%
	3rd	12.5	4.8	-61.6%	4.5	-64.0%
$\ddot{x}_i$ (g)	1st	0.90	0.72	-20.0%	0.80	-11.1%
	2nd	1.13	0.78	-31.0%	0.88	-22.1%
	3rd	1.53	0.87	-43.1%	0.99	-35.3%

6.5 DISCUSSION

A comparison of the responses for a three-storey building is listed in Table 6.6

Table 6.6 A comparison between an MRF damper and MRE device

	Case		MRF	MRE	Percentage
Dissipation Energy (N mm)	Passive Off		9663	8130	-16.0%
	Passive On		32123	24022	-25.0%
x_i(mm)	Passive Off	1st	-66.2%	-63.4%	-2.8%
		2nd	-66.4%	-62.6%	-3.8%
		3rd	-64.8%	-61.6%	-3.2%
	Passive On	1st	-81.7%	-78.9%	-2.8%
		2nd	-71.0%	-68.2%	-2.8%
		3rd	-66.4%	-64.0%	-2.4%
$\ddot{x}_i$ (g)	Passive Off	1st	-24.4%	-20.0%	-4.4%
		2nd	-35.4%	-31.0%	-4.4%
		3rd	-46.4%	-43.1%	-3.3%
	Passive On	1st	+4.4%	-11.1%	+15.5%
		2nd	-27.4%	-22.1%	-5.3%
		3rd	-40.5%	-35.3%	-5.2%

From table 6.6, we find that the dissipation energy of an MRE device are both less than the MRF damper with the peak control force criteria, especially the passive on control logic where dissipation energy in the MRE device was about 25% less than the MRF damper. However, the control performance of the MRE device is slightly inferior to the MRF damper. For example the control performances are between 2% to 5% less than the MRE device which demonstrates that the control performances of the MRE device in acceleration and displacement has almost the same effect as those applied by the MRF damper. In addition, the MRE device controlled first floor acceleration better than the MRF damper when the passive on control logic was applied. First-floor acceleration increased by 4.4% when the passive on control logic incorporating MRF damper was operating, had a negative effect on building. However, a building that incorporates an MRE device can still reduce the acceleration on the first-floor by 11.1% by using the passive on control logic.

6.6 CONCLUSION

In this chapter the performance of an MRF damper and an MRE device in controlling the structure of a three storied building was compared and evaluated using the equivalent peak control force as the criteria in this evaluation process. In other words the peak value of the forces due to the MRF damper and MRE isolator were assigned the same. By applying related parameters in a viscoelastic model to the MRE device, the displacement and acceleration of a three storied building were compared with the responses of an MRF damper. The dissipation energy of an MRF damper and MRE device were also compared. The dissipation energy of an MRE device is about 25% less than a MRF damper, but the displacement and acceleration of a structure incorporating the MRE device are slightly inferior to the MRF damper. This comparison again demonstrated the effectiveness that the MRE bearing has in structural control.

CHAPTER 7

CONCLUSIONS AND FUTURE WORK

The MRE devices presented in this thesis are proposed to be applied to structural control. This project attempted to explore MRE material as smart materials to control the structural displacement and acceleration for different types of ground excitation. In the first part of this chapter, the main contributions of this project will be summarised and the characteristics of this system will be outlined. The second part will suggest a direction for further research work.

7.1 SUMMARY

The main contributions of this project can be divided into four parts: 1) An experimental study of a multi-layer MRE bearing, 2) A four-parameter viscoelastic phenomenological model proposed to describe the behaviour of MRE materials and devices, 3) A simulation program of a typical three-storey building incorporating MRE devices on the ground floor, and 4) An evaluation of the performance of an MRE device and MRF damper incorporated into a three-storey building.

7.1.1 An experimental study of a multi-layer MRE bearing

Experimental studies of the steady and dynamic properties of MRE materials and MRE device were presented in this thesis. Factors such as strain amplitude, magnetic density and frequency input were studied and typical characteristics of MRE materials and devices were discussed.

7.1.2 A four-parameter viscoelastic phenomenological model

A four-parameter viscoelastic model was proposed to describe the behaviour of MRE materials. The characteristics of MRE materials were studied by applying the

four-parameter phenomenological model based on hysteresis loops obtained from experimental results. Furthermore, this phenomenological model was extended to describe the performance of an MRE device. A comparison between the analytical and experimental results showed that the four parameters viscoelastic model to be an effective model for MRE materials, a finding that is very useful for structural control.

7.1.3 A simulation program for building structures

The study of dynamic performance for a typical three storied building installed with MRE devices on the ground floor was another goal of this thesis. This work was based on previous research on MR fluids damper used to control structural responses. Our simulation program was developed using the MATLAB SIMULATION program. The four parameter viscoelastic model was also used to simulate an MRE device installed on the ground floor of the building. By comparing the results of simulating the displacement and acceleration for different ground excitations, the results of effective control can be clearly shown.

7.1.4 Performance evaluation

Based on the equivalent peak control force, the performance of building model incorporating an MRE device and an MRF damper were compared by using the MATLAB SIMULINK program. The dissipation energies of the MRF damper and MRE device were also compared. The displacement and acceleration of a structure incorporating an MRE device are slightly inferior to an MRF damper, but the dissipation energy of the MRE device is about 25% less than the MRF damper when the passive on control logic was applied. Thus, the MRE device demonstrated its effectiveness in the area of structural control.

7.2 FUTURE WORK

To verify the positive effects of displacement and acceleration for buildings, related experiments should be implemented in the future. By comparing the responses of displacement and acceleration on each floor, the advantages of MRE devices can be shown. Future work for this project is divided into three main parts:

(1) A scaled MRE isolator will be developed to control practical building model. This MRE isolator will be installed on the ground floor of the building and can generate a force sufficient to control the structural responses.

(2) Implement and find optimal control logics for structural control. By comparing the structural responses of displacement and acceleration on each floor with different control logics, a reasonable control logic with satisfactory control will be selected and studied.

(3) Find an industrial partner to apply this technology for commercialisation (domestic and international). The commercial implementation of MRE technology is also considered to be a key work in the future. MRE technology still requires the support of industrial applications to achieve effective structural control.

References

[1] Gong X. L., Zhang X. Z. and Zhang P. Q., 2005, "Fabrication and Characterization of Isotropic Magnetorheological Elastomers", *Polymer Testing*, 24(5): 669–676

[2] Song H. J., Wereley N. M., Bell R. C., Planinsek J. L. and Filer II J. A., 2009, "Field Dependent Response of Magnetorheological Elastomers Utilizing Spherical Fe Particles Versus Fe Nanowires", *Journal of Physics: Conference Series*, 149

[3] Zhou G. Y., 2003, "Shear properties of mag-netorheological elastomers", *Smart Material. Struct*, 12: 139-46.

[4] Jolly M. R., Carlson J. D. and Munoz B. C., 1996, "A model of the behaviour of magnetorheological materials", *Smart Mater. Struct.*, 5: 607-614.

[5] Koo J. H., Khan F., Jang D. D. and Jung H. J., 2009, "Dynamic Characterization and Modelling of Magneto-Rheological Elastomers Under Compressive Loadings", *Journal of Physics*, 10: 149.

[6] Zhang X. Z., Li W. H. and Gong X. L., 2008, "The rheology of shear thickening fluid (STF) and the dynamic performance of an STF-filled damper", *Smart Mater. Struct.*, 17: 1-7.

[7] Davis L. C., 1999, "Model of magnetorheological elastomers", *J. Applied Phys.*, 85(6): 3348-3351.

[8] Carlson J. D. and Jolly M. R., 2000, "MR Fluid, Foam and Elastomer Devices", *Mechatronics*, 10: 555–569.

[9] Lokander M. and Stenberg B., 2003, "Performance of isotropic magnetorheological rubber materials", *Polymer Testing*, 22: 245-251.

[10] Watson J. R., 1997, *U.S. Patent*, 5609353, EP0784163 Ford Motor Co, GB.

[11] Jiles D., 1994, "Introduction to magnetism and magnetic materials". *Chapman and Hall.*

[12] De Buyl F. 2001, "Silicone sealants and structural adhesives", I*nternational Journal of Adhesion & Adhesives*, 21: 411-422.

[13] Wacker Silicones, 2003, "Material safety data sheet", *Elastosil M4644A, M4644B*.

[14] Leblanc J. L., 2002, "Rubber-filler interactions and rheological properties in filled compounds", *Prog. Polym. Sci.*, 27: 627-687.

[15] Li W. H., Du H., Chen G. and Yeo S. H., 2001, "Viscoelastic properties of MR fluids under oscillatory shear", *Smart Structures and Materials 2001: Damping and Isolation. Inman, D.J. (Ed.). Proceedings of SPIE*, 4331: 333-342.

[16] Borcea L. and Bruno O., 2001, "On the magneto-elastic properties of elastomerferromagnet composites", *J. Mechanics and Physics of Solids*, 49: 2877-2919.

[17] Lokander M. and Stenberg B., 2003, "Improving the magnetorheological effect in isotropic magnetorheological rubber materials", *Polymer Testing*, 22: 677-680.

[18] Shiga T., Okada A. and Kurauchi T., 1995, "Magnetroviscoelastic behaviour of composite gels", *J. Applied Polymer Science*, 58: 787-792.

[19] Yalcintas M. and Dai H., 2004, "Vibration suppression capabilities of magnetorheological materials based adaptive structures", *Smart Mater. Struct.*, 13: 1-11.

[20] Zhou G. Y. and Jiang Z. J., 2004, "Deformation in magnetorheological elastomer and elastomer-ferromagnet composite driven by a magnetic field", *Smart Mater. Struct.*, 13: 309-316.

[21] Ginder J. M., Schlotter W. F. and Nichols M. E., 2001, "Magnetorheological elastomers in tunable vibration absorbers", *Smart Structures and Materials, 2001: Damping and Isolation. Inman, D.J (Ed.). Proceedings of SPIE*, 4331: 103-110.

[22] Ginder J. M., Clark S. M., Schlotter W. F. and Nichols M. E., 2002, "Magnetostrictive phenomena in magnetorheological elastomers", *Int. J. Modern Phys. B*, 16: 2412-2418.

[23] Demchuk S. A. and Kuzmin V. A., 2002, "Viscoelastic properties of magnetorheological elastomers in the regime of dynamic deformation", *Journal of Engineering Physics and Thermophysics*, 75(2): 396-400.

[24] Bellan C. and Bossis G., 2002, "Field dependence of viscoelastic properties of MR elastomers", *Int. J. Modern Phys. B*, 16: 2447-2453.

[25] Dorfmann A. and Ogden R. W., 2003, "Magnetoelastic modeling of elastomers", *European Journal of Mechanics A/ Solids*, 22: 497-507.

[26] Farshad M. and Benine A., 2004, "Magnetoactive elastomer composites", *Polymer Testing*, 23: 347-353.

[27] Yang G., 2001, "Large-Scale Magnetorheological Fluid Damper for Vibration Mitigation: Modeling, Testing and Control", *PhD dissertation*, University of Notre Dame, Indiana.

[28] Gamota D. R. and Filisko F. E., 1991, "Dynamic mechanical studies of electrorheological materials: moderate frequencies", *J. Rheology*, 35: 399-425.

[29] Shames I. H. and Cozzarelli F. A., 1992, "Elastic and inelastic stress analysis", *Prentice-Hall, Inc.*, Englewood Cliffs, N. J.

[30] Stanway R., Sproston J. L. and Stevens N. G., 1985, "Non-linear identification of an electrorheological vibration damper", *IFAC Identification and Sys. Parameter Estimation*, 195-200.

[31] Stanway R., Sproston J. L. and Stevens N. G., 1987, "Non-linear modelling of an electro-rheological vibration damper", *J. Electrostatics*, 20: 167-184.

[32] Wereley N. M., Pang L. and Kamath G. M., 1998, "Idealized hysteresis modeling of electrorheological and magnetorheological dampers", *J Intell Mater Syst Struct*, 9: 642-649.

[33] Spencer Jr. B. F., Dyke S. J., Sain M. K. and Carlson J. D., 1997, "Phenomenological Model for Magnetorheological Dampers", *Journal of Engineering Mechanics*, 123: 230-252.

[34] Choi S. B. and Lee S. K., 2001, "A hysteresis model for the field-dependent damping force of a magnetorheological damper", *J Sound Vib*, 245(2): 375-383.

[35] Dominguez A., Sedaghati R. and Stiharu I., 2006, "A new dynamic hysteresis model for the magnetorheological dampers", *Smart Mater Struct*, 15(5): 1179-1189.

[36] Wang E. R., Ma X. Q., Rakheja S. and Su C. Y., 2003, "Modelling the Hysteric Characteristics of a Magnetorheological Fluid Damper", *J Automobile Eng., In: proc Inst. Mech. Engrs.* 217 (Part. D).

[37] Spencer Jr. B. F., Dyke S. J. and Deoskar H. S., 1998, "Benchmark problems in strucutural control: Part I – Active mass drive system", *Earthquake Engineering and Structural Dynamics*, 27: 1127-1139.

[38] Chew C. M., Hong G. S. and Zhou W., 2006, "Series damper actuator system based on MR fluid damper", *Earthquake Engineering and Structural Dynamics*, 24: 699-710.

[39] Choi K. M., Cho S. W., Jung H. J. and Lee I. W., 2004, "Semi-active fuzzy control for seismic response reduction using magnetorheological dampers", *Earthquake Engineering and Structural Dynamics*, 33: 723-736.

[40] Fan Y. C., Loh C. H., Yang J. N. and Lin P. Y., 2008, "Experimental performance evaluation of an equipment isolation using MR dampers", *Earthquake Engineering and Structural Dynamics*, 10: pp1-24.

[41] Guo Y. Q., Fei S. M. and Xu Z. D., 2008, "Simulation Analysis on intelligent structures with magnetorheological dampers", *Journal Of Intelligent Material Systems And Structures*, 19: 715-726

[42] Frahm H., 1909, "Device for Damping Vibrations of Bodies", *US Patent*, No. 989958.

[43] Librescu L. and Hause T., 2000, "Recent developments in the modeling and behavior of advanced sandwich constructions: a survey Compos", *Struct.*, 48: 1–17.

[44] Zhou G. Y. and Wang Q., 2006, "Study on adjustable rigidity of magnetorheological-elastomer-based sandwich beams", *Smart material and structures*, 15: 59-74.

[45] Si H., Penf X. and Li X., 2008, "A Micromechanical Model for Magnetorheological Fluids", *Journal of Intelligent Material Systems and Structures*, 19: 19-23

[46] Gandhi F. and Bullough W. A., 2005, "On the Phenomenological Modeling of Electrorheological and Magnetorheological Fluid Preyield Behavior", *Journal of Intelligent Material Systems and Structures*, 16: 237-248

[47] Matsagar V. A. and Jandig R. S., 2004, "Influence of isolator characteristics on the response of base-isolated structures", *Engineering Structures*, 26: 1735-1749.

[48] Ni Z. H., 1986, "Damping", in *Vibrations mechanics*, Xi'an Jiao Tong university press, Xi'an, 128-135.

[49] Chung L. L., Lin R. C., Soong T. T. and Relnhorn A. M., 1989, "Experimental Study of Active Control For MDOF Seismic Structures", *Journal of Engineering Mechanics*, 115: 1609-1627.

[50] Dyke S. J., Spencer Jr. B. F., Sain M. K. and Carison J. D., 1996, "Modeling and control of magnetorheological dampers for seismic response reduction", *Smart Material and structure*, 5: 565-575.

[51] Dyke S. J., Spencer Jr. B. F., Sain M. K. and Carlson J. D., 1998, "An experimental study of MR dampers for seismic protection", *Smart Materials and structures*, 7: 693-703.

[52] Shook D., Lin P. Y., Lin T. K. and Roschke P. N., 2007, "A Comparative Study In The Semi-active Control Of Isolated Structures", *Smart Materials and Structures*, 16: 1433-1446.

[53] Ramallo J. C., Johnson E. A. and Spencer B. F., 2002, "Smart Base Isolation Systems", *Journal of Engineering Mechanics*, 128(10): 1088-1099.

[54] Kobori T., Takahashi M., Nasu T., and Niwa N., 1993, "Seismic response controlled structure with active variable stiffness system", *Earthquake Engineering and Structural Dynamics*, 22: 925-941.

[55] Pnevmatikos N. G., Kallivokas L. F. and Gantes C. J., 2004, "Feed-forward control of active variable stiffness systems for mitigating seismic hazard in structures", *Engineering Structures*, 26: 471–483.

[56] Spencer Jr. B. F., Dyke S. J., Sain M. K. and Carlson J. D., 1996, "Idealized model of a magnetorheological damper", *Proc. 12th Conf. on Analysis and Computation, ASCE (Chicago, IL, 1996)*, 361–70

Appendix A:

The Stress-Strain relationship of 1% and 5% amplitude input

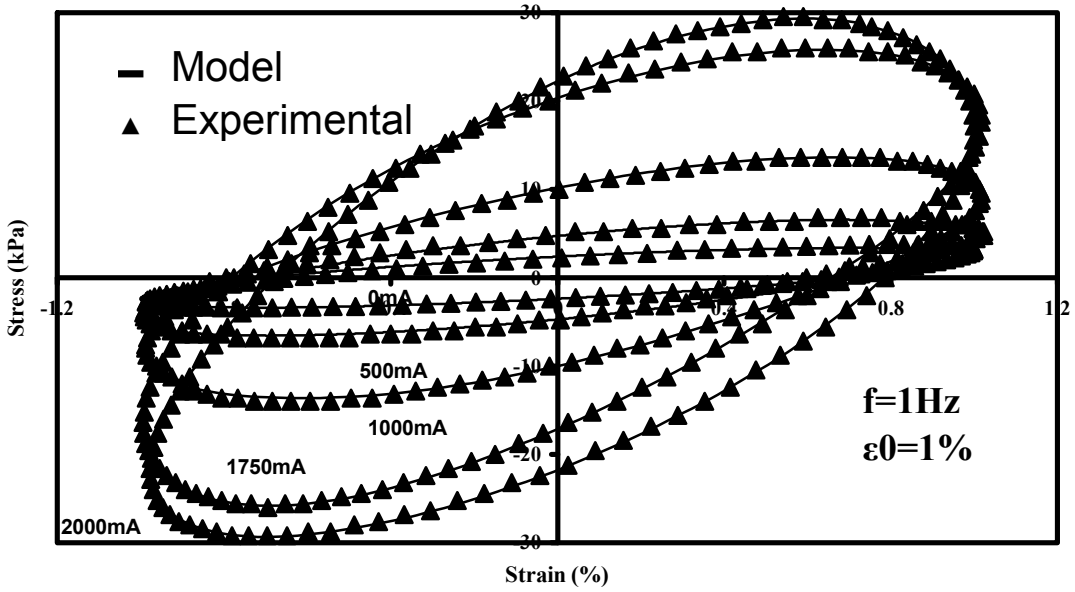

The Stress-Strain relationship of 1% amplitude input

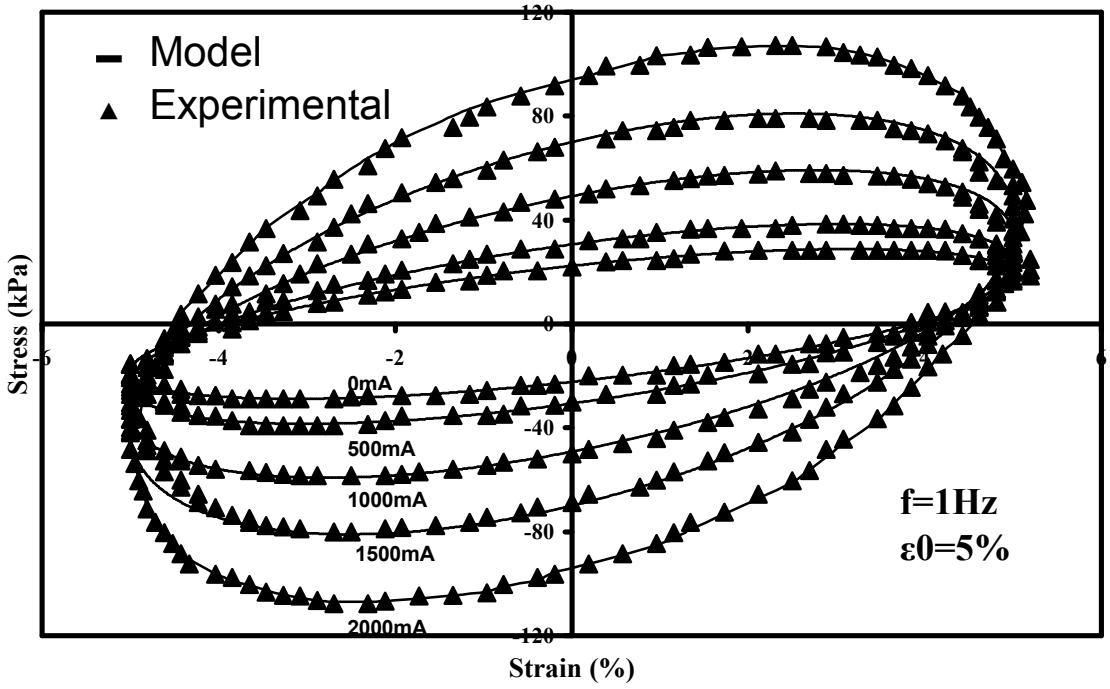

The Stress-Strain relationship of 5% amplitude input

Appendix B:

MATLAB Program of four-parameter viscoelastic model

```
function J=myfunc(coef)
A=csvread('H:\MREmaterial\strainstress.csv');
time=A(:,1)/1000;
stress=A(:,2);
time1=0:0.001:0.99;
[row,col]=size(A);
%assume a model
J=0;
w=2*pi*10;
for i=1:row
    kb=coef(1);
    k1=coef(2);
    k2=coef(3);
    c2=coef(4);
    G1a=(k1*kb+k2*kb+k1*k2)*[(k1+k2)^2+(c2*w)^2]+c2^2*(w^2)*(k1)^2;
    G1b=(k1+k2)*[(k1+k2)^2+(c2*w)^2];
    G1=G1a/G1b;
    G2=(c2*w*k1*k1)/[(k1+k2)^2+(c2*w)^2];
    Gmo=(G1^2+G2^2)^(0.5);
    Gphi=atan(G2/G1);
    stressm(i)=10*Gmo*sin(w*time1(i)+Gphi);
    J=J+(stressm(i)-stress(i))^2;
end
```

Appendix C:

The relationship between magnetic flux density and current intensity

The relationship between Magnetic Flux Density and Current Intensity

No.	Current Intensity (mA)	Magnetic Flux Density (mT)
1	0	0
2	500	118
3	760	191
4	1000	233
5	1500	347
6	2000	459
7	2260	533
8	2500	576

Appendix D:

The simulation program of a three-storey building model

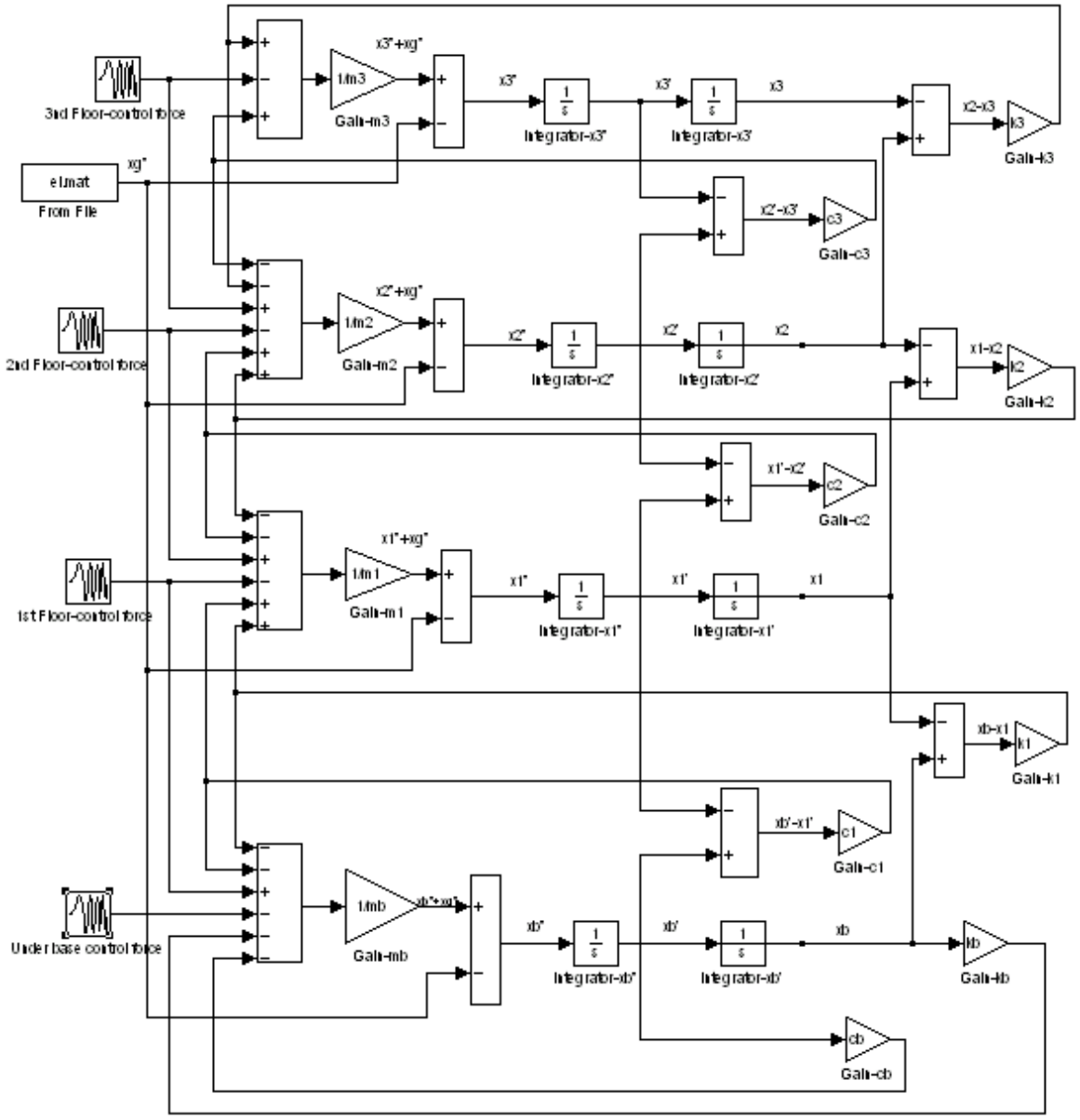

A schematic diagram of simulated system for a 3 storied building

Appendix E:

Peak response of building structure due to Northbridge earthquake

Peak response due to the Northbridge record earthquake

	Floor	Uncontrolled	Passive-off		Passive-on		Bang-bang control	
x_i (mm)	Base	15.3	8.3	-45.8%	4.3	-71.9%	5.1	-66.7%
	1st	19.5	10.2	-47.7%	5.6	-71.3%	6.3	-67.7%
	2nd	23.8	13.9	-41.6%	7.8	-67.2%	8.0	-66.4%
	3rd	26.4	15.2	-42.4%	9.9	-62.5%	10.8	-59.1%
$\ddot{x}_i$ (g)	Base	1.34	0.72	-46.3%	0.97	-27.6%	0.77	-42.5%
	1st	1.49	0.84	-43.6%	1.14	-23.5%	0.92	-38.3%
	2nd	1.72	0.97	-43.6%	1.29	-25.0%	1.09	-36.6%
	3rd	1.85	1.12	-39.5%	1.44	-22.2%	1.21	-34.6%